Charlotte A.G.H. van Gelder

NEUROPROTEOMICS OF THE SYNAPSE

Subcellular quantification of protein networks and signaling dynamics

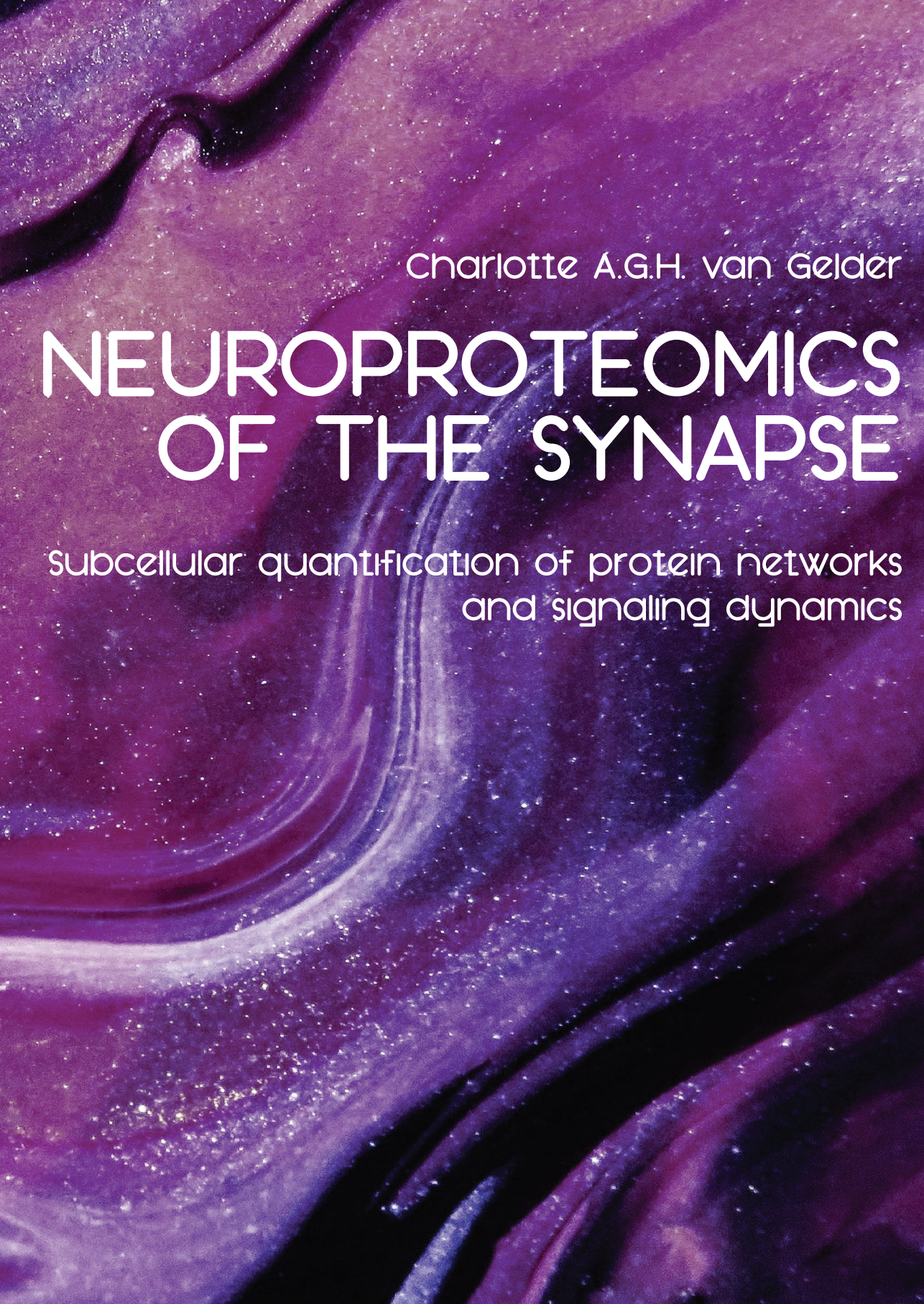

Neuroproteomics of the synapse

Subcellular quantification of protein networks and signaling dynamics

Charlotte van Gelder

Cover design: Stéphanie van Gelder & Charlotte van Gelder
Printed by Proefschriftmaken | proefschriftmaken.nl

ISBN: 978-90-393-7381-1

The research in this thesis was performed in the Biomolecular Mass Spectrometry and Proteomics Group, Utrecht University, Utrecht, The Netherlands.

Neuroproteomics of the synapse

Subcellular quantification of protein networks and signaling dynamics

Neuroproteomics van de synaps

Subcellulaire kwantificatie van eiwitnetwerken en signaleringsdynamiek

(met een samenvatting in het Nederlands)

Proefschrift

ter verkrijging van de graad van doctor aan de
Universiteit Utrecht
op gezag van de
rector magnificus, prof.dr. H.R.B.M. Kummeling,
ingevolge het besluit van het college voor promoties
in het openbaar te verdedigen op

woensdag 9 juni 2021 des middags te 4.15 uur

door

Charlotte Agnes Geertje Hendrika van Gelder

geboren op 29 mei 1990
te Heerlen

Promotoren:

Prof. dr. A.F.M. Altelaar

Prof. dr. A.J.R. Heck

Table of contents

General introduction

Contains sections that are published in:
Laarse S.A.M., van Gelder C.A.G.H.*, Bern M., Akeroyd M., Olsthoorn M.M.A., and Heck A.J.R. Targeting proline in (phospho)proteomics. FEBS J (2020) febs.15190*

Part I - The Dynamic Brain

The mammalian brain

The mammalian brain consists of two major cell types: neurons and glial cells. Glial cells have traditionally been classified as supportive cells, as microglia are known to protect the brain by regulating immune responses and providing structural support, while oligodendrocytes are responsible for the characteristic isolation layer on neuronal axons, which forms the white matter. The grey matter is mostly made up of neuronal cell bodies and their projections[1]. Although there are many types of neurons, the general anatomy of a neuron is described in Figure 1A, where most organelles are found in the cell body, molecules can be transported away from the cell body via one axon, and towards the cell body via many dendrites.

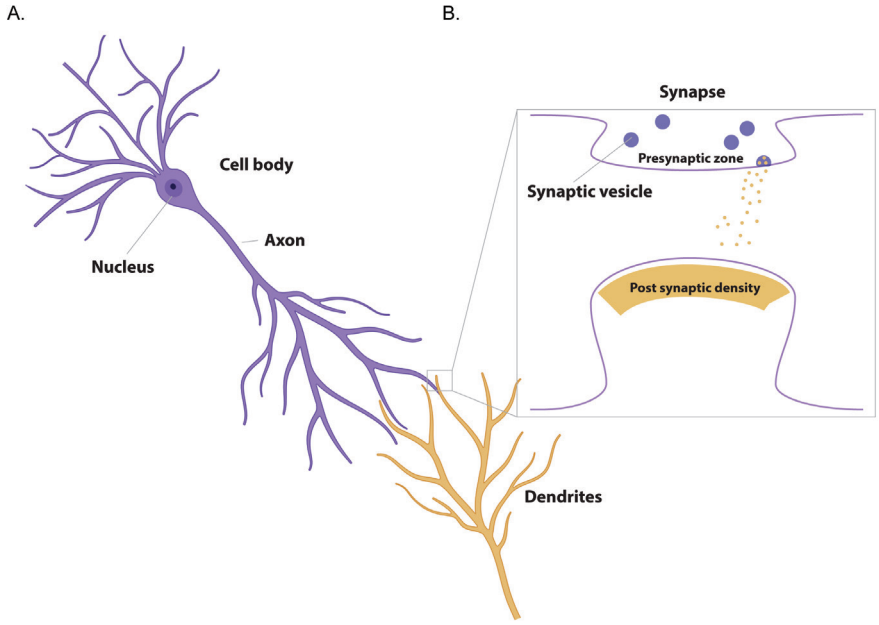

Figure 1. General anatomy of a neuron. **(A)** A neuron consists of a cell body, which contains all essential organelles, including a nucleus, and a variety of protrusions, depending on the type of neuron. Multiple dendrites receive information from other cells, while one axon is responsible for transport away from the cell body, towards another neuron. **(B)** Cell-to-cell communication is achieved via a synapse, where a neurotransmitter molecule is released from the axon terminal of the sending cell, and subsequently stimulates receptors on the postsynaptic density of the receiving cell.

Cell-to-cell signaling

Communication between neuronal cells mostly takes place in synapses, where the axon of one neuron is in close proximity of one of many dendrites of the receiving neuron (Figure 1B). Cell-to-cell signaling can be achieved both electrically and chemically. In chemical synapses, a chemical mediator called a neurotransmitter is released from the pre-synapse into the synaptic cleft, where it diffuses to membrane receptors on the receiving cell, initiating a response. There are many types of neurotransmitters in the

brain, which can exert both excitatory and inhibitory responses, depending on many factors including receptor subtypes. The major excitatory neurotransmitter in the brain is glutamate[2–4].

Glutamate receptors
There are two main types of glutamate receptors, ionotropic and metabotropic receptors. Ionotropic receptors are ligand-gated ion channels and can be divided into three subgroups, being a-amino-3-hydroxy-5-methyl-4-isoxazolepropionic acid (AMPA) receptors, N-methyl-D-aspartate (NMDA), and kainate receptors. Metabotropic glutamate receptors (mGluR) are G-protein coupled receptors and can be placed into three subclasses based on their respective g-proteins, where groups II and III are coupled to inhibitory g-proteins, while group I receptors are coupled to excitatory g-proteins[5–7].

Stimulation of class I mGluRs activates $G_{aq/11}$. Stimulation of the mGlu5 receptor causes the associated enzyme phospholipase C (PLC) to hydrolyze phosphoinositide phospholipids in the cell's plasma membrane. This leads to the formation of inositol 1,4,5-triphosphate (IP3) and diacylglycerol (DAG). Due to its hydrophilic character IP3 can travel to the endoplasmic reticulum where it induces, via fixation on its receptor, the opening of calcium channels, thereby increasing the cytosolic calcium concentrations. The lipophilic DAG remains in the membrane, acting as a cofactor for the activation of protein kinase C (PKC)[7–9]. Moreover, GPCRs such as mGluR5 can also initiate G protein independent signaling pathways, which are mainly activated upon activation of arrestin. These membrane associated protein kinase (MAPK) pathways are mostly known for their role in the regulation of transcription, and may thus play an important role in synaptic homeostasis. Furthermore, scaffolding proteins such as Shank and HOMER can activate the mammalian target of rapamycin (mTOR) pathway, which can regulate protein synthesis[7,10].

Synaptic plasticity
One of the most fascinating features of the brain is its continuous ability to adapt to its surroundings, i.e. it is plastic. Synaptic plasticity can be defined as the potential of neurons to adapt synaptic connectivity in response to an experience, such as a stimulus[2–4,8]. The ability of neuronal networks to strengthen, or potentiate, and weaken, or depress, synaptic connections is key to many essential brain functions, such as learning, memory and regulation of emotions. It is therefore not surprising that dysfunction in the synaptic plasticity process is implicated in diseases such as autism spectrum disorders (ASD)[9,11].

In synaptic plasticity, the increase in synaptic strength is referred to as long term potentiation (LTP). Decrease in synaptic connectivity is called long term depression (LTD), which can be mediated via stimulation of NMDA receptors (NMDA-LTD), or via mGlu5 receptors (mGluR5-LTD). LTD can be achieved functionally, for instance via a decrease in surface receptors on the plasma membrane of the receiving cell[12,13]. While synaptic plasticity occurs in numerous brain areas, it is most well-studied in the hippocampus and the cortex[14].

mGluR5 long term depression

mGlu5 receptors are located on dendritic spines, in close proximity of the postsynaptic density (PSD). The PSD is a protein dense thickening in the dendritic spine in which scaffolding proteins that regulate the stability of membrane receptors are abundant. Tetanic electrical stimulation or chemical stimulation of mGluR5 induces LTD, which is characterized by the internalization of AMPA-type receptors (Figure 2). This reduction of surface AMPA receptors, and as a result a decrease in depolarization potential, is a hallmark of LTD and once induced, can be sustained independently for up to two hours. Other key characteristics of LTD are cytoskeleton reorganization, and local, dendritic, protein synthesis[15,16].

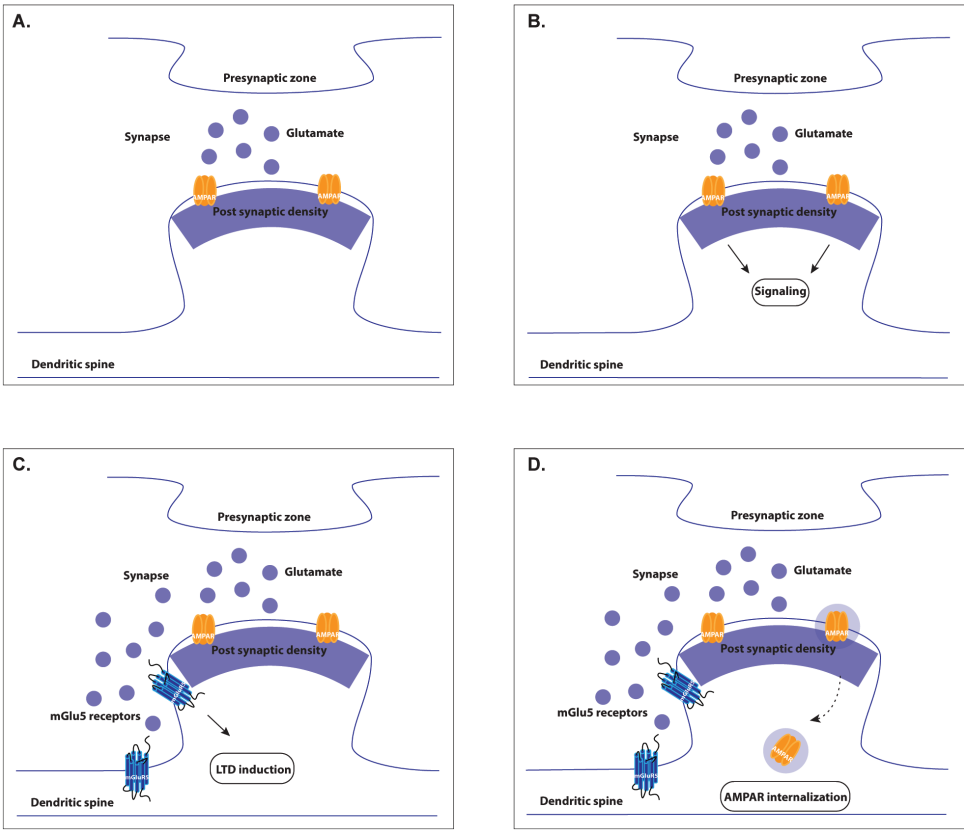

Figure 2. Schematic representation of long term depression. **(A)** Cell-to-cell signaling occurs by releasing the neurotransmitter glutamate from the presynaptic zone into the synaptic cleft. **(B)** Glutamate reaches postsynaptic glutamate receptors, including ionotropic AMPA receptors, promoting signaling in the receiving neuron. **(C)** Excessive glutamate levels in the synaptic cleft activate the perisynaptically located mGluR5, initiating mGluR-LTD, **(D)** leading to the internalization of surface AMPA receptors.

Intracellular GPCRs

In the last decade, a lot of progress has been made concerning the functioning of G protein-coupled receptors. It was first believed that intracellular signaling following stimulation of these receptors was solely caused by G protein-dependent signaling, this view has changed dramatically. GPCRs, including mGluR5, have been demonstrated to be localized on intracellular membranes such as the nucleus. It is believed that stimulation of intracellular mGluR5 leads to differential signaling compared to the extracellular receptors[17]. This raises the question whether intracellular, extracellular or a combination of both receptors are involved in the induction of mGluR-LTD. Much is known about mGluR5 signaling at the cell surface and its corresponding signaling cascades, but less is known about the role of intracellular mGluR5. Recent research by Jong *et al* has shown that stimulation of intracellular mGluR5 can mediate unique signaling pathways when compared to the extracellular receptors. Interestingly, intracellular signaling cascades that seem to be activated include the phosphorylation of extracellular signal-regulated kinase (ERK), a process that is necessary for the synthesis of synaptic plasticity proteins[4]. Even though multiple papers since then have described a differential signal activity between stimulation of extracellular and intracellular mGlu5 receptors, the involved signaling mechanisms remain unknown. Furthermore, conflicting results have been published concerning the role of, among others, ERK1/2, P38 MAPK[18], and the necessity of protein synthesis for the induction of LTD in general[19]. A limiting factor in these studies is the use of gene expression and transcription techniques as a measure for protein activity while focusing on one or more proteins of interest. Since it is still not exclusively shown that mGluR-LTD is protein synthesis dependent, or whether it is dependent on PTM regulation of proteins such as phosphorylation, there is a need for high throughput screening of whole cell proteome and phosphoproteome to identify differences in protein and phosphorylation expression levels upon LTD induction.

Part II - Introduction to Mass Spectrometry-based Proteomics

There is a great need to understand the complexity of the human brain and, in fact, the biological mechanisms underlying the physiology and pathophysiology of the entire human body. Over the last decades, great efforts have been made to achieve this, and with it came the enormous developments in technologies to make it possible. With the completion of the human genome project in 2003, the genomics field was blooming. It was expected that, following the central dogma of biology, mutations in genes would explain the majority of diseases. This dogma, postulated by Crick, describes how DNA is transcribed into mRNA, and subsequently translated into proteins; the functional building blocks of a cell.

Realization came, however, that the transcription of DNA into mRNA, and subsequent translation of mRNA into proteins, was not unidirectional. Alterations in the functional building blocks of the cells, the proteins, could often not be explained by mutations in the genome. On a genetic level, variation is introduced via epigenetic signatures and alternative splicing, among others, while mRNA can be silenced and proteins can undergo interactions (protein-protein interactions; PPIs) and can be regulated by up to 300 different post-translational modifications (PTMs). To understand such complex biological systems, it is essential to study all layers of information in the biological sample in a high-throughput and unbiased manner. The use of mass spectrometry (MS) based proteomics has increased exponentially in the last decades and is now considered the golden standard in proteomics research.

Mass spectrometry-based proteomics

Proteomics encompasses the large-scale study of all proteins in a cell, tissue, or even an entire organism. This includes, but is not limited to, the study of PPIs, protein complexes, and PTMs, of which phosphorylation is most well-known. Three main types of mass spectrometry-based proteomics approaches can be distinguished, based on the size of the protein or peptides that are measured; top-down[20], middle-down[21], and bottom-up[22]. Of these, bottom-up (also called shotgun) proteomics is the most widespread. In shotgun proteomics, proteins are enzymatically digested into peptides, separated by liquid chromatography (LC), and analyzed by tandem mass spectrometry (MS/MS). The resulting fragment ion spectra allow the determination of the amino acid sequence of the originating peptide, ultimately reconstructing the protein of origin in silico (Figure 3). This method allows for fast, high-throughput qualitative and quantitative characterization of thousands of proteins from highly complex samples in a relatively straightforward fashion[22].

The proteomics workflow

A bottom-up proteomics experiment starts with the distortion of cells or tissue to release the protein content. Proteins are extracted with help of chaotropic and/or membrane-solubilizing buffers in combination with mechanical distortion[23]. To prevent proteolysis by endogenous proteases, protease inhibitors are added to the lysis buffer. When interested in protein phosphorylation, phosphatase inhibitors can be added to preserve

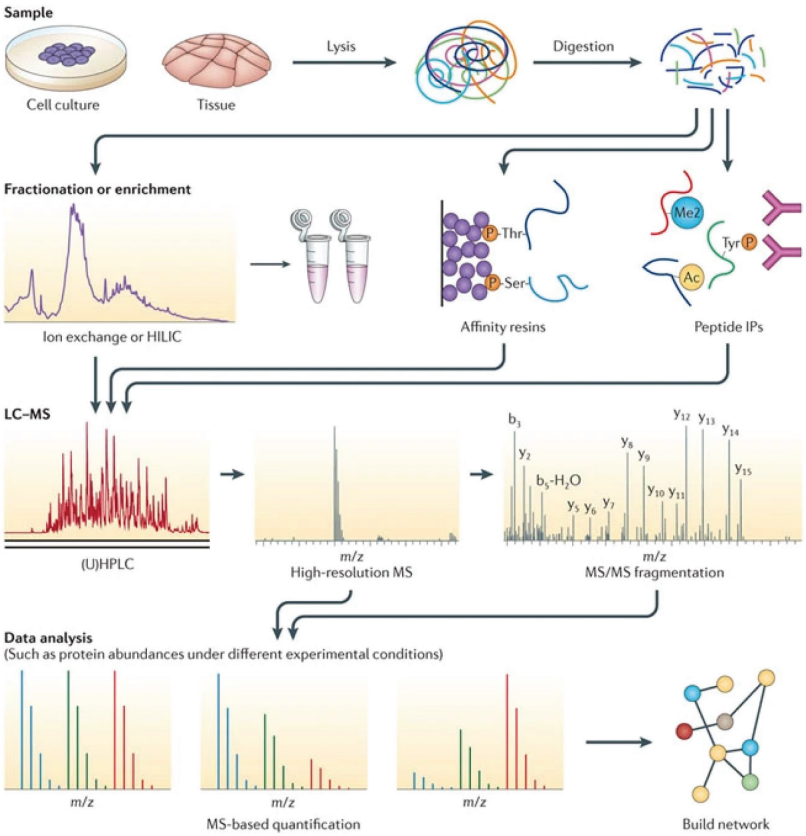

Figure 3. Overview of a generalized bottom-up MS-based proteomics workflow. Biological samples, such as tissue or cultured cells, optionally exposed to a stimulus and/or subjected to metabolic or genetic labeling, are lysed to release their proteins. An enriched set of specific proteins or the full proteome are digested into peptides. Depending on the aim of the experiment, peptides can be fractionated, specific peptides can be enriched using affinity resins or IP approaches, and are ultimately analyzed using LC-MS/MS. Here, the peptide mixture is separated and eluted peptides are introduced in the mass spectrometer, where high-resolution scans are followed by fragmentation of ions, generating tens of thousands of tandem mass spectra. Computer algorithms then match these to proteins from organism specific databases and can compute relative abundances of these proteins. Further statistical and functional analyses can be performed to aid data interpretation and validation. Adapted from Altelaar et al[33].

phosphorylation. Next, proteins are denatured and disulfide bonds are reduced, after which protein refolding is prevented via alkylation of the free thiols. Proteins are then digested into peptides using a sequence-specific protease. The resulting peptide mixture is often subjected to a buffer exchange method, most often using C18 material, so that the sample is cleared of contaminants that will distort mass spectrometric analysis, and to a buffer suitable for subsequent analysis. LC-MS/MS analysis can be separated in three different stages, in which the peptide mixture is first separated using a liquid chromatographic (LC) approach, introduced in the mass spectrometer for detection (MS1) and subsequently fragmented and analyzed (MS2)[24]. Samples are commonly separated using reversed-phase high-performance liquid chromatography (RP-HPLC)[25]. In reversed-

phase separation, analytes are separated based on differential interaction with the hydrophobic stationary phase and a predominantly hydrophilic mobile phase that gradually increases in hydrophobicity. Upon elution from the analytical column, the peptides are ionized, for instance using electrospray ionization (ESI), and the formed ions are introduced into the mass spectrometer.

A full MS spectrum is acquired for peptides eluting from the column at any given time (MS1). Based on method settings, the top n precursor ions (ionized peptides), or precursor ions with a specific mass or charge, are selected for fragmentation. Isolated precursor ions are fragmented by collisions at low energy with an inert gas such as nitrogen (in the case of Collision-induced Dissociation (CID)[26], and Higher-energy Collisional Dissociation (HCD)[27]), or by radical reactions like in Electron Transfer Dissociation (ETD)[28]. Moreover, hybrid techniques such as electron-transfer/ higher-energy collision dissociation (EThcD) exist, allowing for different or supplemental fragmentation depending on precursor characteristics in so-called decision tree methods[29]. The resulting fragment spectrum (MS/MS or MS2 spectrum) contains mass over charge (m/z) and relative intensity values for each fragment. The produced spectra allow for peptide identification through matching against a protein database using a search engine. Search engine algorithms correlate the thousands of experimental spectra generated in each MS run to theoretical spectra of peptides. Several database search engines are available, including Mascot[30] and the freely available Andromeda, which is incorporated into the MaxQuant quantitative proteomics platform[31]. Here, in silico digestion of a defined protein database is performed, taking into account the cleavage specificity of the protease utilized, (post-translational) modifications, missed cleavages, and fragmentation method. Theoretical fragmentation spectra of the in silico peptides are compared to the experimentally generated fragment ions, and resulting Peptide Spectrum Matches (PSMs) are scored and matched to database protein entries. To correct for random spectral matches, a False Discovery Rate (FDR) filter can be applied, both on peptide and protein level. Most commonly, spectra are compared to a randomized decoy sequence database, such as a reversed hit sequence database. Correlation of false versus true matches can then be used to calculate the FDR, which is often set to 1%[32].

The general proteomics workflow can be adjusted and expanded depending on the biological question to be addressed. A variety of labeling, enrichment, and quantification methods utilized in the work presented in this thesis will be discussed in more detail.

Tailoring the proteomics workflow

In the field of neuroproteomics (i.e. proteomics of the neuron), most research questions can be divided into one of two experimental strategies: temporal neuroproteomics, or spatial neuroproteomics. Temporal neuroproteomics studies are aimed at delineating protein expression profiles over time, for instance during neuronal differentiation and neurodevelopment, or upon perturbation of the natural state (Figure 4A). Perturbation can include

drug treatment or gene silencing, or induction of synaptic plasticity. Spatial neuroproteomics studies are focused on the location of protein expression and includes but is not limited to brain region specific protein expression, differences between neuronal cell types, or protein expression profiles within a certain cell type (Figure 4B). Targeted proteomics (Figure 4C) comprises labeling or enrichment techniques to study protein-protein interactions (AP-MS), post-translational modifications (PTMs-MS), subcellular localization of proteins (proximity labeling), and to get structural information about protein complexes (XL-MS). More detailed descriptions of temporal and spatial neuroproteomics studies of the synapse, as well as dedicated proteomics tools for targeted neuroproteomics, are described in **chapter 2**.

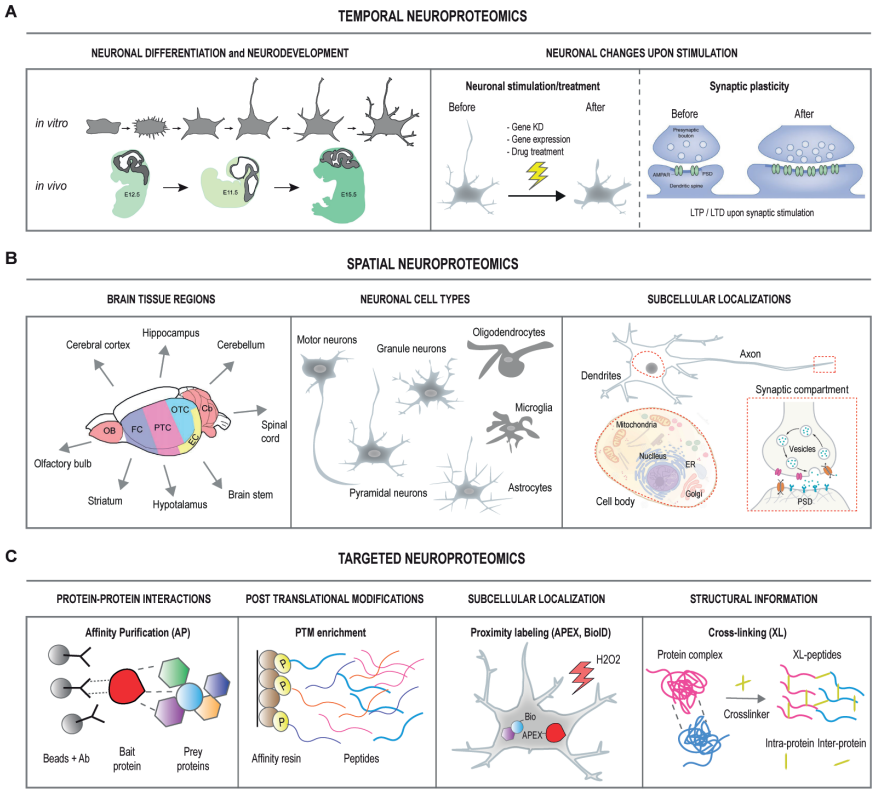

Figure 4. Overview of different neuroproteomics applications. **(A)** Temporal proteomics investigates temporal changes to the proteome, for instance during neuronal differentiation and neurodevelopment, or neuronal changes upon stimulation. **(B)** Spatial proteomics investigates the spatial diversity of proteins in specific brain tissue regions and neuronal cell types, as well as their subcellular localization within different cellular compartments. **(C)** Targeted proteomics comprises labeling or enrichment techniques to study protein-protein interactions (AP-MS), post-translational modifications (PTMs-MS), subcellular localization of proteins (proximity labeling), and to get structural information about protein complexes (XL-MS). Adapted from: Riccardo Stucchi[34].

Proteases

Most proteomic studies use Trypsin for protein digestion as it cleaves with very high specificity C-terminally to arginine (Arg) and lysine (Lys) residues. As both amino acids are basic, the resulting peptides have basic C-termini. This, combined with the free amine at the peptide N-terminus, ensures that tryptic peptides carry a positive charge at either end of the peptide, making them very suitable for fragmentation-based sequencing[35]. In addition, trypsin's high specificity reduces the complexity of the subsequent database searches, as they can be restricted to peptides ending with Arg or Lys, which reduces computational requirements of the search. However, the use of Trypsin also has limitations, and it is not the optimal enzyme for all types of analyses.

Owing to the high specificity of Trypsin, the spacing of Arg and Lys amino acids across the proteome dictate the length of peptides, and thus the number of unique peptides. For standard intracellular proteins, Arg and Lys occur at a high frequency (5.6% and 5.7%, respectively) which leads to the fact that roughly 50% of the peptides produced by Trypsin are too short (<6 amino acids) to be nicely fragmented and uniquely assigned to a protein[36]. Conversely, some proteins, notably membrane proteins, exhibit few tryptic cleavage sites and extreme hydrophobicity, resulting in poor coverage of this class of proteins in Trypsin-based proteomics[37]. These combined effects all contribute to undetected, less visible areas of the proteome. To illustrate this, we have performed an *in silico* digestion of the human proteome using the specificity listed in Table 1, and asked what the upper limit of detection was for each protease using the search and MS settings employed in many standard study setups. For Trypsin, a maximum of 87% of the proteome would in theory be detectable using this proteomics setup, assuming every peptide of suitable characteristics is actually fragmented and identified. To improve on this boundary, efforts have been made to utilize proteases with bottom-up workflows. Several groups have shown that by using proteases that cleave at different amino acid motifs, the number of unique peptides identified, and thus the proteome coverage, can be substantially improved[36,38–41].

Numerous alternative proteases have been used for the digestion of proteins from a lysate, whereby each has its own cleavage specificity and optimal conditions (see Table 1). By combining the proteases either in parallel or sequentially, one is able to improve the proteome coverage through combining the results of individual proteases. For instance, work by Swaney *et al*. nicely illustrated that expanding beyond a single protease can yield a roughly 20% increase in protein identifications and achieved double to proteome sequence coverage[36]. Similarly, our group has shown that the use of multiple proteases in parallel for phosphoproteomics gives rise to highly complementary sets of phosphosites, where only 27% of all identified sites were found in more than one protease dataset[42].

Table 1. Cleavage specificities reported for some of the most commonly used proteases in bottom-up proteomics. Adapted from: van der Laarse S.A.M., van Gelder C.A.G.H. *et al*[43].

Protease	Cleavage site (↓)	Optimal pH	Max Proteome Coverage
Asp-N	↓D	8	78%
LysargiNase	↓K/R	7.5	87%
Lys-C	K↓Xnp	8	79%
Lys-N	↓KXnp	8	78%
Arg-C	R↓Xnp	8	82%
Glu-C	E↓	8	86%
Chymotrypsin	F/W/Y↓	8	87%
Trypsin	K/R↓Xnp	8-9	87%
Sap-9	K/R↓Xnp	6-7	87%

While the combination of proteases has already been shown to aid in expanding the proteome sequence coverage, the presence of (multiple) proline residues presents a particular challenge for many proteases. Proline is a unique amino acid in peptides/proteins as it is the only cyclic amino acid, giving rise to a tertiary amide, limiting hydrogen donating properties and imposing rigid structural constraints on peptide bonds[44,45]. Because of its unique properties, proline often leads to missed proteolytic events during digestion[38], increasing the resultant peptide length and database search complexity. Moreover, proline also affects the fragmentation step during mass analysis, known as the "proline effect"[46], where fragmentation shows enhanced production of y-ions spanning from the proline to the peptide C-terminus due to the enhanced basicity of the proline nitrogen, restricting the peptide sequence coverage[46–48].

To overcome these limitations, research efforts have been directed toward finding a proline-directed protease as such a protease would decrease database search complexity by well-defining the proline position, as well as substantially improve proteome sequence coverage due to its high complementarity to Arg and Lys directed proteases. In 2009, Šebela *et al* evaluated an acidic prolyl endoprotease from Aspergillus niger, called An-PEP, for its use in proteomics and found that the enzyme has potential for in-solution digestion studies[49]. Moreover, our lab showed that An-PEP, also termed EndoPro, exhibited maximum activity at pH = 2 and is active at moderately high urea concentrations and low temperatures, making it very suitable for use in mass spectrometry-based hydrogen-deuterium exchange experiments[50]. In addition, work published on another prolyl endopeptidase originally from Nepenthes ventrata, termed Neprosin, showed that almost half of the sequence coverage achieved by the proline-directed protease on proteins detected in both tryptic and Neprosin digests were not observed when digestion was performed with Trypsin[51]. Collectively, these works suggest huge potential for proline-directed proteases to shed light on previously undetectable areas of the proteome. In phosphoproteomics, however, proline-induced complications are even more prevalent as in

eukaryotic systems around 40% of the phosphorylation events detected are proline-directed, dominated by so-called SP or TP motifs[52]. Hence, in most eukaryotic phosphoproteomics experiments, prolines are highly enriched and even more prevalent than in standard proteomics analysis.
In a recent study, we extended substantially on previous work using proline-directed proteases. We first benchmarked EndoPro versus Trypsin, thereby generating large proteomics datasets on HeLa lysates digested by EndoPro at pH = 2, EndoPro at pH = 5.5 and Trypsin at pH = 8.5. We optimized the peptide ID rates using multiple peptide fragmentation techniques, and the search engine Byonic, allowing us to increase the ID rate substantially to about 40% and 66% of all PSMs for EndoPro and Trypsin, respectively. When using EndoPro at these two different pH values, we found the specificities and activities to be similar. However, our datasets revealed a substantial difference between the peptides generated with EndoPro at pH = 2, EndoPro at pH = 5.5 and Trypsin, indicating the cleavage of different proteins and/or sites at different pH values. Overall, EndoPro enabled us to detect over 2200 unique proteins not observed in our tryptic digests (Figure 5A) and contributed 49% of the total unique phosphosites detected (Figure 5B), making it a protease almost equally powerful as, and complementary, to Trypsin.

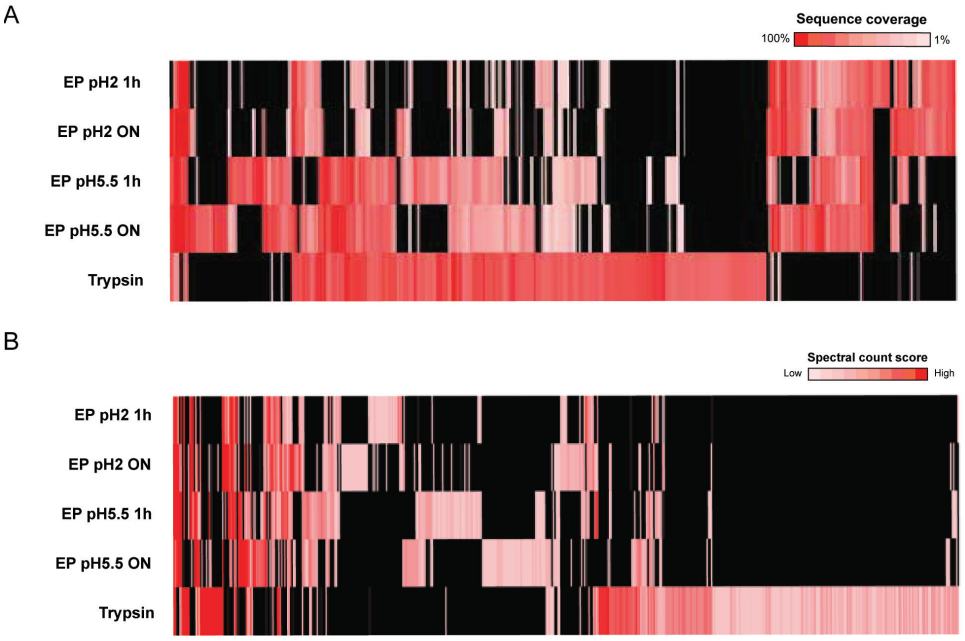

Figure 5. EndoPro is highly complementary to Trypsin in the identification of **(A)** protein identifications and **(B)** site-specific phosphorylation sites. Adapted from: van der Laarse S.A.M., van Gelder C.A.G.H. *et al*[43].

Alternative mass spectrometry approaches

The shotgun proteomics workflow described in this chapter is optimized for discovery or shotgun proteomics. Here, unbiased and complete proteome coverage is desired, which is collected by data-dependent acquisition (DDA) in which the MS automatically fragments the top most abundant peptide peaks in each scan. Mass spectrometric analysis in DDA mode contains a survey scan at high resolution. Next, several peptides are selected for fragmentation, followed by MS2 acquisition, most often based on intensity (so-called top n methods)[53]. An alternative to shotgun acquisition methods is the use of targeted methods. These targeted mass spectrometry-based proteomics approaches, such as selected reaction monitoring (SRM), are hypothesis-driven, and therefore do not rely on stochastic, intensity-based peak picking algorithms. SRM is a popular choice of targeted MS acquisition, because of its high sensitivity and reproducibility in the analysis of a specified subset of peptides of interest, which are selectively isolated and then fragmented over their chromatographic elution time. The use of targeted methods requires dedicated methods, built for experiment-specific target lists. Each of these lists consists of individually optimized assays for every peptide of interest, thereby increasing sensitivity and circumventing missing-value issues often seen for low abundant proteins.

Quantitative proteomics

Cellular proteomes are highly dynamic, and differences between two biological systems are often not just explained by the expression of different proteins, but mostly via changes in PTM or protein abundances. Quantification of proteins and generated peptides is therefore essential in MS-based proteomics studies.

Stable Isotope Labeling by Amino acids in Culture

Labeling techniques are now widely used to allow for relative quantification of proteins between several experimental conditions[54]. The principle of labeling-based quantitation is based on the introduction of heavy stable isotopes that are incorporated in the proteins of interest. Alternatively, proteins or peptides can be chemically labeled during sample preparation. Relative quantification between the heavy and light isotope of the same species can then be determined by comparison of the different signal intensities of the two species, originated by the shift in mass of the heavy isotope. One of the most used in vivo labeling methods is Stable Isotope Labeling with Amino acids in Culture (SILAC)[55]. Although the name suggests that this method can only be used in cell lines, it has been more widely applied, and can be used in tissues, fluids, or even living animals. Despite the wide array of possibilities of SILAC for quantitative proteomics, its use in neuroproteomics has proven difficult. Full incorporation of SILAC labels takes weeks, or preferably some generations of cells, and is therefore not applicable to non-dividing cells such as primary cell lines and neurons[56]. However, pulse labeling with heavy labeled amino acids can be useful in neurons. Short, 'pulsed', exposure of neurons to heavy labeled amino acids allows for monitoring of specific changes in protein expression after a certain stimulus[57].

Tandem Mass Tag labeling
Next to metabolic labeling, different chemical labeling techniques exist. In contrast to SILAC, isobaric labeling reagents[58] such as Tandem Mass Tags (TMT) are introduced at a later stage in sample preparation, mostly at the peptide level. This allows for the use in a much wider range of applications. Quantification is performed at the MS2 level by comparing 'reporter ion' intensities in the tandem mass spectrum. The labeling does not alter the precursor mass in the MS1 spectrum like with SILAC, but fragmentation leads to the formation of specific reporter ion signatures. This allows for extensive multiplexing (there is now TMT-11plex and the recently introduced TMTpro 16plex[59]), meaning that up to 16 samples can be pooled and subsequently measured at the same time. This potentiates the analysis of large sample sets, for instance from comparing multiple time points, treatments, or conditions. Moreover, multiplexing can be extended by the use of multiple labeling sets, in which one label, the reference (most often a pooled mix of all other samples) is equal in all sets, allowing for normalization between pooled sets.

Label Free Quantification
Label-free quantification methods have increased tremendously in popularity, due to the increasing availability of high-resolution mass spectrometers, the low-cost sample preparation (no labels are required), and the flexibility in experimental design. Label-free quantification can be achieved by spectral counting, or by signal intensity measurements of peptide precursor ions across different LC-MS/MS runs. In spectral counting, the number of times a peptide has been selected for fragmentation (i.e. the number of MS/MS spectra, often corrected for the size of the protein) is used as a measure for its abundance[60]. Alternatively, protein abundance can be quantified using precursor ion signal intensities between samples. Here, MS1 signals of each peptide identifying a protein are summed up and subsequently this protein intensity value is compared between the different runs. This method requires robust instrumentation and high reproducibility, since m/z, peak area and retention time of each ion across all runs need to be well aligned. Moreover, additional analysis time is required, because of the lack of multiplexing possibilities.

Normalization is needed to make peptide signals comparable between runs. Due to the stochastic nature of precursor selection in DDA mode, peptide identifications are often missing, especially when derived from low abundant proteins. To overcome the issue of 'missing values' the 'match-between-runs' feature implemented in the MaxQuant software can be used. This employs retention time alignment and allows for transferring of peptide identifications from one LC-MS run to another[61], thus improving label-free quantification by increasing the number of peptides that can be used for quantification beyond those that have been sequenced by MS/MS.

Part III - Scope of this thesis

The advancement in mass spectrometry-based proteomics now allows for the study of highly dynamic, low abundant neuronal processes in specific cellular compartments such as the synapse. In **chapter 2**, we discuss the trends in mass spectrometry-based neuroproteomics of the synapse. We focus on choices in sample types, different labeling and enrichment approaches for the study of protein-protein interactions and protein signaling, and data analysis and interpretation. We highlight studies from the last five years and finally discuss some recent advancements that could benefit the advancement of neuroproteomics studies.

In **chapter 3**, we integrated quantitative high-resolution phosphoproteomics with the analyses of newly synthesized proteins via bio-orthogonal amino acids (azidohomoalanine) in a pulsed labeling strategy combined with tandem mass tag label-based quantification in cultured hippocampal neurons stimulated with DHPG, to study mGluR5-induced protein phosphorylation and translation. We identified several kinases with important roles in DHPG-mGluR-LTD, which we confirmed using small molecule kinase inhibitors. Furthermore, changes in the AMPA receptor endocytosis pathway in both protein synthesis and protein phosphorylation upon mGluR5 activation were identified, whereby Intersectin-1 was validated as a vital player in this pathway. This study revealed several novel insights into the molecular mechanisms underlying mGluR-LTD and provides a broad view on its molecular basis, which serves as a rich resource for further analyses.

In **chapter 4** we describe the optimization and validation of APEX2 fused to the epidermal growth factor receptor (EGFR). We show that with this proximity labeling protocol, we can distinguish the subtle alterations in receptor trafficking upon stimulation with either EGF or TGF-a, resulting in receptor degradation and recycling, respectively. We identified and quantified EGFR stable and transient interactions at different time points after stimulation and were able to use bystander proteins to map EGFR subcellular location at each time point. Utilizing the fast and concise biotinylation of proximity proteins by APEX2, we were able to detect slight differences in early signaling kinetics between TGF-a and EGF, thereby increasing our knowledge on receptor tyrosine kinase signaling and differential trafficking.

In **chapter 5** we continued to use APEX2 and fused it to mGluR5 to study receptor localization bias. We deleted a 25 amino acid sequence in the receptor c-terminal tail, which contains the nuclear localization signal to the inner nuclear membrane (INM) of mGluR5, ΔINM-APEX2, and identified a subset of proteins that were specifically localized to the nuclear fraction of mGluR5. Using siRNA and western blot validation approaches, we confirm the role of these 'bystander' proteins in the differential trafficking of mGluR5 nuclear versus plasma membrane pools. We confirm the role of the coatomer I complex for the retrograde transport of nuclear mGluR5 from the Golgi to the endoplasmic reticulum (ER) and identify casein kinase 2 as an INM-mGluR5-specific kinase. Moreover, we used glycoproteomics to study localization-based differential glycosylation of mGluR5.

References

1. Herculano-Houzel, S. The human brain in numbers: a linearly scaled-up primate brain. Front. Hum. Neurosci. 3, (2009).

2. Kumar, V., Fahey, P. G., Jong, Y.-J. I., Ramanan, N. & O'Malley, K. L. Activation of Intracellular Metabotropic Glutamate Receptor 5 in Striatal Neurons Leads to Up-regulation of Genes Associated with Sustained Synaptic Transmission Including Arc/Arg3.1 Protein. J. Biol. Chem. 287, 5412–5425 (2012).

3. Jong, Y.-J. I., Kumar, V. & O'Malley, K. L. Intracellular Metabotropic Glutamate Receptor 5 (mGluR5) Activates Signaling Cascades Distinct from Cell Surface Counterparts. J. Biol. Chem. 284, 35827–35838 (2009).

4. Jong, Y.-J. I., Sergin, I., Purgert, C. A. & O'Malley, K. L. Location-Dependent Signaling of the Group 1 Metabotropic Glutamate Receptor mGlu5. Mol. Pharmacol. 86, 774–785 (2014).

5. Niswender, C. M. & Conn, P. J. Metabotropic glutamate receptors: physiology, pharmacology, and disease. Annu. Rev. Pharmacol. Toxicol. 50, 295–322 (2010).

6. Purgert, C. A. et al. Intracellular mGluR5 Can Mediate Synaptic Plasticity in the Hippocampus. J. Neurosci. 34, 4589–4598 (2014).

7. Willard, S. S. & Koochekpour, S. Glutamate, Glutamate Receptors, and Downstream Signaling Pathways. Int. J. Biol. Sci. 9, 948–959 (2013).

8. Gladding, C. M., Fitzjohn, S. M. & Molnár, E. Metabotropic Glutamate Receptor-Mediated Long-Term Depression: Molecular Mechanisms. Pharmacol. Rev. 61, 395–412 (2009).

9. D'Antoni, S. et al. Dysregulation of group-I metabotropic glutamate (mGlu) receptor mediated signalling in disorders associated with Intellectual Disability and Autism. Neurosci. Biobehav. Rev. 46, 228–241 (2014).

10. O'Connor, E. C., Bariselli, S. & Bellone, C. Synaptic basis of social dysfunction: a focus on postsynaptic proteins linking group-I mGluRs with AMPARs and NMDARs. Eur. J. Neurosci. 39, 1114–1129 (2014).

11. Jakkamsetti, V. et al. Experience-Induced Arc/Arg3.1 Primes CA1 Pyramidal Neurons for Metabotropic Glutamate Receptor-Dependent Long-Term Synaptic Depression. Neuron 80, 72–79 (2013).

12. Davidkova, G. & Carroll, R. C. Characterization of the role of microtubule-associated protein 1B in metabotropic glutamate receptor-mediated endocytosis of AMPA receptors in hippocampus. J. Neurosci. 27, 13273–13278 (2007).

13. Snyder, E. M. et al. Internalization of ionotropic glutamate receptors in response to mGluR activation. Nat. Neurosci. 4, 1079–1085 (2001).

14. Schaefer, N. et al. The malleable brain: plasticity of neural circuits and behavior - a review from students to students. J. Neurochem. 142, 790–811 (2017).

15. van der Sluijs, P. & Hoogenraad, C. C. New insights in endosomal dynamics and AMPA receptor trafficking. Semin. Cell Dev. Biol. 22, 499–505 (2011).

16. Shepherd, J. D. & Huganir, R. L. The Cell Biology of Synaptic Plasticity: AMPA Receptor Trafficking. Annu. Rev. Cell Dev. Biol. 23, 613–643 (2007).

17. Jong, Y.-J. I., Kumar, V., Kingston, A. E., Romano, C. & O'Malley, K. L. Functional Metabotropic Glutamate Receptors on Nuclei from Brain and Primary Cultured Striatal Neurons. J. Biol. Chem. 280, 30469–30480 (2005).

18. Huang, C.-C., You, J.-L., Wu, M.-Y. & Hsu, K.-S. Rap1-induced p38 Mitogen-activated Protein Kinase Activation Facilitates AMPA Receptor Trafficking via the GDI·Rab5 Complex. J. Biol. Chem. 279, 12286–12292 (2004).

19. Gallagher, S. M., Daly, C. A., Bear, M. F. & Huber, K. M. Extracellular signal-regulated protein kinase activation is required for metabotropic glutamate receptor-dependent long-term depression in hippocampal area CA1. J. Neurosci. 24, 4859–4864 (2004).

20. Heck, A. J. R. Native mass spectrometry: a bridge between interactomics and structural biology. Nat. Methods 5, 927–933 (2008).

21. Cristobal, A. et al. Toward an Optimized Workflow for Middle-Down Proteomics. Anal. Chem. 89, 3318–3325 (2017).

22. Gillet, L. C., Leitner, A. & Aebersold, R. Mass Spectrometry Applied to Bottom-Up Proteomics: Entering the High-Throughput Era for Hypothesis Testing. Annu. Rev. Anal. Chem. 9, 449–472 (2016).

23. Pasing, Y., Colnoe, S. & Hansen, T. Proteomics of hydrophobic samples: Fast, robust and low-cost workflows for clinical approaches. Proteomics 17, 1500462 (2017).

24. de Hoffmann, E. Tandem mass spectrometry: A primer. J. Mass Spectrom. 31, 129–137 (1996).

25. MacNair, J. E., Lewis, K. C. & Jorgenson, J. W. Ultrahigh-Pressure Reversed-Phase Liquid Chromatography in Packed

Capillary Columns. Anal. Chem. 69, 983–989 (1997).
26. Shukla, A. K. & Futrell, J. H. Tandem mass spectrometry: dissociation of ions by collisional activation. J. Mass Spectrom. 35, 1069–1090 (2000).
27. Olsen, J. V et al. Higher-energy C-trap dissociation for peptide modification analysis. Nat. Methods 4, 709–712 (2007).
28. Syka, J. E. P., Coon, J. J., Schroeder, M. J., Shabanowitz, J. & Hunt, D. F. Peptide and protein sequence analysis by electron transfer dissociation mass spectrometry. Proc. Natl. Acad. Sci. 101, 9528–9533 (2004).
29. Frese, C. K. et al. Toward full peptide sequence coverage by dual fragmentation combining electron-transfer and higher-energy collision dissociation tandem mass spectrometry. Anal. Chem. 84, 9668–9673 (2012).
30. Perkins, D. N., Pappin, D. J. C., Creasy, D. M. & Cottrell, J. S. Probability-based protein identification by searching sequence databases using mass spectrometry data. Electrophoresis 20, 3551–3567 (1999).
31. Cox, J. et al. Andromeda: A Peptide Search Engine Integrated into the MaxQuant Environment. J. Proteome Res. 10, 1794–1805 (2011).
32. Jeong, K., Kim, S. & Bandeira, N. False discovery rates in spectral identification. BMC Bioinformatics 13, S2 (2012).
33. Altelaar, A. F. M., Munoz, J. & Heck, A. J. R. Next-generation proteomics: towards an integrative view of proteome dynamics. Nat. Rev. Genet. 14, 35–48 (2013).
34. Stucchi, R. Connecting the neuronal proteome: unraveling protein dynamics in neurons using mass spectrometry-based proteomics. (Utrecht University, 2019).
35. Vandermarliere, E., Mueller, M. & Martens, L. Getting intimate with trypsin, the leading protease in proteomics. Mass Spectrom. Rev. 000–000 (2013).
36. Swaney, D. L., Wenger, C. D. & Coon, J. J. Value of Using Multiple Proteases for Large-Scale Mass Spectrometry-Based Proteomics. J. Proteome Res. 9, 1323–1329 (2010).
37. Eichacker, L. A. et al. Hiding behind Hydrophobicity. J. Biol. Chem. 279, 50915–50922 (2004).
38. Tsiatsiani, L. & Heck, A. J. R. Proteomics beyond trypsin. FEBS J. 282, 2612–2626 (2015).
39. Giansanti, P., Tsiatsiani, L., Low, T. Y. & Heck, A. J. R. Six alternative proteases for mass spectrometry–based proteomics beyond trypsin. Nat. Protoc. 11, 993–1006 (2016).
40. Biringer, R. G. Enhanced sequence coverage of proteins in human cerebrospinal fluid using multiple enzymatic digestion and linear ion trap LC-MS/MS. Briefings Funct. Genomics Proteomics 5, 144–153 (2006).
41. Gauci, S. et al. Lys-N and Trypsin Cover Complementary Parts of the Phosphoproteome in a Refined SCX-Based Approach. Anal. Chem. 81, 4493–4501 (2009).
42. Giansanti, P. et al. An Augmented Multiple-Protease-Based Human Phosphopeptide Atlas. Cell Rep. 11, 1834–1843 (2015).
43. Laarse, S. A. M. et al. Targeting proline in (phospho)proteomics. FEBS J. febs.15190 (2020).
44. Schimmel, P. R. & Flory, P. J. Conformational energies and configurational statistics of copolypeptides containing l-proline. J. Mol. Biol. 34, 105–120 (1968).
45. MacArthur, M. W. & Thornton, J. M. Influence of proline residues on protein conformation. J. Mol. Biol. 218, 397–412 (1991).
46. Vaisar, T. & Urban, J. Probing Proline Effect in CID of Protonated Peptides. J. Mass Spectrom. 31, 1185–1187 (1996).
47. Raulfs, M. D. M. et al. Investigations of the Mechanism of the "Proline Effect" in Tandem Mass Spectrometry Experiments: The "Pipecolic Acid Effect". J. Am. Soc. Mass Spectrom. 25, 1705–1715 (2014).
48. Huo, D., Qin, T. & Zu, L. Energetic switch of the proline effect in collision-induced dissociation of singly and doubly protonated peptide Ala-Ala-Arg-Pro-Ala-Ala. J. Mass Spectrom. 54, 55–65 (2019).
49. Šebela, M. et al. Identification of N-glycosylation in prolyl endoprotease from Aspergillus niger and evaluation of the enzyme for its possible application in proteomics. J. Mass Spectrom. 44, 1587–1595 (2009).
50. Tsiatsiani, L., Akeroyd, M., Olsthoorn, M. & Heck, A. J. R. Aspergillus niger Prolyl Endoprotease for Hydrogen–Deuterium Exchange Mass Spectrometry and Protein Structural Studies. Anal. Chem. 89, 7966–7973 (2017).
51. Schräder, C. U. et al. Neprosin, a Selective Prolyl Endoprotease for Bottom-up Proteomics and Histone Mapping. Mol. Cell. Proteomics 16, 1162–1171 (2017).
52. Chen, X., Wu, D., Zhao, Y., Wong, B. H. C. & Guo, L. Increasing phosphoproteome coverage and identification of phosphorylation motifs through combination of different HPLC fractionation methods. J. Chromatogr. B 879, 25–34 (2011).
53. Aebersold, R. & Mann, M. Mass spectrometry-based proteomics. Nature

422, 198–207 (2003).
54. Craft, G. E., Chen, A. & Nairn, A. C. Recent advances in quantitative neuroproteomics. Methods 61, 186–218 (2013).
55. Ong, S.-E. et al. Stable Isotope Labeling by Amino Acids in Cell Culture, SILAC, as a Simple and Accurate Approach to Expression Proteomics. Mol. Cell. Proteomics 1, 376–386 (2002).
56. Zhang, G., Deinhardt, K. & Neubert, T. A. Stable Isotope Labeling by Amino Acids in Cultured Primary Neurons. in 57–64 (2014).
57. Zhang, G., Deinhardt, K., Chao, M. V. & Neubert, T. A. Study of Neurotrophin-3 Signaling in Primary Cultured Neurons using Multiplex Stable Isotope Labeling with Amino Acids in Cell Culture. J. Proteome Res. 10, 2546–2554 (2011).
58. Thompson, A. et al. Tandem Mass Tags: A Novel Quantification Strategy for Comparative Analysis of Complex Protein Mixtures by MS/MS. Anal. Chem. 75, 1895–1904 (2003).
59. Thompson, A. et al. TMTpro: Design, Synthesis, and Initial Evaluation of a Proline-Based Isobaric 16-Plex Tandem Mass Tag Reagent Set. Anal. Chem. acs. analchem.9b04474 (2019).
60. Liu, H., Sadygov, R. G. & Yates, J. R. A Model for Random Sampling and Estimation of Relative Protein Abundance in Shotgun Proteomics. Anal. Chem. 76, 4193–4201 (2004).
61. Cox, J. et al. Accurate Proteome-wide Label-free Quantification by Delayed Normalization and Maximal Peptide Ratio Extraction, Termed MaxLFQ. Mol. Cell. Proteomics 13, 2513–2526 (2014).


1

2

Neuroproteomics of the synapse: subcellular quantification of protein networks and signaling dynamics

Charlotte AGH van Gelder[1,2] and Maarten Altelaar[1,2]

[1]Biomolecular Mass Spectrometry and Proteomics, Bijvoet Center for Biomolecular Research and Utrecht Institute for Pharmaceutical Sciences, Utrecht University, The Netherlands, [2]Netherlands Proteomics Center, The Netherlands

Manuscript accepted for publication
DOI: https://doi.org/10.1016/j.mcpro.2021.100087

Abstract

One of the most fascinating features of the brain is its ability to adapt to its surroundings. Synaptic plasticity, the dynamic mechanism of functional and structural alterations in synaptic strength, is essential for brain functioning and underlies a variety of processes such as learning and memory. While the molecular mechanisms underlying such rapid plasticity are not fully understood, a consensus exists on the important role of proteins. The study of these neuronal proteins using neuroproteomics has increased rapidly in the last decades, and advancements in mass spectrometry-based proteomics have broadened our understanding of neuroplasticity exponentially. In this review, we discuss the trends in mass spectrometry-based neuroproteomics for the study of synaptic protein-protein interactions and protein signaling dynamics, with a focus on sample types, different labeling and enrichment approaches and data analysis and interpretation. We highlight studies from the last five years, with a focus on synapse structure, composition, functioning, or signaling, and finally discuss some recent developments that could further advance the field of neuroproteomics.

Introduction

Synaptic plasticity is defined as the dynamic process of functional and structural alterations in synaptic strength, where long term potentiation (LTP) implies the strengthening, and long-term depression (LTD) the weakening of synaptic transmission. Dendritic spines, which harbor synapses, are highly abundant on forebrain dendrites, such that a single neuron can contain up to 10,000 synapses[2].

The huge dynamic alterations in spine composition demand the possibility of rapid protein synthesis, degradation, and trafficking[3,4]. Given the fact that the distance between the cell body and a spine can be enormous, these processes cannot be solely attributed to the transport from and to cytoplasmic organelle structures. In the last decade, a plethora of evidence has been gathered to support the existence of so-called satellite synapto-dendritic organelles, that would allow for fast and local turnover of proteins (reviewed in [5]). There is overwhelming evidence on the occurrence of local protein synthesis in mature dendrites (reviewed in [6]), and recent efforts have supported the evidence in mature axons (reviewed in [7]). More than 75% of all excitatory and inhibitory presynaptic terminals were found to contain translational machinery, and distinct patterns of protein synthesis were observed in axonal terminals following three different types of synaptic plasticity[8].

The first synaptoneuroproteomics studies date from the early 2000s, when mass spectrometry-based analysis of postsynaptic density (PSD) fractions was explored[9–17]. These studies have revealed thousands of synaptic proteins and have been fundamental for the development of the neuroproteomics field. However, it is of fundamental importance to understand not only how synapses are organized physically, within synapses, but also spatially, between synapses. It is essential to invest in research focusing on brain areas other than classical synapse brain areas like the hippocampus and cerebral cortex. Therefore, efforts have been made to compare PSD compositions of different brain regions and to link their proteome signatures to both anatomical region and embryonic origin[18]. In the last decade, synaptic proteomics studies have increased significantly, and have contributed to the understanding of brain function, development, and disease states, including a variety of mental disorders (reviewed in [19–22]).

In this review, we highlight the trends in mass spectrometry-based neuroproteomics based on studies from the last five years focussing on synapse structure, composition, functioning, or signaling. We describe several types of sample material and their possible applications, advantages, and drawbacks. Next, we discuss isolation techniques to distinct different cell types, such as astrocytes or specific types of neurons, and for the enrichment of subcellular fractions. We provide an overview of proteomics techniques to study protein-protein interactions, protein synthesis and degradation, and protein signaling dynamics, with a focus on live cell proximity labeling approaches and the use of bio-orthogonal labeling approaches. Finally, we discuss recent developments in the study of proteins and in their analysis by mass spectrometry that could further advance the field of neuroproteomics.

Neuroproteomics

Sample material

In neuroproteomics experiments, the nature of the sample material inherently poses challenges for standard proteomics workflows. Limitations such as low sample amount caused by the use of terminally differentiated, non-dividing cells, and the heterogeneity in cell types have delayed the development of the neuroproteomics field. While earlier studies were mostly performed on brain homogenates, increased sensitivity of mass spectrometers resulted in a shift towards the use of tissue from specific brain regions, and more recently towards more defined and homogeneous primary cultures (Figure 1A). The most represented organisms in neuroproteomics studies are rat and mouse (Figure 1B). Studies of the early 2000s predominantly used rat brain homogenates, as these possess a larger brain mass. Over the years, a slight shift towards mouse models can be observed, which can be correlated to the increase in studies utilizing genetically modified samples. In the last five years, however, primary neuronal cultures derived from rat are increasingly used. Interestingly, the relative contribution of most studied brain regions, the hippocampus and the cortex, has not changed much in the last decades (Figure 1C).

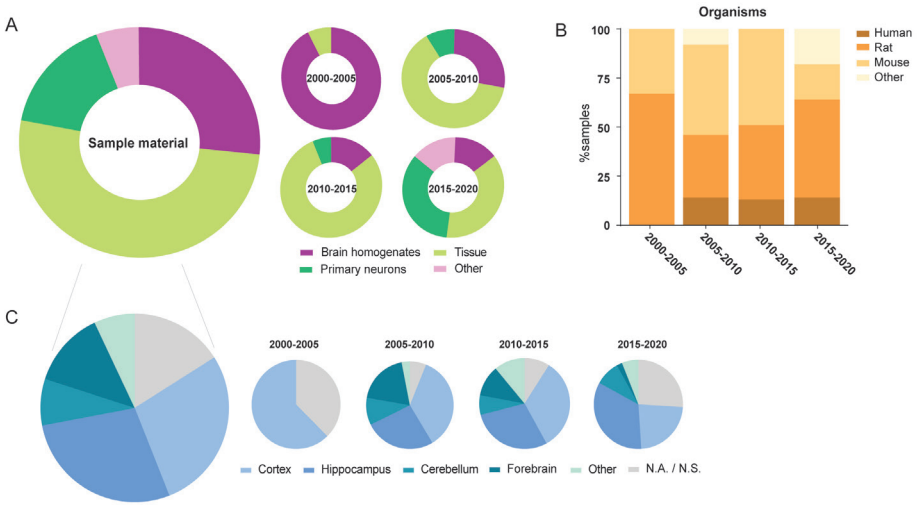

Figure 1. Sample characteristics in neuroproteomics studies of the synapse. **(A)** Contribution of different sample materials. While earlier studies were mostly performed on brain homogenates, increase in sensitivity of mass spectrometers resulted in a shift towards the use of tissue from specific brain regions, and more recently towards more defined and homogeneous primary cultures. **(B)** The most represented organisms in neuroproteomics studies are rat and mouse. While both brain homogenates and primary neurons are predominantly derived from rat, largely due to their larger brain size, genetically modified samples are often derived from mice. **(C)** The distribution of most studied brain regions has not significantly changed during the last decades.

Postmortem and surgical tissue

Human brain samples originate either from neurosurgical biopsies[23,24] or post mortem material[25–27] and are the preferred material source when studying

the molecular fundaments in diseases with an unknown genetic origin. Postmortem material can be matched on sex, age, and several other characteristics, but cannot always be controlled for genetic background, history of drug use, and comorbidity, increasing heterogeneity and thereby complicating data interpretation. Moreover, standardization of sample preservation remains challenging. With average response times of 4 to 7 hours postmortem, protein modification and degradation are expected. While this is less of a concern in surgically obtained material, where samples are dissected, classified into healthy or diseased tissue by an expert, and then snap frozen to guarantee tissue stability, tissue heterogeneity remains an issue. Data interpretation could potentially be aided by the use of internal controls, where diseased and non-diseased tissue from the same patient is compared.

Neurocytometry

One technique with high potential to differentiate between different brain cell populations is fluorescence-activated cell sorting (FACS). Although widely applied to many different cell types, FACS in brain samples, the field of neurocytometry, has been of limited use[28]. This was mainly caused by the need for genetic labeling of cell types[29], difficulties in generation single-cell suspensions, and the lack of cell type-specific markers. For (synapto)proteomics purposes, the main limitation remains cell integrity during dissociation, where cell protrusions are not preserved, and even cell bodies are commonly distorted to the point where many cytoplasmic proteins are lost and the main cell body consists of the nucleus[30]. Moreover, common practice in human brain preservation includes formalin fixation or flash freezing of tissue, both of which are incompatible with FACS. Recently published protocols, however, demonstrate functional neurocytometry for separation of different neuron types following fixation, with preservation of cytoplasmic proteins, and while maintaining RNA integrity[28]. Other examples include Fluorescence-Activated Synaptosome Sorting (FASS), where mice are genetically modified with fluorescent glutamatergic synapses, enabling sorting of synaptosomes with a resealed presynaptic terminal and a PSD[31]. These advances give promise to the use of neurocytometry in neuroproteomics in the future.

Laser capture microdissection

Another possibility for the isolation of specific brain cells is laser capture microdissection (LCM), in which a selection of a tissue of interest is excised using a UV or IF laser, and captured in a collection tube. Advantages of LCM include the use of a wide variety of tissue preparations, its accurate separation of an extremely small number of cells, and even single-cell isolation. However, it is extremely time-consuming and relatively expensive[32]. Its advantages over whole tissue lysate analysis in proteomics studies are increased feature identification, increased peptide identification, and subsequent higher protein identifications and a decrease in missing values[33]. Several studies have shown the use of LCM in combination with LC-MS/MS to study brain tissue abnormalities[34,35].

Cultured primary neurons
One of the major advantages of culturing primary rat or mouse neuronal cells in vitro is that they synchronize prior to differentiation. This makes them very suitable for use in system-wide analyses, such as proteomics studies. Different stages of neuronal development, including axonal outgrowth, dendritogenesis, and ultimately the formation of synapses, can be followed in culture[36].

Induced pluripotent stem cells
In the last decade, tremendous progress has been made in the use of induced pluripotent stem cells (iPSCs)-derived neurons, allowing for cue-specific differentiation into dopaminergic[37,38], serotonergic[39], and glutamatergic[40] neurons; several types of motor neurons were created[41], as well as cortical neurons[42], and various types of glial cells[43,44]. A major limitation in the use of these induced neurons was the representation of brain developmental state, where iPSC-derived neurons often reflect very early developmental stages[45]. This problem was partially solved by protocols using small molecule cues for stepwise differentiation, allowing for the creation of phenotypically more developed neurons, characterized by processes such as synaptogenesis[46]. In recent years, it has become possible to model synaptogenesis and synapse function in several diseases using iPSC-derived neurons (reviewed in [47]).

Species and sex-specificity
Differences in synaptic protein profiles have been observed in a study comparing isolated synaptosomes from hippocampi of four different species. Two rodent proteomes, rat and mouse, and two primate proteomes, marmoset and human, were compared using sequential window acquisition of all theoretical fragment ion spectra (SWATH) mass spectrometry[48]. The most striking differences were observed between rodent and human, and between marmoset and human, while less variance in expression was observed between the two rodent species. Statistical analyses of a predefined set of plasticity-related proteins between the four species showed that especially proteins involved in endocytosis, ionotropic glutamate receptors, and auxiliary subunits were significantly lower expressed in humans compared to the other three species. In contrast, components of the extracellular matrix were higher expressed in humans. Recent findings by Sowers *et al*. indicate that also in synaptic disorders, differences can be observed between sexes. Using label-free quantification (LFQ) quantification of hippocampal slices, they showed that in an FGF14-/- mouse model, the proteomic alterations were mainly sex-specific and that the male proteome could be matched to readily available GWAS data[49].

Cell surface proteins
Over the past two decades, neuroproteomics has provided an incredible amount of data resulting in many new biological insights into the composition and functioning of synapses. However, the majority of studies have focused on intracellular proteins, or the intracellular interactome of transmembrane receptors, leaving cell surface proteins (CSPs) vastly underrepresented. CSPs pose several challenges for the classical proteomics workflows for a number of reasons, including their extensive posttranslational modification patterns, and solubility in standard buffers, which mostly holds for transmembrane

proteins. Secreted proteins add an extra challenge, as they require additional recovery steps (such as collection of cell culture media) and are often contaminated with proteins from different sources.
Interestingly, recent studies employing single-cell sequencing strategies have discovered that different neuronal cell types present a unique set of cell-surface protein combinations. The landscape of proteins present on pre- and postsynaptic membranes, in the extracellular matrix, on glial membranes, as well as secreted proteins, result in the formation of different types of synaptic connections (as reviewed in [50,51]). This notion is especially of interest in the study of connectivity between neurons and more generally the organization of the nervous system, as CSP patterning could hold key information on how and where two brain cells connect.

This was demonstrated in a recent paper by Apostolo *et al*[52]. In this study, mossy fiber synaptosomes were isolated via sucrose gradient centrifugation, making use of the mossy fiber characteristically large size, where a large presynaptic bouton engulfs a series of postsynaptic densities or multi-headed dendritic spines. Analysis of synaptosomes from these mossy fiber microcircuits led to the discovery of more than 75 potential cell surface proteins, most of which (almost 80%) were not previously reported to be localized or functional at the mossy fiber synapse, or any synapse, before. Moreover, the authors were also able to identify over 25 protein-protein interaction pairs among the newly identified CSP using a pairwise high-throughput interaction screen using an enzyme-linked immunosorbent assay (ELISA)-based assay, yielding 38 interaction pairs, of which 10 were not reported before. To achieve this, the extracellular domain of all 73 potential CSPs were fused to alkaline phosphatase or the Fc region of IgG1, and all potential combinations of protein-protein pairs were tested. Following a variety of validation experiments, IgSF8 was identified as a key regulator of the hippocampal CA3 microcircuit, emphasizing the importance of the inclusion of cell surface proteins in neuroproteomics studies.

Contribution of glia in synapse functioning
An important consideration in the data analysis and interpretation of neuroproteomics data is that the obtained information is derived from a mixture of different cell types. Most sample material is in fact comprised of a mix of neuronal cell types and several types of glia, being astrocytes, oligodendrocytes, and microglia. Glia were previously thought to serve merely as a supportive network for neuronal stability and functioning. However, exponential increase in the study of glial cells has highlighted pivotal roles of glia in nervous system development and in the maintenance of homeostasis by for instance the removal of dead neurons and pathogens[53]. A plethora of experimental evidence now supports a pivotal role for glia in synapse formation and functioning. This was corroborated by the introduction of the 'tripartite synapse', where glia are now considered an integral part of the synapse, next to the pre- and postsynaptic parts of the neuron[54]. The relevance of including glia in synapse proteomics studies was emphasized in a recent report where transcriptomic and proteomic data was combined to study the effect of the genetic duplication syndrome Dup15q in Drosophila, which often results in the development of pharmacoresistant epilepsy. In this study, the gene of interest was solely overexpressed in glia, and not

in neurons. Interestingly, the combined analysis of transcriptomic and proteomics data showed downregulation of proteins that regulate synaptic transmission, including neurotransmitter secretion proteins[55]. Another study showed that the neuronal cell adhesion molecule (NRCAM), expressed in astrocytes, interacts with its neuronal counterpart transcellularly, Moreover, loss of astrocytic NRCAM significantly decreased inhibitory synapses and functioning[56]. These examples highlight the necessity of including glia in proteomics analysis of synapse formation and functioning. Current limitations in cell type-specific analyses have limited the number of 'glioproteomics' studies but will most likely gain tremendously by utilizing the combination of sophisticated genetic models and proximity-based proteomics profiling (discussed further on in this review).

In summary, the ideal sample for neuroproteomics studies consists of a single neuronal or glial cell type, as this removes uncertainty of the relative contribution of different cellular origins of proteins of interest that is common on brain lysates, tissue, and to a lesser extent primary neurons. Genetic labeling of specific cell types and subsequent isolation is the most suitable approach to this aim, but lack of cell type-specific labels and low amounts of sample material limit their use. iPSC-derived neurons can be cultured on demand and have the advantage of a specific and human genetic background, and can be labeled, but lack the representation of real life neuronal and glial networks. The fast-developing field of organoid technologies will likely lead towards the creation of the ideal proteomics sample material, as these contain all of the mentioned characteristics of the ideal neuroproteomics sample.

Deciphering protein-protein interactions in protein networks

The subtle changes in protein expression and their recruitment to specific compartments in dendritic spines requires a reduction in sample complexity for specific changes in the synapse to be distinguished from background processes in the cell body. Several strategies exist for the fractionation of sample material to reduce complexity and fractionation is employed in more than 60% of all published proteomics studies focusing on the synapse. Synaptic fractions of synaptosomes, PSD, and the cytomatrix of the active zone can be obtained by Percoll or sucrose gradient centrifugation steps in well-described protocols[1]. Although these protocols allow for in-depth characterization of these specific cellular components, information on inter-compartmental interactions, such as filamentous actin remodeling in dendritic spines, is lost. Moreover, a recent study comparing different synaptosomes preparation protocols revealed considerable variability in synaptosome purity and types of contamination[57]. It is therefore recommended to thoroughly examine the most appropriate isolation technique for each proteomics study. A commonly used practice in the study of axonal proteomes is the use of compartmentalized chambers that separate axons from the cell body, allowing the study of the axonal proteome[58–60]. Figure 2 illustrates the most commonly studied subcellular structures. Such studies are still limited because of the need for robust purification strategies, which are not available for the majority of subcellular structures.

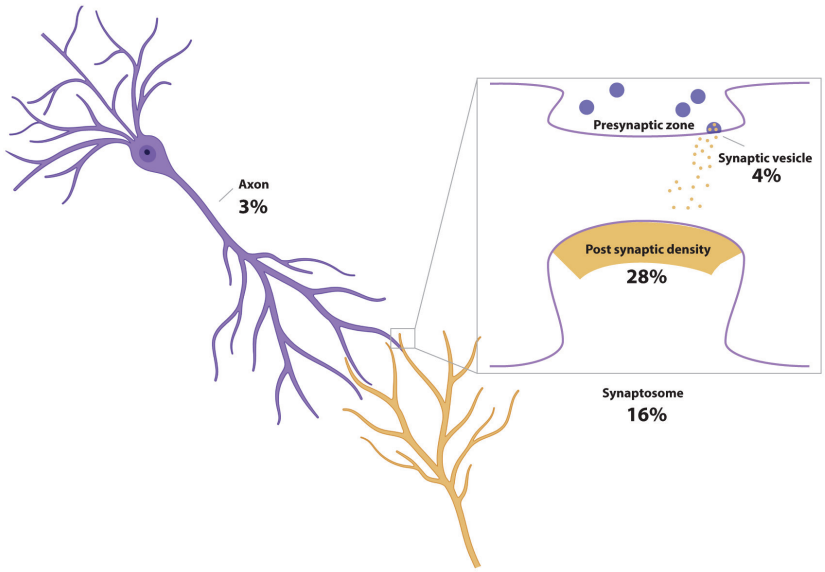

Figure 2. The relative contribution of specific cellular compartments in studies utilizing subcellular fractionation techniques. Percentages reflect the relative contribution of each subcellular fraction to all published studies. In total, 51% of all neuroproteomics studies that were included in this review make use of subcellular fractions.

Affinity purification mass spectrometry

Additional sample preparation steps are required when analyzing protein-protein interactions (PPIs) since classical proteomics workflows do not yield information on the interaction partners of the protein at the time of lysis. Furthermore, PPIs can be dynamic and transient, and therefore call for the use of tailored enrichment methods. When antibodies are available, enrichment can be achieved in near-physiological conditions, making it a popular workflow for the study of protein complexes[61]. Affinity Purification-Mass Spectrometry (AP-MS) experiments can be performed with immobilized antibodies, proteins, peptides, or ligands to isolate protein complexes.

Using antibodies, several postsynaptic complexes have been investigated, including several AMPA receptor subunits[62,63], native AMPA receptor complexes[64], NMDA receptor subunits[62,65], and PSD95[66]. Immunoprecipitation of mGluR1 and mGluR5 in mouse hippocampal and cortical lysates showed that in both regions, mGluR1/5 engage in direct interaction on the postsynapse[67]. An overview of proteomics analyses of postsynaptic protein complexes in relation to neuronal plasticity can be found in[68,69].

Although traditionally less well studied, several efforts have recently been made to elucidate inhibitory synapse complexes. Using AP-MS from transgenic mice with a tagged $GABA_A$ receptor γ2 subunit, Ge *et al* identified and characterized $GABA_A$ receptor-associated proteins that are involved in regulation of surface expression and inhibitory homeostatic plasticity, such as Cleft lip and palate transmembrane protein 1 (Clptm1)[70,71]. Another recent AP-MS study in C. Elegans identified the O-GlcNAc transferase OGT-1 to be an important cofactor in GABA neuron function[72].

For transient and weak interactions, however, detection is limited to classical approaches. Elegant solutions for these technical limitations are the proximity-based labeling approaches.

Proximity labeling approaches

Several proximity-based labeling methods have been developed in recent years that can be used to map any (membrane-bound) micro-domain of a cell. These methods are based on the fusion of a protein of interest to enzymes that can generate a reactive protein label, most commonly biotin, in living cells[73]. These protein labels can subsequently be used for isolation of protein complexes or molecular 'environments' of the protein of interest, for instance with streptavidin-coated beads, and their use in neuroproteomics studies is increasing (Figure 3A).

The most commonly employed proximity-dependent protein biotinylation methods are horseradish peroxidase (HRP), proximity-dependent biotin identification (BioID) and the more recently developed successor TurboID, and the engineered ascorbate peroxidase (APEX). Because the labeling radius of these enzymes is limited (around 10 nm), they can be very suitable to map the population of proteins within a specific structure, as well as their spatial distribution[73]. In BioID, a promiscuous biotin ligase is fused to a distinct subcellular compartment by fusion with a strong targeting motif, which labels proximal proteins in a couple of hours after the addition of a high concentration of biotin[74]. Using in vivo BioID (iBioID), researchers have accomplished in vivo biotinylation of both excitatory and inhibitory synaptic protein complexes in mouse brain[75]. As biotinylation occurred in a native environment, many notoriously difficult proteins, such as membrane proteins, could be identified. TurboID is the result of the directed evolution of BioID's BirA enzyme, decreasing labeling time to 10 minutes[76]. Both peroxidase-based approaches, HRP and APEX, require incubation with a biotin-arylazide such as biotin-phenol and subsequent labeling initiation by addition of H_2O_2. The peroxidase creates a phenoxyl radical with the possibility to covalently tag proximal proteins at electron-rich amino acid side chains, such as tyrosine[77–79]. To be considered, however, is the toxicity of H_2O_2 for living cells. Because the reactive intermediate's half-life in this reaction is much shorter than in BioID approaches, the biotinylation reaction is much faster, and a smaller, more accurate, labeling radius is created. This increase in sensitivity allows to make 'snapshots' of protein interactions over time, so that protein dynamic interactions, as well as cellular localization of the protein of interest, can be deduced[80,81]. APEX labeling of a-synuclein in cortical neurons led to the identification of mRNA translation, endocytosis, and synaptic transmission proteins, indicating that alterations of these pathways in Parkinson's disease could be directly related to a-synuclein spatial localization[82].

For the labeling of extracellular compartments such as synaptic clefts, HRP-fusion constructs, which cannot be used in many intracellular compartments because of their reducing environments, were designed. Using a cell membrane-impermeable biotin phenol conjugation, proteomes of both excitatory glutamatergic, and inhibitory GABAergic synaptic clefts were created[80,83]. A split horseradish peroxidase (sHRP) was created to study

intercellular protein-protein interactions, in which two inactive HRP-fusion constructs are activated upon co-localization of their fusion proteins. Fusion to pre-synaptically localized neurexin, in combination with post-synaptic neuroligin then allowed for synapse detection between two predefined sets of neurons, as demonstrated in vivo in mouse retinal ganglion cells[84]. The labeling of transcellular protein interactions was enabled with the development of Split-TurboID, in which N- and C-terminal TurboID fragments were directed to the extracellular surface of neurons and astrocytes, respectively. When in close proximity, enzymatic activity is recovered and biotinylation of proximity proteins occurs. Interestingly, this approach was applied in living mouse cortex, after local biotin injection[56].

Taken together, proximity-labeling approaches have been embraced by the proteomics community as the new standard for the study of PPIs, as compared to antibody-based affinity approaches. Figure 3B contains an overview of the most commonly employed proximity labeling constructs. However, several limitations have to be taken into consideration. As the construct needs to be inserted into cells, the bait protein is not the endogenous protein, but the fused protein of interest and the enzyme. Transfection protocols need to be optimized to ensure both transfection efficiency, and levels of protein of interest, so that it is comparable to 'native' conditions. Moreover, during construct development, one has to keep in mind that the enzyme placement does not interfere with protein functionality and localization.

Crosslinking mass spectrometry

For the study of protein complexes, chemical cross-linking mass spectrometry (XL-MS) has emerged as a powerful addition to classical AP-MS experiments. In XL-MS experiments, two proximate amino acid residues, most often lysine, are covalently bound by a cross-linking molecule. This crosslinker typically consists of two functionally reactive groups, separated by a spacer. Cross-linked residues are identified via mass spectrometry, and a distance-constraint is determined. The distance-constraint is determined via the sum of the length of the spacer arm, and the side chains of the amino acid residues[85,86]. The resulting crosslink data contains information on both intra- and inter protein interactions, where cross-linked residues originated from the same, or from different proteins, respectively. XL-MS is therefore very suitable to reveal detailed information on PPIs, and yields additional information on the structure of a protein and protein complexes. However, most crosslinking reagents are not cell-permeable, limiting the use of XL-MS to cell lysates for the time being. Using XL-MS, an elaborate interaction atlas of more than 2,000 proteins was made of the mouse synapse, using pooled microsome and synaptosomal fractions of hippocampal and cerebellar tissue. Next to extensive information on PPI, the obtained datasets were used to elucidate specific PPI interaction sites of SNARE proteins, to model the auxiliary AMPAR interaction complex, and to model conformational changes of specific kinase domains[87].

Elucidation of protein complexes in the synapse at spatiotemporal resolution is essential in the journey towards single-synapse proteomic profiling, which was emphasized by the creation of the Mouse Lifespan Synaptome Atlas[88].

Here, a tremendous effort was made to characterize single-synapse compositions of excitatory synapses in more than 100 brain regions in the developing mouse brain, resulting in a publicly available brain-wide atlas of synaptosomes. The atlas was created combing a semi-automated imaging platform of two fluorescently-labeled constituents of multiprotein scaffolding complexes, PSD95 and SAP102, the localization of which led to the classification of 37 subtypes of excitatory synapses[88,89].

Protein synthesis and turn-over dynamics

Bio-orthogonal labeling approaches

The study of dynamic protein expression was aided significantly by the introduction of bio-orthogonal labeling approaches, in which cell culture media is supplemented with unnatural amino acids. These can have heavy labeled carbon and/or nitrogen, such as in Stable Isotope Labeling of Amino acids in Cell culture (SILAC), or are modified with an azide or alkyne moiety, such as Azide Homo Alanine (AHA). Incorporation of AHA in newly synthesized proteins then enables for click-chemistry based enrichment upon lysis, followed by identification and relative quantification of differential protein expression (Figure 3C). The combination with (pulse) SILAC labeling adds an additional layer of confidence on the observation of truly newly synthesized proteins. The use of such bio-orthogonal labeling approaches in living cells or organisms is increasing (Figure 3A) and are especially interesting in synapse proteomics studies where perturbations in protein expression are thought to be small. Advantages of heavy isotope labeling include the possibility to pool multiple samples into one mass spectrometry measurement, while click-chemistry based approaches enable enrichment of proteins of interest, which aids identification of low abundant proteins and allows for the use of smaller sample amounts. Potential hurdles in the use of these labeling approaches include low metabolic flux in terminally differentiated cells, generally leading to reduced labeling efficiency[90,91]. Moreover, depletion of amino acid storage by complete media change is not recommended because of the pivotal role of secreted factors such as neurotransmitters in neuronal health. For the use of short pulse experiments, however, these can be overcome by a competitively high addition of the non-canonical amino acid in preconditioned media. Moreover, mathematical models have been proposed to normalize for discrepancies in labeling efficiency[92]. Since the spatial distribution of methionine does not allow for all tryptic peptides to contain an AHA upon metabolic labeling experiments, extra control conditions such as methionine controls are recommended for increased confidence. The combination pulse of SILAC and AHA allows for the enrichment of labeled proteins and relative quantification of enriched proteins via the heavy labeled n-terminal arginine or lysine present on all tryptic peptides and is therefore often employed. While most studies have relied on label-free quantification approaches (62%), the use of SILAC and isobaric mass tags such as TMT has increased in popularity (Figure 3D). This increase in popularity can mostly be attributed to the possibility of multiplexing of up to sixteen samples in one mass spectrometry measurement, thereby significantly decreasing analysis time. Another advantage of labeling lies in quantification, as the creation of a pooled reference sample that is spiked in each separate sample mix allows for correction of shifts in retention time

and relative intensities. However, the addition of labeling reagents requires additional sample preparation steps, which increases sample variability. Moreover, the number of samples that can be multiplexed are still limited, which creates boundaries in experimental design. Advancements in both the stability of analysis tools, as well as in data analysis software, have increased the confidence in label free quantification strategies.

A potential alternative that does not require depletion of culture media is O-propargyl-puromycin (OPP); an alkyne analog of puromycin. Puromycin, an aminonucleoside antibiotic and structural analog of an aminoacyl-tRNA, blocks protein synthesis via the formation of a non-hydrolyzable peptide bond in the elongating peptide. This terminates protein elongation and produces truncated, puromycin-modified, peptides that with the use of OPP can be enriched and analyzed using mass spectrometry. This approach, called SUnSET[93], was successfully applied ex vivo in axons to identify mTOR-initiated local protein synthesis after nerve injury[94]. Although SUnSET was shown to not interfere with protein synthesis rate[93], one has to keep in mind that the labeled products are in fact not functional proteins, but rather truncated peptides, which very likely affects cell homeostasis and cellular functioning.

In a recent study on the role of protein phosphorylation and translation during the induction and maintenance of mGluR5-induced LTD in hippocampal neurons, short pulses of AHA were used to identify more than 200 newly synthesized proteins[95]. In another study, AHA was used to study protein synthesis during a 24-hour synaptic scaling experiment. Hippocampal neurons were stimulated with either a Na^+ channel antagonist for 24 hours or a $GABA_A$ receptor antagonist, to increase or decrease miniature excitatory postsynaptic current amplitude, respectively. Approximately 300 proteins were found to be differentially regulated, among which proteins involved in excitatory synapses, and glutamate receptor complexes[96]. A follow-up study using biorthogonal non-canonical amino acid tagging (BONCAT) where a temporal trajectory of the homeostatic scaling response was obtained, showed that there was little overlap in newly synthesized proteins between an early (2 hours) and late (24 hours) time point, although similar general functional processes were regulated, indicating that slight alterations in proteomic composition can affect the duration and polarization of synaptic remodeling[97]. Moreover, stable isotope labeling and pulsed AHA was utilized in cultured glial cells derived from a mouse model of Vanishing White Matter (VWM) to identify protein signaling and metabolic pathways affected by a common Eif2b mutation[98].

Incorporation of bio-orthogonal molecules is not limited to amino acids and could therefore also be employed to study the dynamics of other biomolecules such as sugars and lipids. The addition of heavy labeled or enzymatically modified sugars can be used to monitor glycosylation patterns in neurons[99], and heavy labeled lipids and fatty acids are also readily available.

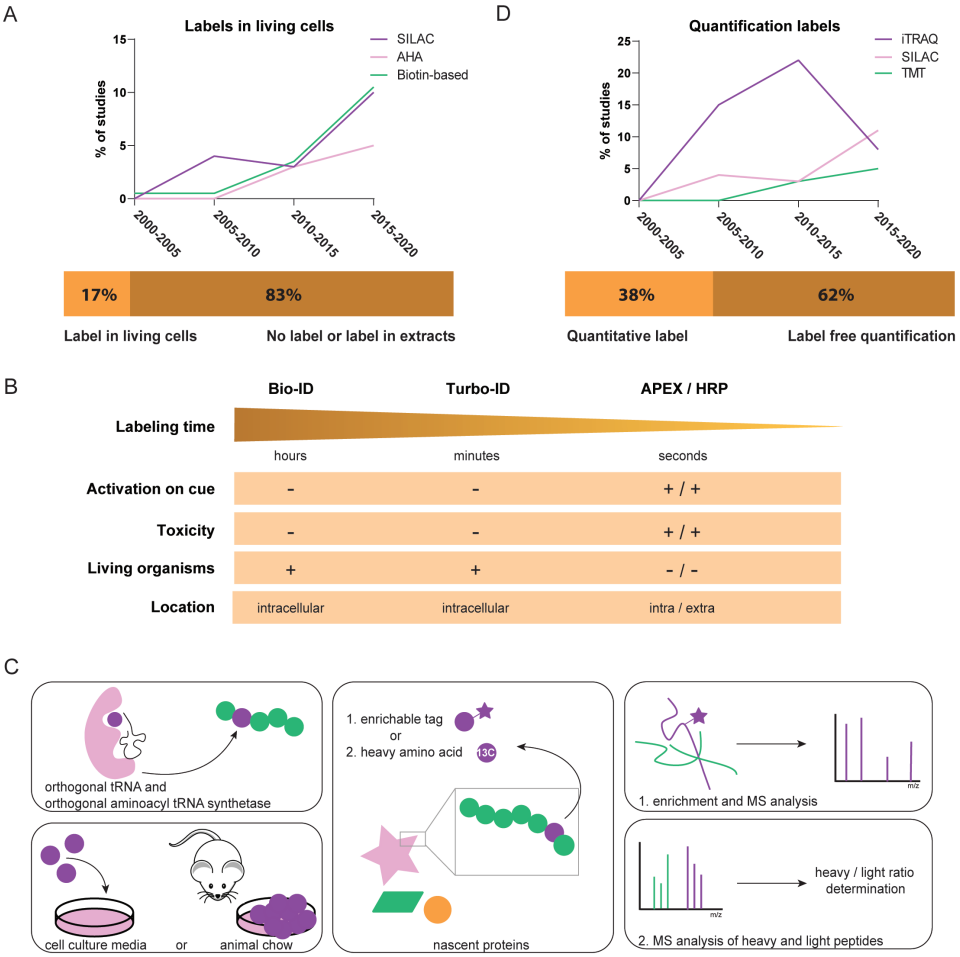

Figure 3. Overview of bio-orthogonal and proximity labeling approaches and prevalence of labels in neuroproteomics studies. **(A)** Prevalence of the use of enrichment labels. In the last decade, an increase in labeling under native conditions (i.e. in living cells or even in living organisms) for labeling of specific cellular structures and/or cellular processes such as protein translation can be observed. **(B)** Characteristics of the most prominently used proximity-labeling constructs. **(C)** Workflow of bio-orthogonal labeling experiments. Unnatural amino acids can be genetically introduced using orthogonal tRNA and an orthogonal aminoacyl tRNA synthetase (upper panel) or supplemented to cell culture media or animal chow. The unnatural amino acid can contain an enrichable tag, or a heavy isotope, so that nascent proteins can either be enriched and subsequently analyzed by mass spectrometry. Alternatively, heavy isotope containing proteins can be analyzed simultaneously with existing, natural proteins, after which the ratio between heavy and light proteins can be determined. **(D)** Prevalence of the use of quantification labels.

Protein degradation

Protein turnover is the net result of the synthesis of nascent proteins and the degradation of mature proteins. This equilibrium does not only allow for the replacement of damaged proteins but has been proven to be essential in dynamic cellular processes, such as synaptic plasticity[100]. The role of ubiquitination and the ubiquitin-proteasome system in synaptic plasticity is reviewed in [101].

The combination of rapid protein turnover and the stability of long-lived synaptic proteins have been shown to be present in both pre- and postsynaptic compartments (reviewed in [102]). Using heavy labeled lysine in mouse chow, followed by a seven-week chase with light labeled lysine, it was recently shown that the majority of heavy-labeled proteins were rapidly degraded in the chase weeks. Cellular fractionation showed that protein turnover is higher in the cytosol compared to synaptosomes. Moreover, protein turnover was activity-dependent, as determined in an enriched environment experiment, in which a group of mice underwent experience-dependent synaptic plasticity[103]. Interestingly, in primary hippocampal cultures, neuronal protein turnover also seems to be influenced by the presence of extracellular matrix compartments, as well as other cell types such as glia. The same study also showed that pre-synaptic proteins tend to have longer half-live than average and that that glutamate receptors exhibit shorter half-lives[104]. Remarkably, inhibition of the proteasome by a variety of proteasome inhibitors does not affect degradation rates of the majority of synaptic proteins, as was determined in cortical neurons where a multiplexed SILAC approach was used to measure protein degradation. This seems to imply that many synaptic proteins are degraded via an alternative route. However, proteasome inhibition did seem to suppress the synthesis of synaptic proteins[105].

Post-translational modifications and protein signaling

The biological functionality of proteins is not solely dependent on their expression levels but can be regulated extensively via more than 100 different post-translational modifications (PTMs). Due to the low stoichiometry of most PTMs, comprehensive analysis requires enrichment steps before mass spectrometric analysis. In the case of phosphorylation, this is often performed using Immobilized Metal Affinity Chromatography (IMAC) approaches in which peptides with a negatively charged phosphogroup are bound to iron. While these strategies typically required milligrams of protein input material, and therefore hampered the analysis of phosphorylation dynamics in precious neuronal samples, recent advances have made it possible to perform sensitive and reproducible enrichment of phosphopeptides with less than 10 µg of protein input material[106]. Adaptations to this protocol have led to the development of a strategy for the identification of mannose-6-phosphate (M6P) modified hydrolases. This very low abundant PTM is critical for the transport of newly synthesized hydrolases from the Golgi apparatus to the lysosome, where they exert their function. Together with selective triggering of the newly identified phosphomannose oxonium fragment marker ions, hundreds of M6P-modified glycopeptides could be identified[107]. While phosphorylation is the most widely studied PTM, other PTMs have gained interest in the last decade (Figure 4A).

Phosphorylation

The first studies on the synaptic phosphoproteome were performed on isolated mouse PSD[108–110], as well as human synaptosomal fractions[111], and identified approximately 300 phosphorylation sites on key synaptic proteins. With the advancements in technology, the number of detected phosphoproteins also increased, enabling the study of activity-dependent phosphorylation

changes, such as the phosphorylation dynamic changes upon naïve and stimulated synaptosomal preparations[112,113], as well as brain-region specific phosphorylation changes[114], and the discovery of a sequence-specific S-Q phosphorylation motif that is regulated during synaptic plasticity[115]. Interestingly, this S-Q phosphoproteome was heavily dependent on $GABA_A$ and NMDA receptor activity, while stimulation of metabotropic glutamate receptors (mGluRs) with DHPG did not influence S-Q phosphorylation. Another recent study performed on primary hippocampal neurons analyzed the phosphorylation dynamics of mGluR-LTD over multiple time points, and quantified over 5,000 phosphorylation sites, mapping important kinases in synaptic plasticity, and identifying new phosphoproteins involved in AMPA receptor trafficking in mGluR-induced LTD[95]. A phosphoproteomics study on neuronal differentiation of SH-SY5Y neuroblastoma cells elegantly showed that upon neuronal differentiation cues, phosphorylation motifs of prominent cell-cycle division kinases were downregulated, while the relative contribution of G protein-coupled receptor kinases (GRKs) and calcium/calmodulin-dependent protein kinase 2 (CaMK2) increased significantly[116]. In the biggest neuronal phosphoproteomics study to date, the (phospho)proteomic effects of in vivo administration of several agonists and antagonists of the kappa opioid receptor (KOR) were studied in four murine brain regions, resulting in the identification and quantification of an astonishing 50,000 phosphorylation sites[117]. The acquired data resulted in the identification of time-dependent, as well as brain region- and stimulus-specific phosphorylation patterns. Another study showed that 30% of the mouse synaptic phosphoproteome showed oscillatory patterns, indicating that phosphorylation of essential synaptic proteins, such as receptors and channels, and especially kinases, are key to essential circadian brain processes such as synaptic excitation and inhibition[118].

Other post-translational modifications

A recent study by Smith *et al* investigated the extent of S-nitrosylation (SNO) in rat cortical neuron nuclear extracts. SNO involves the attachment of a nitric oxide group to cysteine thiol residues. Not only did they identify more than 600 S-nitrosylated proteins, they were also able to generate several lysine-specific SNO motifs, and found that SNO modification of the histone-binding protein RBBP7 was necessary for dendritogenesis[119]. Palmitoylation (or S-acylation), the attachment of the 16-carbon saturated fatty acid palmitate to cysteines, was found to be crucial in neuronal functioning and trafficking of neuronal proteins[120,121]. From all newly identified palmitoylated proteins, many scaffolding and receptor proteins were identified, including NMDA receptor subunits. This is especially interesting since palmitoylation is, like phosphorylation, reversible, and can therefore play an important role in receptor trafficking[120]. As discussed previously, protein degradation plays a pivotal role in synapse biology and is therefore particularly interesting to study. Ubiquitination is a notoriously tricky PTM to enrich for MS analysis, since the di-glycine motif that is typically used for enrichment, is not specific and needs to be performed on peptide level, after digestion[110]. Nevertheless, antibody-based enrichment of this motif has led to a considerable amount of key synaptic proteins[122], and significant differences in ubiquitination were observed in Huntington mouse brain samples[123]. In an alternative approach, the BirA enzyme was fused to multiple copies of ubiquitin modified with a

short N-terminal sequence that can be biotinylated. Next, the polyubiquitin is processed into individual ubiquitin molecules by endogenous deubiquitinating enzymes, which then allows this modified ubiquitin to be readily available for target proteins that can now also be biotinylated by BirA. Using this approach, ubiquitinated proteins in Drosophila embryonic and adult neurons were compared, as well as specific targets E3 ligases Parkin and Ube3a[124,125].

Glycosylation is one of the most common and, at the same time, one of the most complex PTMs. Classical challenges in the study of PTMs, such as the need for enrichment, do not apply here. In fact, the high abundance and heterogeneity of the modification is the major hurdle in accurate analysis[126,127]. Recent advancements, such as the extension of the mass range during electron transfer higher-energy collisional dissociation[128], and the use of alternative dissociation strategies such as activated-ion electron transfer dissociation (AI-ETD)[129], have led to a significant increase in N-glycopeptide identification, and N-glycosite profile mapping, respectively. Using a cerebellum-specific knockout mouse for Srd5a3, a gene that is involved in the initiation steps of N-glycosylation, Medina-Cano *et al* discovered that especially highly glycosylated proteins were affected by the mutation, linking high N-glycan multiplicity to neurite outgrowth and axon guidance processes[114].

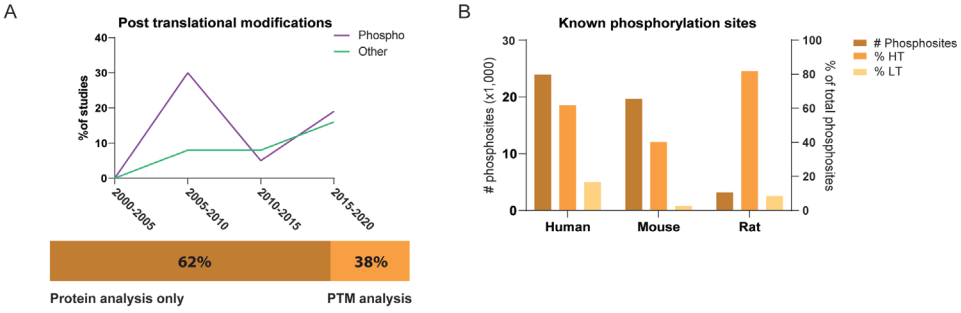

Figure 4. Post-translational modifications in neuroproteomics studies focused on the synapse. **(A)** Only a minority of published studies have analyzed the prevalence of one or more PTMs in their proteomics dataset. While phosphorylation is the most studied PTM, other PTMs such as N-glycosylation and ubiquitination are gaining interest. **(B)** Known phosphorylation sites and supporting evidence from high throughput (HT) and low throughput (LT) studies for the top three used model organisms in neuroproteomics studies. The data used in this graph was taken from the PhosphoSitePlus knowledgebase[134].

PTM interplay

Interestingly, an emerging line of research is focused on the crosstalk, or interplay, of multiple PTMs on a single amino acid residue. Most prominently, a study on the crosstalk between O-GlcNAcylation and phosphorylation on murine synaptosomes found that more than 5% of their identified O-GlcNAcylated serine and threonine residues were also phosphorylated, and protein kinases were prominently enriched, indicating that the crosstalk could be regulating enzymatic activity[130]. A challenge in the study of PTM crosstalk, however, is the necessity of enrichment before mass spectrometric

analysis, limiting the possibility of detecting both PTMs in a single analysis.

Data analysis and interpretation

Databases containing localization of new PTM sites has expanded tremendously with the arrival of large shotgun mass spectrometry experiments and other high throughput analysis methods. With the increase in detectable phosphorylation events, comes the laborious task of data interpretation and validation. Only 5.3% of all identified human phosphorylation sites reported in the PhosphoSitePlus database that have been detected in high throughput studies have a reported function, as determined by low throughput validation studies[131]. Low throughput studies are needed to study the role of these prominently identified phosphorylation sites and to increase the validity of phosphoproteomics analyses. Studies of phosphorylation status increase in complexity through the fact that an increase in phosphorylation does not necessarily mean an increase in activity and vice versa. Even more complicated are phosphorylated proteins or even single peptides with multiple phosphorylation sites.

Since functional PTMs are likely to be evolutionarily conserved between species, it is an often-used criterion for selecting a specific phosphorylation event for further characterization. However, a comparison of PTMs between species can be complicated, since many modification sites are located in disordered regions[132]. Moreover, the rate of identification and functional characterization of phosphorylation sites is not linear across species, as illustrated in Figure 4B. In humans, almost 240,000 phosphosites have a reported function in PhosphoSitePlus, while they only represent 62% and 17% of the total identified phosphosites in high throughput (HT) and low throughput (LT) studies, respectively[133]. Almost 80% fewer phosphosites are reported for rat, the model system most often used in neuroproteomics studies. This makes phosphoproteomics data interpretation and analysis significantly less informative and more laborious since efforts have to be made to translate gene, protein, and phosphorylation site data from human to rat.

The study of multiple PTMs is hampered by the limitations in computational analysis. The immense amount of data that results from a mass spectrometry-based proteomics experiment necessitates automated ways of data analysis and interpretation that goes beyond the annotation of spectra and database searching. Several data repositories have been created, specifically focused on the synaptic proteome, to structure the increasing amount of data[134–136]. A frequently employed strategy during the data interpretation process is the use of gene ontology (GO) enrichment analyses to gain insight into the overrepresentation of genes or proteins in the data set involved in a particular biological process (BP), with a specific molecular function (MF), or present in a defined cellular component (CC). While its use has been helpful in the understanding of several big synaptic datasets[137], the lack of annotation and expert curation of synapse-specific gene and therefore gene products such as proteins, limited its potential and interpretation of results. With the release of SynGO, 'an interactive knowledge base that accumulates available research about synapse biology using GO annotations to novel

ontology terms'[138], more than 1,000 genes with localization or function in the synapse were annotated and expert-curated, improving the interpretation of large synaptic –OMICS datasets. Moreover, analysis tools for integration and interpretation of phosphoproteomics data are being developed to deal with some of these challenges. PhophOrtolog for instance, was developed to map protein modification sites between species[132], and several tools have been developed to aid integration of kinase activation state with known targets and known PPIs (such as INKA[139] and PHOTON[140]), and visualization of dynamics in temporal phosphorylation datasets, such as the Cytoscape plugin PhosphoPath[141].

Computational modeling

Genome-wide association studies (GWAS) have contributed tremendously to the identification of risk genes for many neurological disorders, including psychiatric disorders such as schizophrenia. However, in the majority of cases, these findings did not translate linearly with alterations in the proteome or neuronal phenotypes. Strategies combining several research techniques might contribute to our understanding of these complex, multifactorial diseases. While the combination of RNA sequencing and proteomics is most often employed, it is becoming increasingly clear that these are difficult to integrate and interpret. However, integration of mRNA and proteome datasets can contribute to our understanding of essential brain processes, as was shown in a study where both transcriptome and proteome alterations were followed during normal sleep and high sleep pressure in mice. Both the proteome and transcriptome showed circadian oscillations, but these almost completely abolished in the synaptic proteome during sleep deprivation, while the transcriptome was much less affected[142]. A recently published study by Rosato *et al* employed a different strategy, combining so-called cellomics and proteomics experimental data to investigate neuronal phenotypes of schizophrenia risk genes. To this end, they studied the phenotypic alterations in primary cultured neurons upon knockdown of more than 40 candidate schizophrenia risk genes. They grouped the knock-down induced phenotypes and performed proteomics analysis to identify the molecular pathway underlying the shared risk of these genes, thereby enhancing the understanding of the molecular fingerprint of schizophrenia[143]. Approaches like these can greatly contribute to our knowledge on so-called synaptopathies, a term applied to diseases with synaptic dysregulation (reviewed in [144,145]).

With the exponential increase in proteomics data from a variety of cell types, model systems, modifications, and perturbations that has been generated over the last decades, another challenge has emerged: the integration of these data to not only strengthen the knowledge that has already been gained but also to predict understanding of brain processes and circuitry complexity. Systems biology approaches, where biological data is combined with computational modeling and mathematics, are being developed. In short, more and more layers of complexity are added to the understanding of molecular networks that underlie brain function in both health and disease, as more and more information becomes available. For instance, the first layer exists of the classical neuronal signaling model, only considering the pre- and postsynaptic terminals. A second

layer is created where information from glia cells is included, a third with molecular elements of the extracellular matrix, then the neurovascular unit, the immune system, etcetera. Moreover, on a molecular level, information on expression, interactions, structural organization, and turnover of proteins creates additional layers of information that need to be taken into account. Modular systems biology tries to organize already available data of big datasets, including genomics, epigenomics, transcriptomics, proteomics, metabolomics, and others, into mathematical and computational models to get a more in-depth view of the mechanisms of complex biological processes. These include, but are not limited to, the identification of key pathways, and even predictions of how different modules in a network will respond to perturbations in a system, such as synaptic plasticity. The most recent evidence of the major pathways that should be considered in the development of a modular and computational model of synapse formation and functioning are reviewed in [54].

New techniques

The wide variety of cell types in the brain poses one of the major challenges in the neuroproteomics field. The majority of experimental studies focusing on synapse biology require the use of either brain tissue samples, or cultured primary neurons, which both contain a plethora of different cell types. The possibility of selective enrichment of specifically defined cell populations could significantly aid the neuroproteomics field. A big step forward was made with the introduction of inducible genetic labels. Using a Cre-recombinase system to express a methionyl-tRNA synthetase (MetRS) with an expanded amino acid binding site, researchers are now able to label specific cell types using cell type-specific promotors. MetRS enables the methionine tRNA to be charged with the unnatural azidonorleucine (ANL), which can then be easily enriched using classic click-chemistry methods[146]. In neurons, a similar approach using trans-cyclooct-2-ene (TCO*)-modified L-lysine (TCO*-A) was introduced into different transmembrane AMPAR regulatory proteins (TARPs) to study TARP modulation over AMPA receptors in living neurons using fluorescence microscopy[147]. Similarly, cell type-specific expression of proximity labeling constructs can achieve cell-type-specific labeling of PPIs[148]. It has to be noted, however, that these approaches can only be applied successfully if one can find a cell-type-specific protein to label.

Single-cell proteomics

Processes like LTP or LTD are known to be cell – and even synapse-specific, and the possibility of measuring at single-cell sensitivity could therefore contribute to our understanding of synaptic plasticity on a molecular level. Next to the obvious benefits (less sample material is needed, less variation is expected because of increased homogeneity of the obtained sample material), confidence in the obtained results is expected to increase, since many more biological replicates can be measured. One of the biggest challenges in single-cell proteomics is the detection of proteins that are present in low copy numbers. In addition to instrumental improvements, such as a faster duty cycle, research focuses on decreasing sample complexity by fractionation more extensively before mass spectrometry

analysis. Traditionally, an orthogonal separation is employed offline, before standard online reversed-phase LC-MS/MS, such as high pH or size exclusion chromatography. Alternatively, Choi *et al* have recently developed a near single-cell method with trace-level sensitivity by coupling offline reversed-phase fractionation and capillary electrophoresis mass spectrometry. This approach allowed for the detection of more than 700 protein groups using only 1 ng of protein digest, the equivalent of five neurons[149].

Targeted mass spectrometry

Concerning mass spectrometry analysis, we can see some general trends in the direction of parallel (PRM) and selected reaction monitoring (SRM) types of analysis. Advantages of these targeted assays include increased sensitivity and accuracy as compared to traditional discovery-based methods, where the stochastic selection of ions often leads to incomplete information and a bias towards a subset of proteins [150]. SRM was successfully used to study a subset of synaptic proteins in cerebrospinal fluid (CSF) of Alzheimer's disease patient cohorts, where synaptic proteins were found to be reduced already in preclinical Alzheimer's, preceding clinical symptoms[151]. Alternatively, quantification of synaptic proteins of interest can be improved using parallel reaction monitoring (PRM), as was shown in PSD fractions of WT versus Shank3B cortical tissue[152]. Comparable to SRM, PRM is based on the isolation of a preset precursor ion, after which fragments, or transitions, are measured and used for quantification. However, instead of a triple quadrupole setup, an orbitrap replaces the third quadrupole, and unlike SRM, all transitions of a given precursor ion are scanned, i.e. parallel monitoring of all fragments takes place[153]. Because PRM assays can be performed on the more commonly used Q Exactive mass spectrometers, it is a promising addition to the neuroproteomics toolbox.

In summary, two decades of synapse proteomics research, with the identification of more than 2,000 synapse proteins, tens of thousands of phosphorylation sites, transient and time-resolved information on protein-protein interactions and structures, has significantly increased our knowledge of the molecular composition and functioning of the synapse. Moreover, with the majority of mass spectrometry-based proteomics datasets freely available in data repositories such as ProteomeXchange[154], the neuroscience community has gained a variety of valuable data resources. To advance the field of neuroproteomics further, the combination of spatial and temporal information is essential. Most improvements can be achieved in the experimental steps preceding typical proteomics sample preparation, and begin with the choice of organism, brain region, and sample type. Increased sensitivity of instrumentation has significantly decreased the amount of sample material needed for proteomics analysis. This now allows for the use of single-cell types, such as differentiated iPSCs and primary neuronal cultures, as well as for the enrichment of low abundant proteins and subcellular structures. In the last decade there has been constant improvement in enrichment methods, both in living organisms or cells (such as proximity labeling approaches and non-canonical amino acid), and in sample preparation processes (such as the enrichment of PTMs). Indeed, we can see a clear shift in the use of both of these areas (Table 1), thereby constantly increasing our knowledge of activity- and compartment

dependent protein expression, modification, and interaction profiles in synaptic compartments, and even in cell type-specific synapses.

Table 1. Overview of neuroproteomics studies employing labeling techniques in living systems. N.A. - not applicable, N.S. - not specified.

Labeling technique	Reference	Organism	Sample type	Brain region	Cellular compartment
BioID	[76]	Mouse	Tissue	Hippocampus Cortex	N.A.
	[125]	Fly	Homogenates	N.A.	N.A.
HRP	[84]	Rat	Primary neurons	Cortex	N.A.
	[81]	Rat	Primary neurons	Cortex	N.A.
APEX	[83]	Rat	Primary neurons	Cortex	N.A.
Turbo-ID	[56]	Mouse	Tissue	Cortex	N.A.
SILAC	[105]	Rat	Primary neurons and glia	Hippocampus	N.A.
	[59]	Xenopus Laevis	Cultured eyes	N.A.	Axon
	[60]	Xenopus Laevis	Cultured eyes	N.A.	Axon
	[151]	Rat	Primary neurons	Hippocampus Cortex	N.A.
	[106]	Rat	Primary neurons	Hippocampus	N.A.
AHA	[96]	Rat	Primary neurons	Hippcampus	N.A
	[97]	Rat	Primary neurons	Hippocampus	N.A.
	[98]	Rat	Primary neurons	Hippcampus	N.A.
15N	[152]	Rat	Tissue	Whole brain	Nucleus, ER, cytoplasm, mitochondria
	[153]	Mouse	Tissue	Barrel cortex	Synaptosome
ANL	[143]	Mouse	Tissue or extracts	N.S.	N.S.
FASS	[35]	Mouse	Tissue	Forbrain	Synaptosome

Acknowledgments

We would like to thank Saar van der Laarse for help with the data that was incorporated in Figure 4B.

References

1. Dieterich DC, Kreutz MR. Proteomics of the Synapse – A Quantitative Approach to Neuronal Plasticity. Mol Cell Proteomics. 2016;15(2):368-381.

2. Sorra KE, Harris KM. Overview on the structure, composition, function, development, and plasticity of hippocampal dendritic spines. Hippocampus. 2000;10(5):501-511.

3. Hanus C, Ehlers MD. Secretory outposts for the local processing of membrane cargo in neuronal dendrites. Traffic. 2008;9(9):1437-1445.

4. Hanus C, Schuman EM. Proteostasis in complex dendrites. Nat Rev Neurosci. 2013;14(9):638-648.

5. Nakahata Y, Yasuda R. Plasticity of Spine Structure: Local Signaling, Translation and Cytoskeletal Reorganization. Front Synaptic Neurosci. 2018;10.

6. Glock C, Heumüller M, Schuman EM. mRNA transport & local translation in neurons. Curr Opin Neurobiol. 2017;45:169-177.

7. Biever A, Donlin-Asp PG, Schuman EM. Local translation in neuronal processes. Curr Opin Neurobiol. 2019;57:141-148.

8. Hafner A-S, Donlin-Asp PG, Leitch B, Herzog E, Schuman EM. Local protein synthesis is a ubiquitous feature of neuronal pre- and postsynaptic compartments. Science. 2019;364(6441):eaau3644.

9. Walikonis RS, Jensen ON, Mann M, Provance DW, Mercer JA, Kennedy MB. Identification of proteins in the postsynaptic density fraction by mass spectrometry. J Neurosci. 2000;20(11):4069-4080.

10. Satoh K, Takeuchi M, Oda Y, et al. Identification of activity-regulated proteins in the postsynaptic density fraction. Genes Cells. 2002;7(2):187-197.

11. Jordan BA, Fernholz BD, Boussac M, et al. Identification and verification of novel rodent postsynaptic density proteins. Mol Cell Proteomics. 2004;3(9):857-871.

12. Li KW, Hornshaw MP, Van Der Schors RC, et al. Proteomics analysis of rat brain postsynaptic density. Implications of the diverse protein functional groups for the integration of synaptic physiology. J Biol Chem. 2004;279(2):987-1002.

13. Li K wan, Hornshaw MP, van Minnen J, Smalla K-H, Gundelfinger ED, Smit AB. Organelle proteomics of rat synaptic proteins: correlation-profiling by isotope-coded affinity tagging in conjunction with liquid chromatography-tandem mass spectrometry to reveal post-synaptic density specific proteins. J Proteome Res. 4(3):725-733.

14. Peng J, Kim MJ, Cheng D, Duong DM, Gygi SP, Sheng M. Semiquantitative proteomic analysis of rat forebrain postsynaptic density fractions by mass spectrometry. J Biol Chem. 2004;279(20):21003-21011.

15. Yoshimura Y, Yamauchi Y, Shinkawa T, et al. Molecular constituents of the postsynaptic density fraction revealed by proteomic analysis using multidimensional liquid chromatography-tandem mass spectrometry. J Neurochem. 2004;88(3):759-768.

16. Liu S-H, Cheng H-H, Huang S-Y, Yiu P-C, Chang Y-C. Studying the protein organization of the postsynaptic density by a novel solid phase- and chemical cross-linking-based technology. Mol Cell Proteomics. 2006;5(6):1019-1032.

17. Jordan BA, Fernholz BD, Neubert TA, Ziff EB. New Tricks for an Old Dog: Proteomics of the PSD.; 2006.

18. Roy M, Sorokina O, McLean C, et al. Regional Diversity in the Postsynaptic Proteome of the Mouse Brain. Proteomes. 2018;6(3):31.

19. Ramadan N, Ghazale H, El-Sayyad M, El-Haress M, Kobeissy FH. Neuroproteomics Studies: Challenges and Updates. Methods Mol Biol. 2017;1598:3-19.

20. Reig-Viader R, Sindreu C, Bayés À. Synaptic proteomics as a means to identify the molecular basis of mental illness: Are we getting there? Prog Neuro-Psychopharmacology Biol Psychiatry. 2018;84:353-361.

21. Natividad L, Buczynski M, McClatchy D, Yates J. From Synapse to Function: A Perspective on the Role of Neuroproteomics in Elucidating Mechanisms of Drug Addiction. Proteomes. 2018;6(4):50.

22. Wang Y-Z, Savas J. Uncovering Discrete Synaptic Proteomes to Understand Neurological Disorders. Proteomes. 2018;6(3):30.

23. Bayés À, Collins MO, Croning MDR, van de Lagemaat LN, Choudhary JS,

Grant SGN. Comparative study of human and mouse postsynaptic proteomes finds high compositional conservation and abundance differences for key synaptic proteins. PLoS One. 2012;7(10):e46683.
24. Bayés À, van de Lagemaat LN, Collins MO, et al. Characterization of the proteome, diseases and evolution of the human postsynaptic density. Nat Neurosci. 2011;14(1):19-21.
25. Gong Y, Lippa CF, Zhu J, Lin Q, Rosso AL. Disruption of glutamate receptors at Shank-postsynaptic platform in Alzheimer's disease. Brain Res. 2009;1292:191-198.
26. Sun Y, Dierssen M, Toran N, Pollak DD, Chen W-Q, Lubec G. A gel-based proteomic method reveals several protein pathway abnormalities in fetal Down syndrome brain. J Proteomics. 2011;74(4):547-557.
27. Manavalan A, Mishra M, Feng L, Sze SK, Akatsu H, Heese K. Brain site-specific proteome changes in aging-related dementia. Exp Mol Med. 2013;45:e39.
28. Martin D, Xu J, Porretta C, Nichols CD. Neurocytometry: Flow Cytometric Sorting of Specific Neuronal Populations from Human and Rodent Brain. ACS Chem Neurosci. 2017;8(2):356-367.
29. Lobo MK, Karsten SL, Gray M, Geschwind DH, Yang XW. FACS-array profiling of striatal projection neuron subtypes in juvenile and adult mouse brains. Nat Neurosci. 2006;9(3):443-452.
30. Guez-Barber D, Fanous S, Harvey BK, et al. FACS purification of immunolabeled cell types from adult rat brain. J Neurosci Methods. 2012;203(1):10-18.
31. Biesemann C, Grønborg M, Luquet E, et al. Proteomic screening of glutamatergic mouse brain synaptosomes isolated by fluorescence activated sorting. EMBO J. 2014;33(2):157-170.
32. Chung S, Shen W. Laser capture microdissection: from its principle to applications in research on neurodegeneration. Neural Regen Res. 2015;10(6):897.
33. De Marchi T, Braakman RBH, Stingl C, et al. The advantage of laser-capture microdissection over whole tissue analysis in proteomic profiling studies. Proteomics. 2016;16(10):1474-1485.
34. Hondius DC, Eigenhuis KN, Morrema THJ, et al. Proteomics analysis identifies new markers associated with capillary cerebral amyloid angiopathy in Alzheimer's disease. Acta Neuropathol Commun. 2018;6(1):46.
35. Hondius DC, Hoozemans JJM, Rozemuller AJM, Li KW, Smit AB. A Laser Microdissection–Liquid Chromatography–Tandem Mass Spectrometry Workflow for Post-mortem Analysis of Brain Tissue. In: ; 2018:371-383.
36. Frese CK, Mikhaylova M, Stucchi R, et al. Quantitative Map of Proteome Dynamics during Neuronal Differentiation. Cell Rep. 2017;18(6):1527-1542.
37. Nguyen HN, Byers B, Cord B, et al. LRRK2 Mutant iPSC-Derived DA Neurons Demonstrate Increased Susceptibility to Oxidative Stress. Cell Stem Cell. 2011;8(3):267-280.
38. Byers B, Cord B, Nguyen HN, et al. SNCA Triplication Parkinson's Patient's iPSC-derived DA Neurons Accumulate α-Synuclein and Are Susceptible to Oxidative Stress. Chin W-C, ed. PLoS One. 2011;6(11):e26159.
39. Lu J, Zhong X, Liu H, et al. Generation of serotonin neurons from human pluripotent stem cells. Nat Biotechnol. 2016;34(1):89-94.
40. Liu J, Kościelska KA, Cao Z, et al. Signaling defects in iPSC-derived fragile X premutation neurons. Hum Mol Genet. 2012;21(17):3795-3805.
41. Maury Y, Côme J, Piskorowski RA, et al. Combinatorial analysis of developmental cues efficiently converts human pluripotent stem cells into multiple neuronal subtypes. Nat Biotechnol. 2015;33(1):89-96.
42. Paşca SP, Portmann T, Voineagu I, et al. Using iPSC-derived neurons to uncover cellular phenotypes associated with Timothy syndrome. Nat Med. 2011;17(12):1657-1662.
43. Kondo T, Funayama M, Tsukita K, et al. Focal Transplantation of Human iPSC-Derived Glial-Rich Neural Progenitors Improves Lifespan of ALS Mice. Stem Cell Reports. 2014;3(2):242-249.
44. Wang S, Bates J, Li X, et al. Human iPSC-Derived Oligodendrocyte Progenitor Cells Can Myelinate and Rescue a Mouse Model of Congenital Hypomyelination. Cell Stem Cell. 2013;12(2):252-264.
45. Zhang Y, Pak C, Han Y, et al. Rapid Single-Step Induction of Functional Neurons from Human Pluripotent Stem Cells. Neuron. 2013;78(5):785-798.

46. Varderidou suzy, Verheijen BM, Schätzle P, Hoogenraad CC, Pasterkamp RJ, Altelaar M. Deciphering the protein dynamics of iPSC-derived neurons. J Proteome Res. May 2020:acs.jproteome.0c00070.
47. Habela CW, Song H, Ming G. Modeling synaptogenesis in schizophrenia and autism using human iPSC derived neurons. Mol Cell Neurosci. 2016;73:52-62.
48. Koopmans F, Pandya NJ, Franke SK, et al. Comparative Hippocampal Synaptic Proteomes of Rodents and Primates: Differences in Neuroplasticity-Related Proteins. Front Mol Neurosci. 2018;11.
49. Sowers ML, Re J Di, Wadsworth PA, et al. Sex-Specific Proteomic Changes Induced by Genetic Deletion of Fibroblast Growth Factor 14 (FGF14), a Regulator of Neuronal Ion Channels. Proteomes. 2019;7(1):5.
50. de Wit J, Ghosh A. Specification of synaptic connectivity by cell surface interactions. Nat Rev Neurosci. 2016;17(1):4-4.
51. Apóstolo N, de Wit J. Compartmentalized distributions of neuronal and glial cell-surface proteins pattern the synaptic network. Curr Opin Neurobiol. 2019;57:126-133.
52. Apóstolo N, Smukowski SN, Vanderlinden J, et al. Synapse type-specific proteomic dissection identifies IgSF8 as a hippocampal CA3 microcircuit organizer. Nat Commun. 2020;11(1):5171.
53. Jha MK, Kim J-H, Suk K. Proteome of brain glia: The molecular basis of diverse glial phenotypes. Proteomics. 2014;14(4-5):378-398.
54. De Luca C, Colangelo AM, Virtuoso A, Alberghina L, Papa M. Neurons, Glia, Extracellular Matrix and Neurovascular Unit: A Systems Biology Approach to the Complexity of Synaptic Plasticity in Health and Disease. Int J Mol Sci. 2020;21(4):1539.
55. Hope KA, Johnson D, Miller PW, Lopez-Ferrer D, Kakhniashvili D, Reiter LT. Transcriptomic and proteomic profiling of glial versus neuronal Dube3a overexpression reveals common molecular changes in gliopathic epilepsies. Neurobiol Dis. 2020;141:104879.
56. Takano T, Wallace JT, Baldwin KT, et al. Chemico-genetic discovery of astrocytic control of inhibition in vivo. Nature. 2020;588(7837):296-302.
57. Gulyássy P, Puska G, Györffy BA, et al. Proteomic comparison of different synaptosome preparation procedures. Amino Acids. 2020;52(11-12):1529-1543.
58. Cagnetta R, Wong HH-W, Frese CK, Mallucci GR, Krijgsveld J, Holt CE. Noncanonical Modulation of the eIF2 Pathway Controls an Increase in Local Translation during Neural Wiring. Mol Cell. 2019;73(3):474-489.e5.
59. Cagnetta R, Frese CK, Shigeoka T, Krijgsveld J, Holt CE. Rapid Cue-Specific Remodeling of the Nascent Axonal Proteome. Neuron. 2018;99(1):29-46.e4.
60. Chuang C-F, King C-E, Ho B-W, Chien K-Y, Chang Y-C. Unbiased Proteomic Study of the Axons of Cultured Rat Cortical Neurons. J Proteome Res. 2018;17(5):1953-1966.
61. Altelaar AFM, Munoz J, Heck AJR. Next-generation proteomics: towards an integrative view of proteome dynamics. Nat Rev Genet. 2013;14(1):35-48.
62. Collins MO, Husi H, Yu L, et al. Molecular characterization and comparison of the components and multiprotein complexes in the postsynaptic proteome. J Neurochem. 2006;97 Suppl 1:16-23.
63. Fukata Y, Tzingounis A V, Trinidad JC, et al. Molecular constituents of neuronal AMPA receptors. J Cell Biol. 2005;169(3):399-404.
64. Schwenk J, Harmel N, Brechet A, et al. High-resolution proteomics unravel architecture and molecular diversity of native AMPA receptor complexes. Neuron. 2012;74(4):621-633.
65. Husi H, Ward MA, Choudhary JS, Blackstock WP, Grant SG. Proteomic analysis of NMDA receptor-adhesion protein signaling complexes. Nat Neurosci. 2000;3(7):661-669.
66. Dosemeci A, Makusky AJ, Jankowska-Stephens E, Yang X, Slotta DJ, Markey SP. Composition of the synaptic PSD-95 complex. Mol Cell Proteomics. 2007;6(10):1749-1760.
67. Pandya NJ, Klaassen R V., van der Schors RC, et al. Group 1 metabotropic glutamate receptors 1 and 5 form a protein complex in mouse hippocampus and cortex. Proteomics. 2016;16(20):2698-2705.
68. Baucum AJ. Proteomic Analysis of Postsynaptic Protein Complexes Underlying Neuronal Plasticity. ACS

Chem Neurosci. 2017;8(4):689-701.
69. Park J. Phosphorylation of the AMPAR-TARP Complex in Synaptic Plasticity. Proteomes. 2018;6(4):40.
70. Ge Y, Kang Y, Cassidy RM, et al. Clptm1 Limits Forward Trafficking of GABAA Receptors to Scale Inhibitory Synaptic Strength. Neuron. 2018;97(3):596-610.e8.
71. Noam Y, Tomita S. On the Path from Proteomics to Function: GABAAR Trafficking Takes a Turn. Neuron. 2018;97(3):479-481.
72. Giles AC, Desbois M, Opperman KJ, Tavora R, Maroni MJ, Grill B. A complex containing the O -GlcNAc transferase OGT-1 and the ubiquitin ligase EEL-1 regulates GABA neuron function. J Biol Chem. 2019;294(17):6843-6856.
73. Kim DI, Roux KJ. Filling the Void: Proximity-Based Labeling of Proteins in Living Cells. Trends Cell Biol. 2016;26(11):804-817.
74. Roux KJ, Kim DI, Burke B. BioID: A Screen for Protein-Protein Interactions. In: Current Protocols in Protein Science. Hoboken, NJ, USA: John Wiley & Sons, Inc.; 2013:19.23.1-19.23.14.
75. Uezu A, Kanak DJ, Bradshaw TWA, et al. Identification of an elaborate complex mediating postsynaptic inhibition. Science. 2016;353(6304):1123-1129.
76. Branon TC, Bosch JA, Sanchez AD, et al. Efficient proximity labeling in living cells and organisms with TurboID. Nat Biotechnol. 2018;36(9):880-887.
77. Kotani N, Gu J, Isaji T, Udaka K, Taniguchi N, Honke K. Biochemical visualization of cell surface molecular clustering in living cells. Proc Natl Acad Sci. 2008;105(21):7405-7409.
78. Rhee H-W, Zou P, Udeshi ND, et al. Proteomic Mapping of Mitochondria in Living Cells via Spatially Restricted Enzymatic Tagging. Science (80-). 2013;339(6125):1328-1331.
79. Hung V, Udeshi ND, Lam SS, et al. Spatially resolved proteomic mapping in living cells with the engineered peroxidase APEX2. Nat Protoc. 2016;11(3):456-475.
80. Loh KH, Stawski PS, Draycott AS, et al. Proteomic Analysis of Unbounded Cellular Compartments: Synaptic Clefts. Cell. 2016;166(5):1295-1307.e21.
81. Martell JD, Deerinck TJ, Sancak Y, et al. Engineered ascorbate peroxidase as a genetically encoded reporter for electron microscopy. Nat Biotechnol. 2012;30(11):1143-1148.
82. Chung CY, Khurana V, Yi S, et al. In Situ Peroxidase Labeling and Mass-Spectrometry Connects Alpha-Synuclein Directly to Endocytic Trafficking and mRNA Metabolism in Neurons. Cell Syst. 2017;4(2):242-250.e4.
83. Cijsouw T, Ramsey A, Lam T, Carbone B, Blanpied T, Biederer T. Mapping the Proteome of the Synaptic Cleft through Proximity Labeling Reveals New Cleft Proteins. Proteomes. 2018;6(4):48.
84. Martell JD, Yamagata M, Deerinck TJ, et al. A split horseradish peroxidase for the detection of intercellular protein–protein interactions and sensitive visualization of synapses. Nat Biotechnol. 2016;34(7):774-780.
85. Liu F, Heck AJ. Interrogating the architecture of protein assemblies and protein interaction networks by cross-linking mass spectrometry. Curr Opin Struct Biol. 2015;35:100-108.
86. Klykov O, Steigenberger B, Pektaş S, Fasci D, Heck AJR, Scheltema RA. Efficient and robust proteome-wide approaches for cross-linking mass spectrometry. Nat Protoc. 2018;13(12):2964-2990.
87. Gonzalez-Lozano MA, Koopmans F, Sullivan PF, et al. Stitching the synapse: Cross-linking mass spectrometry into resolving synaptic protein interactions. Sci Adv. 2020;6(8):eaax5783.
88. Cizeron M, Qiu Z, Koniaris B, et al. A brain-wide atlas of synapses across the mouse lifespan. Science. June 2020:eaba3163.
89. Zhu F, Cizeron M, Qiu Z, et al. Architecture of the Mouse Brain Synaptome. Neuron. 2018;99(4):781-799.e10.
90. Spellman DS, Deinhardt K, Darie CC, Chao M V., Neubert TA. Stable Isotopic Labeling by Amino Acids in Cultured Primary Neurons. Mol Cell Proteomics. 2008;7(6):1067-1076.
91. Zhang G, Deinhardt K, Neubert TA. Stable Isotope Labeling by Amino Acids in Cultured Primary Neurons. 2014:57-64.
92. Liao L, Park SK, Xu T, Vanderklish P, Yates JR. Quantitative proteomic analysis of primary neurons reveals diverse changes in synaptic protein content in fmr1 knockout mice. Proc Natl Acad Sci. 2008;105(40):15281-15286.

93. Goodman CA, Hornberger TA. Measuring Protein Synthesis With SUnSET. Exerc Sport Sci Rev. 2013;41(2):107-115.
94. Terenzio M, Koley S, Samra N, et al. Locally translated mTOR controls axonal local translation in nerve injury. Science. 2018;359(6382):1416-1421.
95. van Gelder CAGH, Penning R, Veth T, et al. Temporal quantitative proteomics of mGluR-induced protein translation and phosphorylation in neurons. Mol Cell Proteomics. September 2020:mcp.RA120.002199.
96. Schanzenbacher CT, Sambandan S, Langer JD, Schuman EM. Nascent Proteome Remodeling following Homeostatic Scaling at Hippocampal Synapses. Neuron. 2016;92(2):358-371.
97. Schanzenbächer CT, Langer JD, Schuman EM. Time- and polarity-dependent proteomic changes associated with homeostatic scaling at central synapses. Elife. 2018;7.
98. Wisse LE, Penning R, Zaal EA, et al. Proteomic and Metabolomic Analyses of Vanishing White Matter Mouse Astrocytes Reveal Deregulation of ER Functions. Front Cell Neurosci. 2017;11.
99. Thompson JW, Sorum AW, Hsieh-Wilson LC. Deciphering the Functions of O-GlcNAc Glycosylation in the Brain: The Role of Site-Specific Quantitative O-GlcNAcomics. Biochemistry. 2018;57(27):4010-4018.
100. Klein ME, Castillo PE, Jordan BA. Coordination between Translation and Degradation Regulates Inducibility of mGluR-LTD. Cell Rep. 2015;10:1459-1466.
101. Tsai N-P. Ubiquitin proteasome system-mediated degradation of synaptic proteins: An update from the postsynaptic side. Biochim Biophys Acta - Mol Cell Res. 2014;1843(12):2838-2842.
102. Cohen LD, Ziv NE. Neuronal and synaptic protein lifetimes. Curr Opin Neurobiol. 2019;57:9-16.
103. Heo S, Diering GH, Na CH, et al. Identification of long-lived synaptic proteins by proteomic analysis of synaptosome protein turnover. Proc Natl Acad Sci U S A. 2018;115(16):E3827-E3836.
104. Dörrbaum AR, Kochen L, Langer JD, Schuman EM. Local and global influences on protein turnover in neurons and glia. Elife. 2018;7.
105. Hakim V, Cohen LD, Zuchman R, Ziv T, Ziv NE. The effects of proteasomal inhibition on synaptic proteostasis. EMBO J. 2016;35(20):2238-2262.
106. Post H, Penning R, Fitzpatrick MA, et al. Robust, Sensitive, and Automated Phosphopeptide Enrichment Optimized for Low Sample Amounts Applied to Primary Hippocampal Neurons. J Proteome Res. 2016;16(2):728-737.
107. Čaval T, Zhu J, Tian W, et al. Targeted Analysis of Lysosomal Directed Proteins and Their Sites of Mannose-6-phosphate Modification. Mol Cell Proteomics. 2019;18(1):16-27.
108. Collins MO, Yu L, Coba MP, et al. Proteomic analysis of in vivo phosphorylated synaptic proteins. J Biol Chem. 2005;280(7):5972-5982.
109. Trinidad JC, Thalhammer A, Specht CG, Schoepfer R, Burlingame AL. Phosphorylation state of postsynaptic density proteins. J Neurochem. 2005;92(6):1306-1316.
110. Trinidad JC, Specht CG, Thalhammer A, Schoepfer R, Burlingame AL. Comprehensive identification of phosphorylation sites in postsynaptic density preparations. Mol Cell Proteomics. 2006;5(5):914-922.
111. DeGiorgis JA, Jaffe H, Moreira JE, et al. Phosphoproteomic Analysis of Synaptosomes from Human Cerebral Cortex. J Proteome Res. 2005;4(2):306-315.
112. Munton RP, Tweedie-Cullen R, Livingstone-Zatchej M, et al. Qualitative and quantitative analyses of protein phosphorylation in naive and stimulated mouse synaptosomal preparations. Mol Cell Proteomics. 2007;6(2):283-293.
113. Kolodziej A, Smalla K-H, Richter S, et al. High Resolution Quantitative Synaptic Proteome Profiling of Mouse Brain Regions After Auditory Discrimination Learning. J Vis Exp. 2016;(118).
114. Trinidad JC, Thalhammer A, Specht CG, et al. Quantitative analysis of synaptic phosphorylation and protein expression. Mol Cell Proteomics. 2008;7(4):684-696.
115. Siddoway B, Hou H, Yang H, Petralia R, Xia H. Synaptic activity bidirectionally regulates a novel sequence-specific S-Q phosphoproteome in neurons. J Neurochem. 2014;128(6):841-851.
116. Murillo JR, Goto-Silva L, Sánchez A, Nogueira FCS, Domont GB, Junqueira M. Quantitative proteomic analysis identifies

proteins and pathways related to neuronal development in differentiated SH-SY5Y neuroblastoma cells. EuPA Open Proteomics. 2017;16:1-11.
117. Liu JJ, Sharma K, Zangrandi L, et al. In vivo brain GPCR signaling elucidated by phosphoproteomics. Science. 2018;360(6395):eaao4927.
118. Brüning F, Noya SB, Bange T, et al. Sleep-wake cycles drive daily dynamics of synaptic phosphorylation. Science. 2019;366(6462):eaav3617.
119. Smith JG, Aldous SG, Andreassi C, Cuda G, Gaspari M, Riccio A. Proteomic analysis of S-nitrosylated nuclear proteins in rat cortical neurons. Sci Signal. 2018;11(537):eaar3396.
120. Kang R, Wan J, Arstikaitis P, et al. Neural palmitoyl-proteomics reveals dynamic synaptic palmitoylation. Nature. 2008;456(7224):904-909.
121. Collins MO, Woodley KT, Choudhary JS. Global, site-specific analysis of neuronal protein S-acylation. Sci Rep. 2017;7(1):4683.
122. Na CH, Jones DR, Yang Y, Wang X, Xu Y, Peng J. Synaptic Protein Ubiquitination in Rat Brain Revealed by Antibody-based Ubiquitome Analysis. J Proteome Res. 2012;11(9):4722-4732.
123. Sap KA, Guler AT, Bezstarosti K, et al. Global Proteome and Ubiquitinome Changes in the Soluble and Insoluble Fractions of Q175 Huntington Mice Brains. Mol Cell Proteomics. May 2019:mcp.RA119.001486.
124. Ramirez J, Martinez A, Lectez B, et al. Proteomic Analysis of the Ubiquitin Landscape in the Drosophila Embryonic Nervous System and the Adult Photoreceptor Cells. McCabe BD, ed. PLoS One. 2015;10(10):e0139083.
125. Martinez A, Ramirez J, Osinalde N, Arizmendi JM, Mayor U. Neuronal Proteomic Analysis of the Ubiquitinated Substrates of the Disease-Linked E3 Ligases Parkin and Ube3a. Biomed Res Int. 2018;2018:1-14.
126. Trinidad JC, Schoepfer R, Burlingame AL, Medzihradszky KF. N - and O -Glycosylation in the Murine Synaptosome. Mol Cell Proteomics. 2013;12(12):3474-3488.
127. Medina-Cano D, Ucuncu E, Nguyen LS, et al. High N-glycan multiplicity is critical for neuronal adhesion and sensitizes the developing cerebellum to N-glycosylation defect. Elife. 2018;7.
128. Čaval T, Zhu J, Heck AJR. Simply Extending the Mass Range in Electron Transfer Higher Energy Collisional Dissociation Increases Confidence in N-Glycopeptide Identification. Anal Chem. July 2019:acs.analchem.9b02125.
129. Riley NM, Hebert AS, Westphall MS, Coon JJ. Capturing site-specific heterogeneity with large-scale N-glycoproteome analysis. Nat Commun. 2019;10(1):1311.
130. Trinidad JC, Barkan DT, Gulledge BF, et al. Global Identification and Characterization of Both O -GlcNAcylation and Phosphorylation at the Murine Synapse. Mol Cell Proteomics. 2012;11(8):215-229.
131. Hornbeck P V, Kornhauser JM, Latham V, et al. 15 years of PhosphoSitePlus®: integrating post-translationally modified sites, disease variants and isoforms. Nucleic Acids Res. 2019;47(D1):D433-D441.
132. Chaudhuri R, Sadrieh A, Hoffman NJ, et al. PhosphOrtholog: a web-based tool for cross-species mapping of orthologous protein post-translational modifications. BMC Genomics. 2015;16(1):617.
133. Hornbeck P V., Zhang B, Murray B, Kornhauser JM, Latham V, Skrzypek E. PhosphoSitePlus, 2014: mutations, PTMs and recalibrations. Nucleic Acids Res. 2015;43(D1):D512-D520.
134. Pielot R, Smalla K-H, Müller A, et al. SynProt: A Database for Proteins of Detergent-Resistant Synaptic Protein Preparations. Front Synaptic Neurosci. 2012;4:1.
135. Pirooznia M, Wang T, Avramopoulos D, et al. SynaptomeDB: an ontology-based knowledgebase for synaptic genes. Bioinformatics. 2012;28(6):897-899.
136. von Eichborn J, Dunkel M, Gohlke BO, et al. SynSysNet: integration of experimental data on synaptic protein–protein interactions with drug-target relations. Nucleic Acids Res. 2012;41(D1):D834-D840.
137. Distler U, Schmeisser MJ, Pelosi A, et al. In-depth protein profiling of the postsynaptic density from mouse hippocampus using data-independent acquisition proteomics. Proteomics. 2014;14(21-22):2607-2613.
138. Koopmans F, van Nierop P, Andres-

Alonso M, Byrnes A, Cijsouw T. SynGO: An Evidence-Based, Expert-Curated Knowledge Base for the Synapse. Neuron. 2019;103:1-18.
139. Beekhof R, Alphen C, Henneman AA, et al. INKA, an integrative data analysis pipeline for phosphoproteomic inference of active kinases. Mol Syst Biol. 2019;15(4).
140. Rudolph JD, de Graauw M, van de Water B, Geiger T, Sharan R. Elucidation of Signaling Pathways from Large-Scale Phosphoproteomic Data Using Protein Interaction Networks. Cell Syst. 2016;3(6):585-593.e3.
141. Raaijmakers LM, Giansanti P, Possik PA, et al. PhosphoPath: Visualization of Phosphosite-centric Dynamics in Temporal Molecular Networks. J Proteome Res. 2015;14(10):4332-4341.
142. Noya SB, Colameo D, Brüning F, et al. The forebrain synaptic transcriptome is organized by clocks but its proteome is driven by sleep. Science. 2019;366(6462):eaav2642.
143. Rosato M, Stringer S, Gebuis T, et al. Combined cellomics and proteomics analysis reveals shared neuronal morphology and molecular pathway phenotypes for multiple schizophrenia risk genes. Mol Psychiatry. May 2019.
144. Grant SG. Synaptopathies: diseases of the synaptome. Curr Opin Neurobiol. 2012;22(3):522-529.
145. Lepeta K, Lourenco M V., Schweitzer BC, et al. Synaptopathies: synaptic dysfunction in neurological disorders - A review from students to students. J Neurochem. 2016;138(6):785-805.
146. Alvarez-Castelao B, Schanzenbächer CT, Hanus C, et al. Cell-type-specific metabolic labeling of nascent proteomes in vivo. Nat Biotechnol. 2017;35(12):1196-1201.
147. Bessa-Neto D, Kuhlemann A, Beliu G, et al. Bioorthogonal labeling of transmembrane proteins with non-canonical amino acids allows access to masked epitopes in live neurons. Prepr bioRxiv. 2021.
148. Wilson RS, Nairn AC. Cell-Type-Specific Proteomics: A Neuroscience Perspective. Proteomes. 2018;6(4):51.
149. Choi SB, Lombard-Banek C, Muñoz-LLancao P, Manzini MC, Nemes P. Enhanced Peptide Detection Toward Single-Neuron Proteomics by Reversed-Phase Fractionation Capillary Electrophoresis Mass Spectrometry. J Am Soc Mass Spectrom. 2018;29(5):913-922.
150. Pontes AH, de Sousa M V. Mass Spectrometry-Based Approaches to Understand the Molecular Basis of Memory. Front Chem. 2016;4.
151. Lleó A, Núñez-Llaves R, Alcolea D, et al. Changes in Synaptic Proteins Precede Neurodegeneration Markers in Preclinical Alzheimer's Disease Cerebrospinal Fluid. Mol Cell Proteomics. 2019;18(3):546-560.
152. Wilson R, Rauniyar N, Sakaue F, Lam T, Williams K, Nairn A. Development of Targeted Mass Spectrometry-Based Approaches for Quantitation of Proteins Enriched in the Postsynaptic Density (PSD). Proteomes. 2019;7(2):12.
153. Peterson AC, Russell JD, Bailey DJ, Westphall MS, Coon JJ. Parallel Reaction Monitoring for High Resolution and High Mass Accuracy Quantitative, Targeted Proteomics. Mol Cell Proteomics. 2012;11(11):1475-1488.
154. Deutsch EW, Csordas A, Sun Z, et al. The ProteomeXchange consortium in 2017: supporting the cultural change in proteomics public data deposition. Nucleic Acids Res. 2017;45(D1):D1100-D1106.
155. Cohen LD, Zuchman R, Sorokina O, et al. Metabolic Turnover of Synaptic Proteins: Kinetics, Interdependencies and Implications for Synaptic Maintenance. Akaaboune M, ed. PLoS One. 2013;8(5):e63191.
156. Toyama BH, Savas JN, Park SK, et al. Identification of Long-Lived Proteins Reveals Exceptional Stability of Essential Cellular Structures. Cell. 2013;154(5):971-982.
157. Butko MT, Savas JN, Friedman B, et al. In vivo quantitative proteomics of somatosensory cortical synapses shows which protein levels are modulated by sensory deprivation. Proc Natl Acad Sci. 2013;110(8):E726-E735.

Temporal quantitative proteomics of mGluR5-induced protein translation and phosphorylation in neurons

Charlotte AGH van Gelder[1,2*], Renske Penning[1,2*], Tim S Veth[1,2], Lisa AE Catsburg[3], Casper C Hoogenraad[3], Harold D MacGillavry[3,], and Maarten Altelaar[1,2]

[1]Biomolecular Mass Spectrometry and Proteomics, Bijvoet Center for Biomolecular Research and Utrecht Institute for Pharmaceutical Sciences, Utrecht University, The Netherlands, [2]Netherlands Proteomics Center, The Netherlands, [3]Cell Biology, Department of Biology, Faculty of Science, Utrecht University, The Netherlands.

**Both authors contributed equally to this work*

Published in Mol Cell Proteomics (2020) mcp.RA120.002199

Abstract

At neuronal synapses, activation of group I metabotropic glutamate receptors (mGluR1/5) triggers a form of long-term depression (mGluR-LTD) that relies on new protein synthesis and the internalization of AMPA-type glutamate receptors. Dysregulation of these processes has been implicated in the development of mental disorders such as autism spectrum disorders and therefore merit a better understanding on a molecular level. Here, to study mGluR-induced signaling pathways, we integrated quantitative phosphoproteomics with the analyses of newly synthesized proteins via bio-orthogonal amino acids (azidohomoalanine) in a pulsed labeling strategy in cultured hippocampal neurons stimulated with DHPG, a specific agonist for group I mGluRs. We identified several kinases with important roles in DHPG-induced mGluR activation, which we confirmed using small molecule kinase inhibitors. Furthermore, changes in the AMPA receptor endocytosis pathway in both protein synthesis and protein phosphorylation were identified, whereby Intersectin-1 was validated as a novel player in this pathway. This study revealed several new insights into the molecular pathways downstream of group I mGluR activation in hippocampal neurons, and provides a rich resource for further analyses.

Introduction

Activation of metabotropic glutamate receptors (mGluRs) initiates a broad array of signaling pathways that collectively modulate the efficiency of neuronal communication. mGluR-dependent signaling has been linked to cognitive functions such as attention, learning and memory, and disrupted mGluR signaling has been implicated in neurological disorders such as Fragile X Syndrome, mental retardation, schizophrenia, addiction and autism spectrum disorders[1–3]. In particular, group I mGluRs (mGluR1 and mGluR5), generally localized at the postsynaptic membrane, significantly contribute to synaptic function by modulating synaptic excitability, and inducing or facilitating different forms of synaptic plasticity[4–8]. Probably the best characterized form of plasticity mediated by group I mGluRs is the long-term depression of synaptic strength referred to as mGluR-LTD[9]. In contrast to NMDA receptor-dependent forms of LTD, the major mechanism of mGluR-LTD expression relies on the rapid and local synthesis of new proteins in dendrites[10], although not all forms of mGluR-LTD require protein synthesis[11,12]. Thus, defining the signaling pathways downstream of mGluR that control translational regulation, and identifying the proteins that are newly synthesized in response to mGluR activation, are important goals in an effort to better understand mGluR-dependent plasticity mechanisms.

Postsynaptic mGluRs canonically link to Gaq/11 G-proteins, which activate phospholipase C (PLC) to form diacylglycerol (DAG) and inositol tris-phosphate (IP3). IP3 in turn triggers the release of Ca2+ from internal stores, resulting in an increase in the Ca2+ concentration and activation of protein kinase C (PKC)[3]. Apart from these pathways, mGluR stimulation has been found to activate a wide range of other downstream effectors, including c-Jun N-terminal kinase JNK1[13], casein kinase 1, cyclin-dependent kinase 5 (CDK5)[14], and components of the ERK-MAPK[15–17], and PI3K-Akt-mTOR[18–20] signaling pathways. In particular, induction of these latter two pathways are essential for the expression of mGluR-LTD, mainly because these converge on the regulation of translation initiation factors such as Mnk1, eIF4E and 4EBPs[18,21].

mGluR-LTD induces an acute wave of new protein synthesis that is required for the long-term reduction in surface a-amino-3-hydroxy-5-methyl-4-isoxazolepropionic acid receptors (AMPAR) underlying the depression of synaptic responses[10,22]. The generation of these "LTD proteins" is directly related to the rate of AMPAR endocytosis, and the rapid synthesis of proteins is required for the internalization of AMPARs and mGluR-LTD[23–30]. However, it is unclear what other molecular processes are working in parallel to sustain mGluR-LTD. Thus, even though some of the key mechanisms underlying mGluR-LTD have been identified, characterizing the full repertoire of molecular events that are initiated by mGluR activation would greatly enhance our understanding of mGluR-LTD.

Here, to identify the phosphorylation dynamics initiated by mGluR activation in hippocampal neurons, we applied a phosphoproteomics approach using high-resolution LC-MS/MS. The sensitivity of our approach allowed us to profile multiple time-points over the course of DHPG-induced mGluR activation. In addition, to identify newly synthesized proteins in response to mGluR

activation, we used an azidohomoalanine (AHA) labeling strategy[31] in combination with tandem mass tag (TMT) labeling for accurate quantification of translated proteins. Based on the observed phosphorylation dynamics we identified several kinases important in the regulation of DHPG-mGluR signaling, which we confirmed using specific kinase inhibitors. Furthermore, we uncovered a broad spectrum of protein synthesis and phosphorylation dynamics in the AMPA receptor endocytosis pathway. We thereby highlight several novel insights into the signaling mechanisms upon mGluR activation and AMPAR internalization, and validated Intersectin-1 (Itsn1) to play an important role in mGluR-mediated AMPAR trafficking.

Experimental Procedures

Ethics statement
All animal experiments were performed in compliance with the guidelines for the welfare of experimental animals issued by the Government of The Netherlands. All animal experiments were approved by the Animal Ethical Review Committee (DEC) of Utrecht University.

Neuronal cultures
Hippocampal cultures were prepared from embryonic day 18 (E18) rat brains as described in. Dissociated neurons were plated on poly-L-lysine (30 µg/ml) and laminin (2 µg/ml) at a density of 200,000 neurons per well. Cultures were grown in Neurobasal medium (NB) supplemented with B27, 0.5 mM glutamine, 12.5 µM glutamate, and penicillin / streptomycin at 37°C/5% CO_2. Neurons were transfected at DIV10-14 with indicated constructs using Lipofectamine 2000 (Invitrogen) and experiments were performed 5 – 7 days later.

Phosphopeptide analysis
Experimental Design and Statistical rationale. Primary hippocampal neurons were stimulated with DHPG for 5, 10, or 20 minutes, or not stimulated (control, 0 min). This experiment was repeated three times, resulting in three biological replicate samples from separate cultures. No technical replicates were measured. The samples were grouped in triplicates (0 min, 5 min, 10 min, 20 min) and identifications were subsequently filtered for phosphosites having at least two valid values in at least one treatment group. Differences in intensity between different treatment groups was determined with an ANOVA using $p<0.05$ as a significance threshold.

DHPG stimulation and protein digestion. At DIV14-17 neurons were stimulated with 100 µM DHPG for 0, 5, 10, or 20 minutes. Neurons were washed three times with PBS and harvested directly in 8 M Urea lysis buffer supplemented with phosphatase inhibitor (PhosSTOP, Roche) and protease inhibitor (cOmplete mini EDTA-free, Roche). Neurons were lysed at 4°C with the Bioruptor Plus (Diagenode) by sonicating for 15 cycles of 30 sec. Protein content was determined with a Pierce BCA protein quantification assay (Thermo Fisher). Equal amounts of protein (45 µg of each sample) were heated at 95°C for 5 minutes and then reduced (4 mM DTT) for 20 minutes at 56°C and alkylated

(8 mM IAA) for 25 minutes in the dark at room temperature. The proteins were then digested with Lys-C (1:75, Wako) for 4h at 37°C, after which the samples were diluted to a urea concentration of 2M and trypsin (1:50, Sigma Aldrich) was added overnight. The peptides were acidified to a total concentration of 1% Formic Acid (Merck). Samples were cleaned up using OASIS sample cleanup cartridges (Waters) and dried in vacuo.

Phosphorylated peptide enrichment
Phosphorylated peptides were enriched using Fe(III)-NTA cartridges (Agilent technologies) in an automated fashion using the AssayMAP Bravo Platform (Agilent technologies). The cartridges were primed with 0.1% TFA in ACN and equilibrated with loading buffer (80% ACN/0.1% TFA). Samples were suspended in loading buffer and loaded onto the cartridge. The peptides bound to the cartridges were washed with loading buffer and the phosphorylated peptides were eluted with 1% ammonia directly into 10% formic acid, leading to an average phosphopeptide purity of 91%. Samples were dried in vacuo and stored at -80 °C until LC-MS/MS analysis.

Mass spectrometry and data-acquisition
The phosphorylated peptide enriched samples were analyzed with an UHPLC 1290 system (Agilent technologies) coupled to an Orbitrap Q Exactive Plus mass spectrometer (Thermo Scientific). Before separation peptides were first trapped (Dr Maisch Reprosil C18, 3 µm, 2 cm x 100 µm) and then separated on an analytical column (Agilent Poroshell EC-C18, 2.7 µm, 50 cm x 75 µm). Trapping was performed for 10 min in solvent A (0.1% FA) and the gradient was as follows; 4 - 8% solvent B (0.1% FA in acetonitrile) in 2 min, 8 - 24% in 71 min, 24 - 35% in 16 min, 35 - 60% in 7 min, 60 - 100% in 2 min and finally 100 % for 1 min. Flow was passively split to 300 nl/min. The mass spectrometer was operated in data-dependent mode. At a resolution of 35.000 m/z at 400 m/z, MS full scan spectra were acquired from m/z 375–1600 after accumulation to a target value of 3e6. Up to ten most intense precursor ions were selected for fragmentation. HCD fragmentation was performed at normalised collision energy of 25% after the accumulation to a target value of 5e4. MS/MS was acquired at a resolution of 17,500. Dynamic exclusion was enabled with an exclusion list of 500 and a duration of 18s.

Data analysis
RAW data files were processed with MaxQuant (v1.6.0.1[92]) and MS2 spectra were searched with the Andromeda search engine against the TrEMBL protein database of Rattus Norvegicus (28,080 entries, downloaded 08/08/2017) spiked with common contaminants. Cystein carbamidomethylation was set as a fixed modification and methionine oxidation, protein N-term acetylation, and phosphorylation of serine, threonine, and tyrosine were set as variable modifications. Trypsin was specified as enzyme and up to two miss cleavages were allowed. Filtering was done at 1% false discovery rate (FDR) at the protein and peptide level. The mass tolerance was set to 4.5 ppm for the precursor ions and 20 ppm for the fragment ions. Label-free quantification (LFQ) was performed, and "match between runs" was enabled. The data was further processed using Perseus 1.6.0.7[93], WebLogo [94,95], MotifX[96,97], and SynGO[34].

pAHA & TMT labeling

Experimental Design and Statistical rationale. Primary hippocampal neurons were stimulated with DHPG and subsequently incubated with L-AHA (n=4, experimental condition). For each studied time point (15, 45, and 90 minutes), control experiments were included where either AHA was supplemented to unstimulated neurons, to define the set of proteins that are truly being translated in response to DHPG (n=4), or neurons were stimulated with DHPG in methionine-supplemented media in the absence of AHA (n=4), to control for non-specific binding during the enrichment process. TMT reagents 126 – 130C were used to label the nine experimental conditions, and these were mixed in a 1:1 ratio. The TMT 131 label served as a reference 'pool' between biological replicates and consisted of an equal mix of all nine experimental conditions of biological replicate 1, and was mixed in equal ratios with the other TMT labels. All biological replicates were injected twice (technical replicates) and searched as one result file. Only DHPG specific and AHA enriched proteins that had a higher relative expression than in the control conditions, in at least one of the time points, were taken for further analysis.

Stimulation and lysis. DIV12 hippocampal neurons were incubated in NB media (Gibco life technologies) supplemented with B27, 0.5 µM glutamine and penicillin/streptomycin (supplemented NB) and either with 4 mM L-azidohomoalanine (L-AHA) (Bachem) or 4 mM L-Methionine (Sigma-Aldrich) and in parallel stimulated with 100 µM DHPG or vehicle for 5 minutes at 37°C/5% CO_2. Neurons were then moved into freshly supplemented NB media with either 4 mM L-AHA or 4 mM L-methionine and incubated at 37°C/5% CO_2 until the end of the experiment (15, 45, and 90 minutes after initial DHPG stimulation). Harvest followed three washes with PBS, directly into urea lysis buffer (Click-it Protein enrichment kit, Invitrogen C10416) supplemented with protease inhibitor (cOmplete mini EDTA-free, Roche).

Enrichment and digestion. Neurons were lysed at 4°C with the Bioruptor Plus (Diagenode) by sonicating for 10 cycles of 30 sec. Protein content was determined with a Pierce BCA protein quantification assay (Thermo Fisher). Newly synthesized proteins were then enriched from 100 µg of protein material per sample using the Click-it protein enrichment kit for chemistry capture of azide modified proteins (Invitrogen C10416) following the manufactures protocol with small modifications. In short, protein lysate volume was adjusted to equal protein input for each sample per biological replicate and final volume was adjusted by adding Milli-Q. Lysates were added to washed resin and was incubated end to end rotating overnight. Resins were washed with Milli-Q and SDS buffer was added. Proteins were reduced (1M DTT) for 15 minutes at 70 °C and alkylated (40 mM IAA) for 30 minutes in the dark at room temperature. The resins were then transferred to the supplied filter columns and extensively washed with subsequently SDS wash buffer, 8 M urea with 100 mM Tris pH 8, 20% ACN and 50 mM Ammonium Bicarbonate (AMBIC). Resins were transferred to a new tube and proteins were digested with 0.1 µg Lys-C for 2h at 37°C and 0.5 µg trypsin (Promega) overnight at 37 °C. Samples were centrifuged and the supernatant was taken. Sample cleanup was performed using the OASIS sample cleanup cartridges (Waters). Samples were dried *in vacuo* and stored at -80 °C.

TMT labeling. TMT labeling was performed according to the manufacturer's instructions using the TMT10plex Isobaric Label Reagent Set (Thermo Scientific). In brief, samples were reconstituted in 100 µl 87.5% HEPES buffer pH 8.5 / 12.5% ACN, and TMT reagents in 41 µl anhydrous ACN. Full contents of the reagents were added to the samples and incubated at room temperature for one hour, after which the reaction was quenched with 5% hydroxylamine. Labeled mixtures were cleaned using the OASIS sample cleanup cartridges (Waters), dried in vacuo and stored at -80 °C until further processing.

Mass spectrometry and data-acquisition. Fractions were reconstituted in 10% FA and analyzed in two technical replicates with a UHPLC 1290 system (Agilent technologies) coupled to an Orbitrap Q Exactive X mass spectrometer (Thermo Scientific). Peptides were trapped on an in house made trap column (Dr Maisch Reprosil C18 column, 3 µm, 2 cm x 100 µm) and separated on an analytical column (Agilent Poroshell EC-C18, 2.7 µm, 50 cm x 75 µm). Trapping was performed for 5 min in solvent A (0.1% FA) and separation was performed using a 85 min linear gradient from 15% to 45% solvent B. Flow was passively split to 300 nl/min. The mass spectrometer was operated in data-dependent mode. At a resolution of 60,000 at 200 m/z, MS full scan spectra were acquired from 375 – 1600 m/z after accumulation to a target value of 3e6. Up to 15 most intense precursor ions were selected for HCD fragmentation at a normalized collision energy of 32% after accumulation to a target value of 5e4. MS/MS was acquired at a resolution of 60,000, with a fixed first mass of 120 m/z. Dynamic exclusion was enabled with a duration of 12s.

Data analysis. RAW data files were processed using Thermo Proteome Discoverer (version 2.2.0.338) and Mascot search engine (v2.6.1), allowing for variable methionine oxidation, protein N-terminal acetylation, and methionine replacement by AHA. Carbamidomethylation of cysteines was set as a fixed modification. The protein database consisted of the TrEMBL protein database of Rattus Norvegicus (28,080 entries, downloaded 08/08/2017) spiked with common contaminants. Enzyme specificity was set for trypsin, with a maximum of two allowed missed cleavages. The precursor mass tolerance was 50 ppm, and fragment mass tolerance was set to 0.05 Da. TMT 10plex was set as quantification method, and only unique peptides were used for quantification. Normalization mode was disabled, and reporter abundances were based on signal to noise values in all cases. Results were filtered using a 1% FDR cut-off at the protein and peptide level.

Selective Reaction Monitoring

Spectral library generation. Spectral libraries were used to determine peptide fragmentation characteristics and their indexed retention time, which are key for the identification of peptides in the tier 2 SRM assay. The custom mix of heavy labelled peptides (JPT) was mixed with iRT peptides (Biognosys), and analysed using an Orbitrap Q-Exactive HF (Thermo Scientific). An unscheduled parallel reaction monitoring (PRM) method was use that scanned for the +2 and +3 charged peptides, including all possible methionine oxidations. Peptides were separated using a 2h gradient and at least a 30k resolution was used for the PRM assay, resulting in a minimum of 5 spectra per peptide. Raw files were analysed using MaxQuant (version

1.6.10.43), carbamidomethyl cysteine as fixed modification, and the variable modifications serine/threonine/tyrosine phosphorylation, methionine oxidation, and isotope labels. The search results were filtered using a 1% FDR cut off, subsequently using Skyline (version 20.1.1.83) pseudo-MS2 spectra were generated which were used as the peptide library.

SRM assay development. The SRM assay was developed using previous described methods 72,98. The assay was developed on a TSQ Altis (Thermo Scientific) and a TSQ Vantage (Thermo Scientific). In brief, the 6 most intense fragment ions from the library were used as initial transitions, to which essential transitions for identification were added, such as transitions that validate phosphorylation on specific residues. These transitions were used to optimize multiple parameters such as retention time and collision energy. Collision energy was optimized per transition using Skyline, with the TSQ Vantage CE formula as starting point (CE = 0.03m/z + 2.905 for doubly charged precursors and CE = 0.038m/z + 2.281 for precursor charges of three and higher), and optimized using steps of 1 voltage.

SRM LC-MS/MS setup. Samples were analysed on a TSQ Altis (Thermo Scientific) coupled to an UltiMate 3000 (Thermo Scientific), and an easy spray analytical column (ES802A, 25 cm, 75 mm ID PepMap RLSC, C18, 100 A˚, 2 mm particle size column (Thermo Scientific)). First, samples were reconstituted in 2% LC-MS grade formic acid, containing the heavy labelled peptides. Samples were loaded on a trap column (Acclaim™ PepMap™ 100 C18 HPLC Column 0.3x5mm with 5um particles (Thermo Scientific)) with Buffer A (0.1% FA), and subsequently separated using 0-35% buffer B (80%ACN, 0.1%FA) in 50 minutes at 300nL/min, followed by a 10 minute column wash with 99% buffer B at 300nL/min. The TSQ Altis spray voltage was set at 1.9 kV and fragmented at 1.5 mTorr in the second quadrupole. The first quadrupole was set at 0.7 da FWHM, and the third quadrupole at 1.2 da FWHM. All transitions were measured with an optimized collision energy and a dwell time of 5 ms.

SRM data assessment. All experiments were analysed using Skyline (version 20.1.1.83). Quality of the peptides was assessed mainly on the signal similarity between the heavy and the light peptides. Most important aspects were perfect co-elution, peak shape, and relative contributions of each transition between the heavy and the light peptide. A rdotp > 0.95 was maintained as an indicator of the similarity between the heavy and the light peptide. To normalize the endogenous peptides an in-house Python script compared the relative intensity of the heavy peptides between two time points. The relative difference was used as multiplier for the endogenous signal.

DNA constructs

The Itsn1 miRNA knockdown construct was generated by annealing oligos containing the 21-nucleotide targeting sequences described in [78] and ligating in the miRNA expression plasmids pSM155-GFP (provided by G. Du; University of Texas, Houston, TX) digested with BsmBI.

Kinase inhibitor assay

For the kinase inhibitor assays, neurons were pre-incubated with KN-93

(10 µM), staurosporine (1 µM), or roscovitine (20 µM) for 30 minutes before induction of mGluR-LTD. Neurons were stimulated with DHPG (100 µM) for 5 minutes, returned to original medium and fixed 30 minutes later. Blockers were present during the entire experiment.

Immunofluorescence and confocal microscopy
To induce mGluR-LTD, hippocampal neurons were stimulated with DHPG for 5 minutes and then returned to the original culture medium. After 30 minutes, neurons were fixed with 4% paraformaldehyde / 4% sucrose in phosphate-buffered saline (PBS) for 8 – 10 minutes. Fixed neurons were blocked with 10% normal goat serum in PBS for 30 – 60 minutes at room temperature, stained with rabbit anti-GluA1 (1:100; Calbiochem), or anti-ITSN1 and labeled with fluorescent goat anti-rabbit secondary antibodies. Confocal images were taken with a Zeiss LSM 710 with 63x 1.40 oil objective. Images consist of a z-stack of 7-9 planes at 0.39 µm interval, and maximum intensity projections were generated for analysis and display. GluA1 cluster intensity was measured using the ParticleAnalyzer function in ImageJ and analyzed per region of interest.

Results

Protein synthesis upon activation of mGluR-LTD via DHPG
To study the downstream effects of group I mGluR activation, primary hippocampal cultures were stimulated with (s)-3,5-dihydroxyphenylglycine (DHPG), a specific agonist of group I mGluRs. We confirmed that this induced a reduction in surface GluA1 expression (Figure S1A) as has been established before[9,32]. To identify proteins that are synthesized de novo in response to mGluR activation by DHPG, we used a pulsed-AHA approach[31,33]. Cultured hippocampal neurons were stimulated with DHPG in the presence of the bio-orthogonal methionine analogue AHA to label newly synthesized proteins. Since these primary neuron cultures are limited in sample material, which poses a challenge in sensitivity to determine truly newly synthesized proteins, we decided to incorporate two control conditions. In one condition we performed DHPG stimulation in the presence of methionine to control for non-specific binding during the enrichment process. Additionally, we included a control in which unstimulated neurons were supplemented with AHA, to define the set of proteins that are translated only in response to DHPG. To profile the temporal induction of protein synthesis, neurons were harvested and lysed at different time points up to 90 minutes after a 5-minute DHPG stimulation (Figure 1A). AHA-incorporated proteins were consecutively enriched via click-chemistry, digested by a combination of Lys-C and trypsin and analyzed using high-resolution nanoLC-MS/MS. Only DHPG specific and AHA enriched proteins that had a higher relative expression than in the control conditions, in at least one of the time points, were taken for further analysis. GO enrichment analysis against a full brain background using SynGO[34] confirmed enrichment of postsynaptic over presynaptic localization, as well as a clear enrichment in, among others, postsynaptic cytoskeleton and ribosome (Figure 1B). Among the newly synthesized proteins are hallmark mGluR-LTD proteins involved in translation, such as translation initiation factor 4a (Eif4a2) and elongation factor 2 (Eef2)[22], which demonstrates the effectiveness of this experimental set up

to identify protein translation upon DHPG-induced mGluR activation (Figure 1C, Figure S2B).

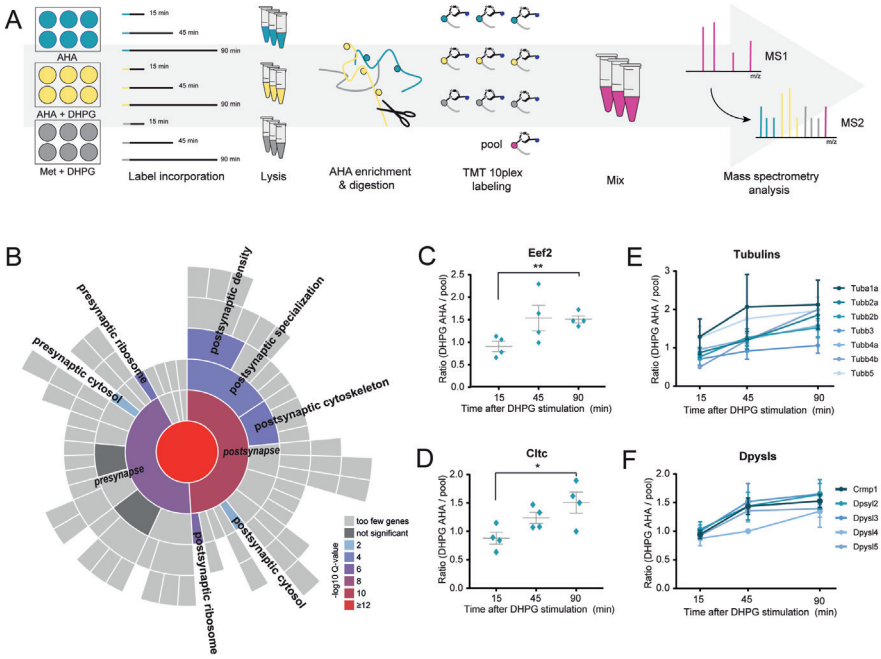

Figure 1. Identification of protein translation following DHPG-induced group I mGluR activation. **(A)** Workflow: neurons were stimulated with DHPG for 5 minutes in combination with methionine (negative control, to control for non-specific binding during the enrichment process, N=4) or the methionine substitute AHA (N=4). An extra control was included in which unstimulated neurons were supplemented with AHA, to define the set of proteins that are truly being translated in response to DHPG (N=4). After DHPG removal, translation was followed for a total of 15, 45, and 90 minutes. Newly synthesized proteins were enriched, digested and labeled with TMT10plex. **(B)** SynGO cellular location enrichment analysis of newly translated proteins (1% FDR) revealed enrichment of postsynaptic over presynaptic localization. **(C)** Induction of mGluR-LTD using DHPG leads to identification of proteins involved in translation, such as Eef2, as well as **(D)** in receptor endocytosis, such as clathrin, showing increasing protein abundance over time. **(E)** This enrichment and labeling approach reducibly identifies multiple members of the same protein families during mGluR-LTD, including subunits of both alpha and beta tubulins and **(F)** Dpysls. Data are represented as mean±SEM, * p<0.05, p<0.01, as determined with a one-way ANOVA.

DHPG-induced activation of group I mGluR stimulates augmented internalization of AMPARs[9,10,27,29,30]. Accordingly, we found many newly synthesized proteins with functions related to receptor endocytosis and recycling. Examples include the adaptor protein complex AP-2 subunit alpha1 adaptin (Ap2a1), the GTPase Cdc42, and the neuronal migration protein doublecortin (Dcx), which is a known interactor of clathrin adaptor complexes[35] (Table S1). In line with this observation, we identified DHPG-dependent translation of the heavy chain of clathrin (Cltc), a key protein for the formation of coated vesicles, which was steadily being translated

over all three time points (Figure 1D, Figure S2C).

In line with the findings that reorganization of the actin cytoskeleton underlies the expression of mGluR-LTD[36], and is for instance thought to cause the changes in spine morphology that are associated with mGluR-LTD[37], we observed several proteins with known roles in structural plasticity processes, including stathmins (Stmn1 and Stmn2), profilin (Pfn2), and neuromodulin (Gap43), as well as cofilin-2 (Cfl2) (Table S1). Interestingly, apart from these actin regulators we also observed profound translation of microtubule-associated proteins (Map2, Map6, Mapre1, Map1lc3b, and Mapt), as well as numerous subunits of both alpha and beta tubulins over all time points (Figure 1E). Since the microtubule cytoskeleton is largely excluded from spines, these results suggest that postsynaptic mGluR activation has even wider effects, potentially reorganizing the microtubule cytoskeleton in the dendritic shaft to facilitate microtubule-based transport.

Interestingly, we also identified and measured the translation of several protein families and complexes over time, such as several proteasomal subunits, ribosomal proteins, 14-3-3 proteins, tubulins, and dihydropyrimidinase-related proteins, which are also known as the collapsing response mediator protein family (CRMPs) (Figure 1F). These versatile proteins are involved in a variety of developmental and plasticity-related brain processes, and have been shown to also localize in the PSD[38]. Interestingly, the CRMP family of proteins were recently identified as some of the most stable, long-lived proteins in neurons[39].

To generate a more in-depth overview of the type of proteins being translated, and which processes they represent, we performed a k-means interaction-based clustering analysis using the protein-interaction database STRING (Table S1)[40]. GO analysis of these resulted in the enrichment of six biological processes, visualized using the geneMANIA app in Cytoscape[41]. This interaction-based clustering approach highlights interactions between proteins as identified by, among others, physical interactions, co-expression data and co-localization data, retrieved from a wide variety of assays, organisms, and cell types. With these combined data, we can identify groups of proteins with similar functions in relevant biological processes underlying mGluR signaling cascades.

Figure 2 displays the interaction network with representative proteins of each of these processes, as well as their z-score normalized expression levels over all pooled experimental conditions. As expected, we identify several protein clusters with an enrichment in biological processes related to protein translation. The first cluster contains proteins involved in the processing of mRNA, and includes several splicing factors (Srsf2 and Srsf3) and ribonucleoproteins (e.g. Snrnp70), as well as binding proteins (Nono and Pcbp2). The second cluster, with a clear enrichment in proteins regulating translation, includes translation initiation factor Eif4a2, and elongation factors (Eef1g, Eef2, and Tufm), as well as multiple ribosomal proteins, both from the 40S (e.g. Rps2 and Rps7) and 60S ribosome (e.g. Rpl3 and Rpl22). This suggests that mGluR group I activation initiates the formation of new ribosomes, presumably to meet the demands of an increased rate of protein

synthesis. Cluster 3 contains proteins involved in protein folding, including several heat shock proteins (e.g. Hsp90aa1 and Hsp90ab1), as well as several subunits of the t-complex (e.g. Cct2 and Cct5), which are molecular chaperones in protein folding[42]. These clusters, where protein translation and folding are the main biological processes, are part of what can be described as a 'first wave' of protein synthesis, which is initiated rapidly and already shows considerable new protein translation in the early time points (predominantly from the 45 minute time point on). A 'second wave' of protein synthesis seems to be initiated at a later stage (45 to 90 minute time point, as demonstrated in clusters 4 and 5), and contains proteins, amongst others, related to protein degradation. Recently, a dynamic interplay between protein translation and degradation has been described to be crucial for mGluR-LTD[43,44]. Inhibition of the proteasome rescued impairments in mGluR-LTD induction caused by blockage of protein translation[43], suggesting that a fine coordination between protein translation and degradation of proteins by the UPS is key for the efficient induction of mGluR-LTD. In line with this, we observed translation of many proteins involved in protein degradation in cluster 4, including several subunits of the proteasome (e.g. Psma2, Psma3, Psmb1 and Psmb7). Finally, we identified two protein clusters with a similar enrichment in GO terms, containing proteins involved in the organization of cellular components (cluster 5) and, more specifically, cytoskeleton organization (cluster 6). While both clusters contain multiple tubulins, cluster 5 also contains several 14-3-3 proteins, which have been studied extensively in relation to their function in the regulation of actin filaments[45]. In addition to tubulins, cluster 6 also contains several actin regulating proteins (e.g. Arpc1a and Wdr1).

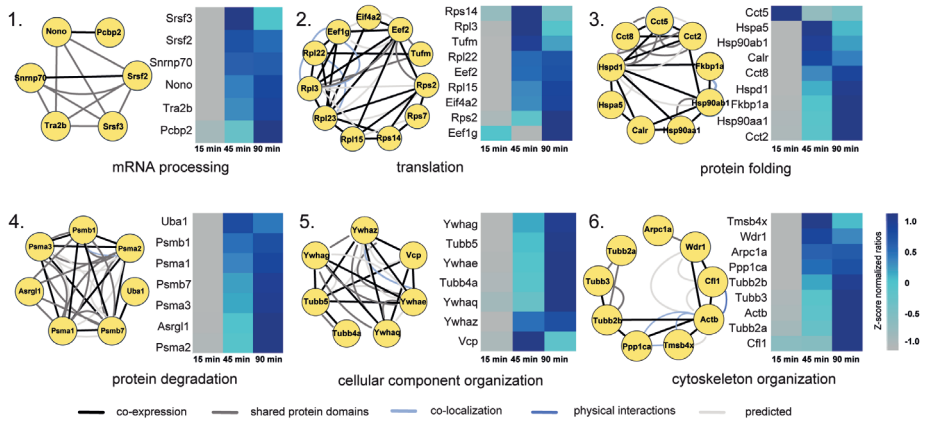

Figure 2. Interaction-based protein clusters with distinct biological processes involved in mGluR activation. GO enrichment analysis of k-means based interaction clusters resulted in six main clusters with a clear enrichment in a biological process. Proteins from each cluster are displayed with their known interaction profiles. Heatmaps represent the z-score normalized ratio DHPG AHA / pool over the three measured time points.

Phosphoproteomics of group I mGluR activation in primary neurons reveals defined clusters of phosphosite regulation with a strong synaptic signature

Due to the low stoichiometry of phosphorylation events in the proteome, phosphoproteomics analysis involves dedicated enrichment strategies. These strategies typically require milligrams of protein input material[46–48], hampering analysis of phosphorylation dynamics in primary neurons. Recently, we have shown that automated phosphopeptide enrichment using Fe(III)-IMAC cartridges on a Bravo AssayMap platform allows sensitive and reproducible enrichment of several thousands of unique phosphopeptides starting with only 1-10 µg of protein input material. Moreover, we showed that from a single neuronal culture plate, 200,000 cells delivering ~50 µg of protein, we could identify biological relevant phosphorylation events among the ~7,000 observed phosphosites[49]. This now allowed us to study phosphorylation events on multiple time-points after DHPG stimulation in primary hippocampal neurons, without the need for combining extensive amounts of input material. The proteomics analysis of Fe(III)-IMAC enriched phosphorylated peptides was performed after stimulating rat hippocampal neurons for 0, 5, 10 or 20 minutes with DHPG. The applied workflow is outlined in Figure 3A.

The phosphoproteomics screen resulted in the identification of 17,556 phosphosites with a localization probability >0.75, of which 5,423 could be quantified in at least two biological replicates in at least one experimental condition and were used for subsequent analysis (Table S2). Phosphopeptide abundance showed a normal distribution (Figure S3A) and a high degree of overlap between the identified phosphoproteins from both the 5, 10 and 20 minutes DHPG-stimulated neurons could be observed compared to control (Figure S3B). The distribution of phosphosites on serine, threonine and tyrosine residues is in line with previous publications[46,49,50] (Figure S3C). The reproducibility of the experimental procedure was assessed between biological replicates, and between the different time points. A high degree of correlation between the biological replicates could be observed, suggesting that a small, but distinct subset of signaling pathways is activated by DHPG, consistent with the notion that DHPG activates local dendritic signaling pathways, rather than a robust, cell-wide response. Nevertheless, the DHPG-treated samples could still be clearly distinguished from the control samples (Figure S3D). Furthermore, SynGO enrichment analysis of biological function compared to a full brain background resulted in a significant enrichment for PSD organization, regulation of postsynaptic neurotransmitter receptor activity and localization, and organization of the postsynaptic actin skeleton (Figure S3E).

To identify phosphosites regulated over time, a multiple-samples ANOVA was performed, resulting in a total of 504 phosphosites that were significantly regulated in response to DHPG ($p<0.05$). Unsupervised fuzzy clustering of the proteins from which these regulated phosphosites originated revealed five distinct clusters (Figure 3B)[51]. The proteins grouped in cluster 1 are characterized by an increasing trend in phosphorylation and are enriched in multiple GO terms compared to the full phosphoproteome, such as actin binding and microtubule cytoskeleton organization (Figure 3C). In cluster 2, showing a distinct pattern starting with immediate de-phosphorylation

upon DHPG stimulation followed by re-phosphorylation at later time points, we observe enrichment in processes involved in signaling, such as protein kinase binding and serine/threonine kinase activity. Cluster 3, containing proteins involved in cytoskeleton organization and microtubule binding (e.g. Map1b and Mapt), shows initial phosphorylation followed by dephosphorylation at the later time points. Both clusters 4 and 5 show a steady trend in phosphorylation over all time points, where proteins are either steadily dephosphorylated over time (cluster 4), or phosphorylated over time (cluster 5). Both clusters are enriched for proteins associated with microtubule binding (e.g. Map2, Map4 and Macf1), small GTPase regulator activity, and more generally protein phosphorylation.

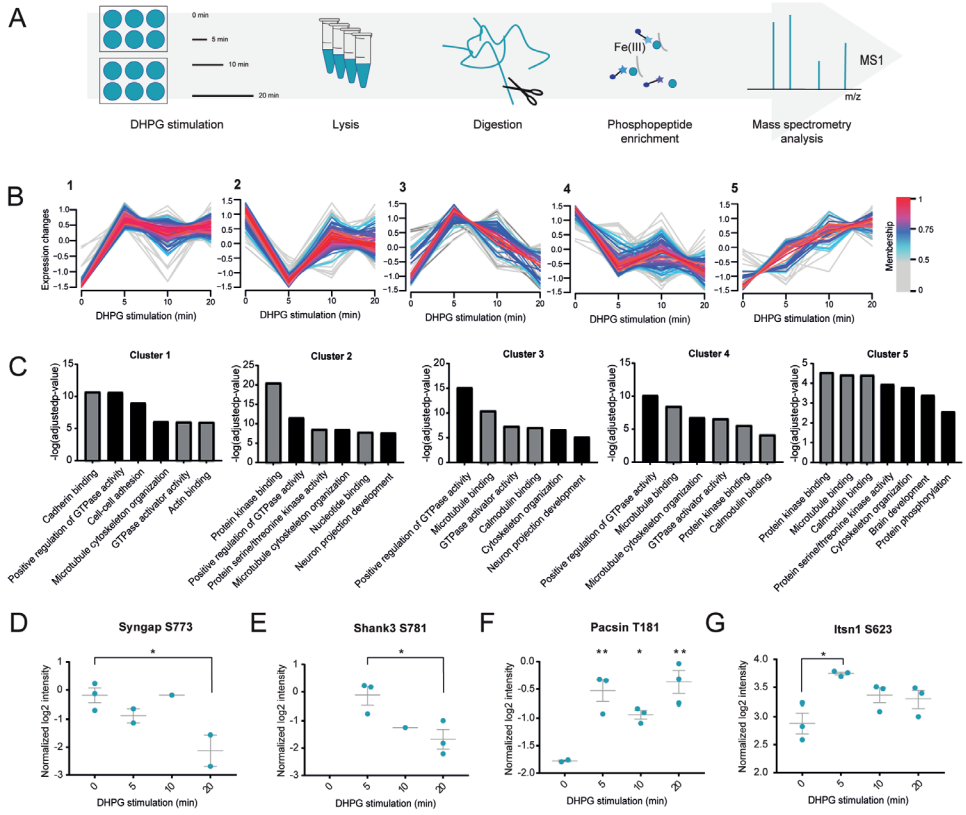

Figure 3. Quantitative phosphoproteomics of mGluR signaling in hippocampal neurons stimulated with DHPG. **(A)** Quantitative phosphoproteomics workflow: samples were taken at 0, 5, 10 and 20 minutes after the addition of DHPG. **(B)** Unsupervised clustering reveals five distinct clusters for the regulated phosphosites. **(C)** GO-term enrichment analysis for molecular function (grey) and biological process (black). **(D-G)** Normalized log2 intensities of regulated phosphosites upon DHPG stimulation. Data are represented as mean±SEM, * $p<0.05$, ** $p<0.01$, as determined with a one-way ANOVA.

Taken together, we can use the phosphorylation patterns from these five clusters to generate a general timeline of biological processes, where some fast and short-acting processes such as protein kinase binding and

kinase activity precede more general and longer-acting processes such as microtubule binding and cytoskeleton organization.

Phosphorylation dynamics in relation to DHPG-activated group I mGluRs
Regulation of major signaling pathways by kinases and phosphatases underlies various dynamic processes in cellular functioning, including mGluR-LTD[16,18,52–54]. A selection of several kinases can influence important nodes of these signaling pathways. One kinase shown before to be important in mGluR-LTD is Ca2+/calmodulin-dependent protein kinase II (CaMKII). We found subunit CaMKIIβ to be dephosphorylated in our dataset at S315 following DHPG stimulation. This is in contrast with observations in mature Purkinje cells, where DHPG stimulation drastically increased phosphorylation of S315, thereby decreasing its F-actin binding and bundling activity. In this system, CaMKIIβ was found to be directly phosphorylated by PKCγ, via the mGluR IP3R1/Ca2+-dependent PKC pathway[55]. Next to CaMKII, we observed dephosphorylation, and thus activation, of Eef2 at T57, the major target of the Ca2+/calmodulin-dependent protein kinase eEF2K[56]. Interestingly, one hour after DHPG stimulation, Eef2 phosphorylation has been shown to result in mGluR-LTD related protein translation of Arc/Arg3.1 and inhibition of global protein translation in mouse hippocampal slices[57].

Next to protein translation, several proteins involved in protein degradation showed regulation by phosphorylation upon DHPG stimulation. Among these are the T273 phosphosite of the Psmd1, and T9 of the Psmd2 regulatory subunits of the 26S proteasome, several other proteasome subunits (Psma5 and Psmc3), and several ubiquitin-related enzymes.

Multiple integral proteins of the PSD showed regulation at the phosphorylation level. For instance, the protein SynGAP1, an important negative regulator of AMPAR insertion at the membrane of the PSD[58], was significantly dephosphorylated over time at S773 (Figure 3D). Phosphorylation of the S773 site alone has been shown to inhibit GAP activity, while concurrent phosphorylation of both S773 and S802 increased GAP activity[59]. GAP activity is necessary for the inactivation of Ras and Rap, which are involved in AMPAR trafficking[59]. Our data thus suggest that dephosphorylation of SynGAP1 at S773 in response to DHPG changes the Ras/Rap activation balance, perhaps promoting AMPAR endocytosis.

Significant changes in phosphorylation status were also found in several PDZ domain-containing proteins (Table S2). We observed alterations in phosphorylation in prominent synaptic scaffolding proteins such as Dlg2 (PSD-93), Dlg3 (SAP-102), Shank2 and Shank3. The latter was found to be phosphorylated already five minutes after mGluR stimulation at S781 (Figure 3E), a site that has not previously been identified in rat, but was recently shown to be induced by an LTP protocol in mouse PSD fractions[60]. Other regulated PDZ proteins include microtubule-associated serine/threonine-protein kinase 2 (Mast2) at two distinct phosphorylation sites, as well as Rho GTPase-activating proteins Arhgap21 and Arhgap23. Also identified to be phosphorylated, but not found to be significantly regulated in this data set, is the PDZ scaffold protein GRIP, which is involved in AMPAR trafficking[61,62].

Multiple proteins involved in endocytosis show significant regulation at the phosphorylation level, including Syndapin-1 (Pacsin1) and β-Pix (Arhgef7). Syndapin-1 becomes phosphorylated at the T181 site after DHPG stimulation (Figure 3F). This phosphosite of Syndapin-1 is located in the F-Bar domain of the protein and is important in neuronal membrane tubulation. The F-bar domain is involved in lipid binding and cytoskeleton reorganization[63]. However, this specific phosphosite was not shown to be involved in the regulation of activity-dependent bulk endocytosis. More recently, it was shown that Syndapin-1 also interacts directly with Pick1 via its F-bar domain and that this interaction is important for AMPAR endocytosis in NMDAR-related cerebellar LTD[64]. This might suggest a potential role for this T181 phosphosite in the Syndapin-1 and Pick1 binding following DHPG-induced group I mGluR activation, potentially influencing AMPAR endocytosis. β-Pix is a guanine nucleotide exchange factor and binds the p21–activated kinase Pak1. The site S71 of β-Pix is strongly conserved and has a possible role in its guanine exchange function[65]. In our experiment, the phosphorylation pattern of S71 belongs to cluster 2, where after an initial rapid dephosphorylation, the phosphorylation state after 20 minutes of DHPG stimulation returns close to its initial level. Furthermore, two phosphosites (S623 and S1134) of Itsn1, a protein linked to receptor internalization, were significantly regulated upon DHPG stimulation (Figure 3G). In neurons, Itsn1 was suggested to be involved in presynaptic vesicle recycling[66,67], but was also shown to have a postsynaptic function in AMPAR internalization in invertebrates[68]. The exact role of these phosphosites is still unknown, also in mGluR-LTD, which makes Itsn1 an interesting target for further study.

Activated kinases upon group I mGluR stimulation with DHPG

To assess if certain kinases are specifically involved in the phosphorylation events underlying DHPG-induced group I mGluR signaling, we next performed a phosphorylation site consensus motif analysis of the regulated phosphosites. This allowed us to extract multiple phosphorylation motifs (Figure S5) resulting in four distinct typical kinase motif sequences linked to regulated proteins in our dataset (Figure 4A). The first and most pronounced motif is the proline directed motif at the +1 position, which is a known recognition motif of the cyclin-dependent kinases (CDKs)[69]. Moreover, we identified the threonine directed TPxK motif, which is a known substrate binding site of Cdk5. The third motif is the RxxS motif, which is part of the known targeting sequence for the MAPK-activated protein Kinases (MKs)[70,71]. A double MK2/3 knockout mouse model showed impaired mGluR-LTD and GluA1 endocytosis, indicating a regulatory role for these kinases in the process. This RxxS motif is also described as a consensus motif for CaMKII kinases, as is the KxxS motif, which is also visible as the fourth most dominant motif.

To experimentally validate the activation of these kinases, as well as kinases associated to mGluR5 activation and AMPAR internalization, we performed quantitative selected reaction monitoring (SRM) analysis of activation sites of several of these kinases[72]. With this analysis we were unable to detect the activation site of CDK, however, could clearly show increased phosphorylation of the respective activation sites of CAMKIIa (T285), ERK2/MAPK1 (T182 and Y184) and PKCa (S225 and T227) upon DHPG stimulation

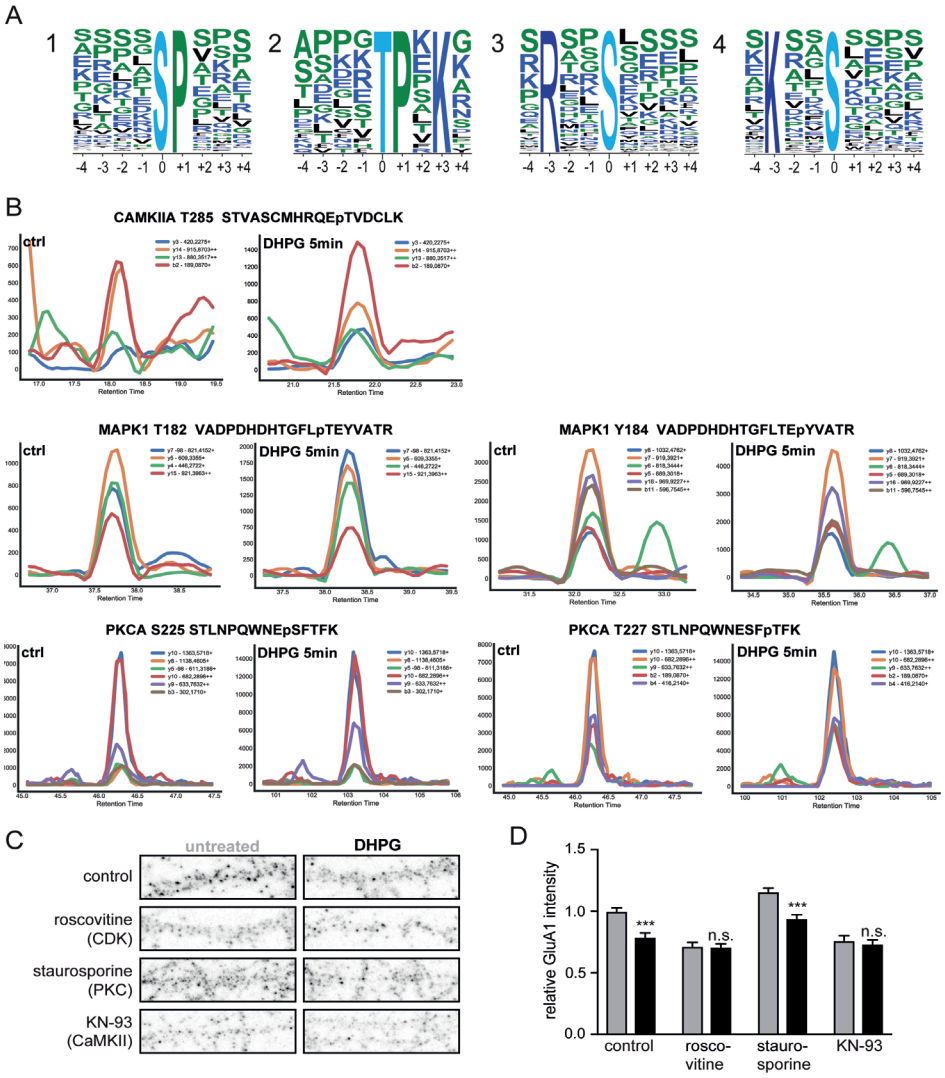

Figure 4. Kinases involved in DHPG-activated mGluR-LTD. **(A)** MotifX sequence motifs of regulated phosphosites (p<0.01) implicated in mGluR-LTD. **(B)** Representative SRM traces of known kinases downstream of mGluR5 activation by DHPG. A clear increase in phosphorylation was observed after 5 minutes of DHPG stimulation compared to control for several activation sites of PKCa, CaMKIIa and MAPK1. **(C)**. Immunostaining of GluA1 subunits at the cell surface after control or DHPG treatment, pre-incubateed with control (untreated, N=19)) or 3 different kinase inhibitors (Roscovitine (CDKs, N=15), staurosporine (PKC, N=12) and KN-93 (CaMKII, N=12)). **(D)** Relative quantification of cell surface GluA1 intensity; pre-incubation with roscovitine (N=13) or KN-93 (N=12) blocked DHPG-induced reduction in surface GluA1 levels in contrary to staurosporine (N=12) pre-incubation which did not prevent mGluR-induced GluA1 internalization. Data are represented as mean±SEM. *** p<0.001, n.s. not significant, as determined with a one-way ANOVA.

(Figure 4B). Next, we used well-characterized pharmacological inhibitors to specifically block the activity of CDKs (roscovitine), or CaMKII (KN-93) before stimulation with DHPG in hippocampal cultures. Confirming the predictions, we found that pre-incubation with roscovitine or KN-93 blocked the DHPG-induced reduction in surface GluA1 levels (Figure 4C,D). On the other hand, pre-incubation with staurosporine, blocking PKC activity did not prevent mGluR-induced GluA1 internalization. These experiments thus confirmed our prediction that the activity of CDKs and CaMKII underlie the DHPG-induced AMPAR internalization.

Further analysis of the most distinguished and characteristic kinase motifs, such as the TPxK motif known for Cdk1, Cdk2, and Cdk5, matched 99 of our significantly regulated phosphosites (Table S2). Here, we could find back known Cdk5 signaling proteins, such as the cyclin-dependent kinase 5 activator 1 (or p35), a neuron specific activator of Cdk5, the membrane associated cytoskeleton protein Amphiphysin, and the microtubule-associated protein Map2. The same group also contains other Maps, including Map1b and Mapt, as well as other cytoskeleton related proteins (i.e. members of the Dpysl family). Other interesting phosphorylation sites from our generated list of potential Cdk substrates include Aak1 T338, which is reported to be phosphorylated by Cdk1 (phosphosite plus). Aak1 in turn phosphorylates AP2 subunits 2m1 and 2m2 (also both found regulated by phosphorylation in our dataset). Based on downstream substrate candidates presented here, Cdk's seem to be involved in initiation of AMPAR endocytosis, next to their known role in cytoskeleton reorganization[73,74].

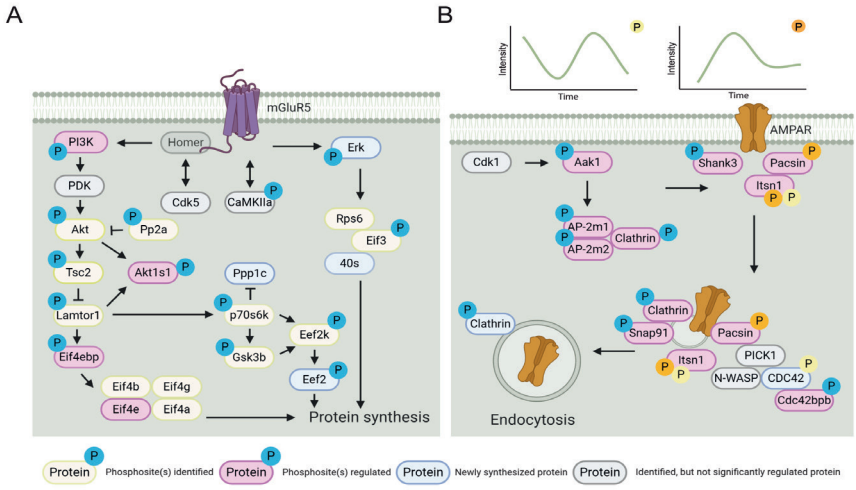

Figure 5. Pathways involved in DHPG-induced mGluR activation and AMPAR internalization. **(A)** Detailed overview of the molecular pathways involved in DHPG-induced mGluR signaling identified in the (phospho)proteomics experiments. **(B)** Visualization of phosphorylated proteins shows the activity of several signaling cascades facilitating and activating AMPAR recycling and internalization. The relative quantification of these phosphorylation events (upper panel) shows distinct phosphorylation patterns over time. Created with BioRender.

Newly translated proteins regulated by phosphorylation

Fifteen proteins were found to be both newly synthesized and regulated by phosphorylation upon DHPG stimulation (Table S2). These proteins include several proteins involved in translation and protein synthesis and degradation, as well as microtubule-associated protein 6 (Map6), neuronal migration protein doublecortin (Dcx) and previously discussed elongation factor (Eef2). It also contains neuromodulin (Gap43), a PKC substrate that is known for its presynaptic role in NMDAR-mediated LTD[75]. More recent studies however, have shown that neuromodulin is also abundantly expressed postsynaptically, where it has to be cleaved by Caspase-3 to regulate LTD[76]. Interestingly, two of its regulated phosphosites (T95 and S96) are located in close proximity to a Caspase-3 cleavage site. Dephosphorylation of two amino acids in this cleavage domain could very well result in a conformational change, making it more accessible to caspase cleavage.

We validated changes in phosphorylation of two of these proteins, and their three significantly regulated phosphosites. We confirmed dephosphorylation of Stmn1 S62 after 5 minutes of DHPG stimulation using SRM (Figure S4A), which matches the unsupervised clustering and GO enrichment profile of this microtubule destabilizing protein (cluster 2, Figure 3B,C). The same holds true for Dcx S331 and S337, (Figure S4B,C), a microtubule-associated protein found in cluster 3 (Figure 3B,C). Both Dcx and Stmn1 are proteins in cytoskeleton and cellular component organization, which are predominantly synthesized in the second wave of protein translation (clusters 5 and 6, Figure 2). These data again highlight the distinct timing of events with a fast response through phosphorylation at 5 minutes followed by translation of the same proteins after ~45 minutes. Integration of the phosphoproteomics and protein synthesis datasets, in combination with the data generated from the kinase motif analysis, resulted in a global view of molecular events triggered by group I mGluR activation in neurons (Figure 5).

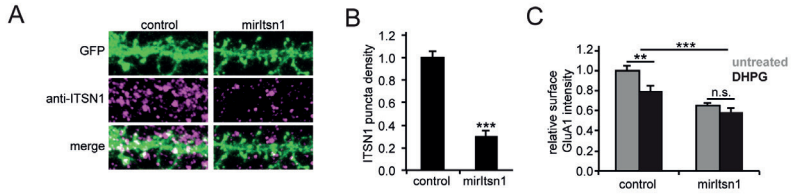

Figure 6. Itsn1 is essential for DHPG-induced AMPAR internalization. **(A)** Immunostaining of GluA1 of transfected neurons with a miRNA-based knockdown construct targeting both the long and short forms of Itsn1 (mirItsn1) or control transfection. **(B)**. Immunostaining of endogenous Itsn1 confirms significant depletion of Itsn1 in mirItsn1-transfected neurons. **(C)** Surface expression of GluA1 was significantly reduced in Itsn1 knockdown neurons under basal conditions and GluA1 surface levels in response to DHPG are severely affected in Itsn1 knockdown neurons. Data are represented as mean±SEM ** $p<0.01$, *** $p<0.001$, n.s. not significant, as determined with a one-way ANOVA.

Itsn1 is essential for DHPG-induced AMPAR internalization

In the phosphorylation data we identified that Itsn1 phosphorylation, a guanine exchange factor (GEF) for the GTPase Cdc42[77], was regulated at two phosphosites (S623 and S1134) upon DHPG stimulation (Figure 3D). To test whether Itsn1 also has a functional role in mGluR-mediated AMPAR internalization, we transfected neurons with a miRNA-based knockdown construct targeting both the long and short forms of Itsn1 (mirItsn1)[78]. Immunostaining of endogenous Itsn1 in control neurons showed a punctate pattern, as described before[78], and confirmed significant depletion of Itsn1 in mirItsn1-transfected neurons (Figure 6A,B). Interestingly, surface GluA1 expression was significantly reduced in Itsn1 knockdown neurons under basal conditions, indicating that Itsn1 is involved in the regulation of AMPAR surface expression. Furthermore, we found that the reduction in GluA1 surface levels in response to DHPG was severely affected in Itsn1 knockdown neurons (Figure 6C), further indicating that Itsn1 contributes to stimulated AMPAR trafficking. The presented experimental confirmation of candidate regulators in AMPAR internalization underlines the strength of this quantitative and high-resolution proteomics approach.

Discussion

Here we used a combination of pulsed AHA and TMT labeling approaches to study protein synthesis in response to group I mGluR activation. This combination ensured for enrichment and MS-based relative quantification of labeled and thus newly synthesized proteins. This enrichment method has been shown to be applicable to different types of cultured cells, including primary cultures like neurons[31,33,79,80]. A major advantage of the use of these pulsed labeling approaches in combination with mass spectrometry analysis is the possibility to identify and quantify subtle alterations in expression of proteins amidst the background of a steady state proteome, even of low abundant proteins. This approach led to the identification of 273 newly synthesized proteins upon mGluR activation, containing both known and novel proteins linked to mGluR-LTD. Here, we identified several proteins previously shown to be involved in mGluR-LTD, such as ERK1[81]and CaMKII, and proteins implicated in endocytosis such as Cdc42[82] and clathrin. Unfortunately, we did not identify some other known mGluR-LTD markers including Arc/Arg3.1, Step or Ophn1[9,22], which might be caused by their expression abundance, the chosen time points of analysis, or the nature of the enrichment method. This could potentially be improved by higher affinity click chemistry enrichment techniques or fractionation before nanoLC-MS/MS analysis. For instance, CaMKIIa was identified as a newly synthesized protein after DHPG stimulation in the proteomics data set but was not included for further analysis due to missing quantitative values. Further, we observed translation of several proteins that are themselves involved in protein synthesis, such as translation initiation and elongation factors, and multiple ribosomal proteins, but also proteins involved in proteasomal degradation, e.g. multiple proteasome subunits and enzymes involved in ubiquitination. These findings hint to the importance of regulating the fine balance between translation and degradation of proteins involved in the induction of mGluR-LTD[43].

Functional clustering of translated proteins DHPG stimulation led to the identification of known mGluR-LTD proteins, and highlighted several functionally relevant proteins with potential roles in mGluR-LTD related processes. Importantly, these functional families of proteins are not limited to the provided clusters, since these are solely based on annotated proteins with known functions or interactions. For instance, the splicing factors in cluster 1 (Figure 2), could potentially be supplemented with less-studied family members, including Srsf1, Srsf4, and Srsf7. This also holds true for, among others, proteasomal subunits and ribosomal proteins. These extended clusters and their corresponding heatmaps can be found in figure S6.

We complemented the protein translation dataset information on the phosphorylation events that potentially drive the signaling pathways downstream of group I mGluR. These events are usually very fast, to allow the cell to rapidly respond to external signals and precede protein translation. This makes phosphorylation likely the first step in the induction of mGluR stimulated signaling pathways, and it could therefore yield valuable information on the underlying molecular events, including mGluR-LTD-associated receptor dynamics. Here, we confirmed the role of CaMKII in mGluR-induced AMPAR internalization in both our sequence motif analysis and kinase inhibitor assay on GluA1 internalization. Multiple studies have shown the importance of kinase and phosphatase activity in the induction and maintenance of mGluR-LTD in general[16,18,53] , emphasizing the importance of phosphorylation in this dynamic process. Involvement of serine/threonine kinase activity has been studied intensively, and have been shown to be prominently involved in the activation of protein translation via the PI3K/Akt and subsequently Tsc and mTOR pathways, while tyrosine phosphatases and kinases are believed to be responsible for AMPAR tagging for internalization, and subsequent degradation[83,84]. Contrary to the intracellular signaling pathways that generally follow Gaq/11 protein stimulation, DHPG-LTD has repeatedly been shown to activate G-protein-independent signaling pathways[85,86]. In line with these findings, we find little phosphorylation, or translation, of proteins of the PLC, DAG, and PKC pathways leading to intracellular calcium release. Furthermore, the kinase inhibitor assay confirmed that inhibition of PKC activity does not influence DHPG-induced GluA1 internalization. This is in line with previous research, which also showed that DHPG induced mGluR-LTD is not dependent on PKC activity[86]. Alternatively, we found significant regulation of CDK-type kinases. Cdk5 is a known regulator of mGluR5 activation, as it controls phosphorylation of the binding site of the adaptor protein Homer to the proline-rich C terminus of group I mGluRs. Via this mechanism, Cdk5 activation is negatively correlated with mGluR5 activation[87]. Moreover, hippocampal slices treated with a Cdk4 inhibitor showed impaired DHPG-induced LTD[88], suggesting that at least two prominent members of the CDK family have functions in synaptic plasticity processes in hippocampal neurons. Our motif analysis indeed confirmed a role for CDK-type kinases in mGluR-LTD, as further demonstrated using the Cdk1, 2 and 5 specific inhibitor Roscovitine, which inhibited GluA1 internalization after DHPG stimulation, however, does not fully distinguish the individual roles of Cdk1, 2 and 5. This also holds true for KN-93, which is does not only block CamKII, but also open voltage-gated potassium channels.

Next to kinase-specific signaling functions, clear regulation of cytoskeleton elements by phosphorylation was observed (Figure 3), suggesting that group I mGluR activation can induce cytoskeleton reorganization. Most prominently, alterations in phosphorylation status of cytoskeletal regulators were observed, some of which were described before[37,89], suggesting acutereorganization suggesting acute microtubule reorganization of both the actin and microtubule cytoskeleton. Indeed, mGluR-induced actin dynamics have been shown to be involved in regulating spine morphology[37]. The effect of mGluR activation on microtubule-associated proteins suggest that mGluR activation can have even wider effects on the microtubule cytoskeleton in the dendritic shaft. Potentially, this could facilitate transport of components of the protein synthesis and degradation machinery. Next to cytoskeleton related processes, GO term analysis on molecular functions of the identified phosphorylated proteins yielded enrichment of regulatory activity of small GTPases. Several members of the Ras GTPase superfamily were found to be newly synthesized upon group I mGluR activation, including members of the Rab and Ran subfamilies, Cdc42, and several of their interacting proteins. Recently, studies have been performed on some small GTPases in relation to several types of synaptic plasticity, shedding light on the possible importance of these types of molecules in mGluR-LTD as well. Overall, these and other data provide evidence for the possible importance of small GTPases in mGluR-LTD, and should be followed up further[90,91].

Itsn1 has not been subjected to extensive analysis in the context of synaptic plasticity before, although it was shown to influence trafficking of the AMPAR subunit GluA1 in C. Elegans[68]. Here, we showed a role for Itsn1 in GluA1 trafficking at dendritic spines in mammals as well. Interestingly, knockdown of Itsn1 reduced the expression of GluA1 in dendritic spines, even in the absence of DHPG. Importantly, the induction of AMPAR internalization upon DHPG stimulation was not observed in the knockdown neurons, emphasizing a central role of Itsn1 in basal and activity-induced GluA1 internalization. The exact mechanism by which Itsn1 influences receptor trafficking remains to be studied further. An interesting question is whether Itsn1 exerts its functionality mostly via posttranslational modifications such as the here identified phosphorylation sites, or via one of its interacting domains with other proteins. Previous research showed that its DH domain was critical for Cdc42 activation, and its SH3 domain for N-WASP interaction[77]. Although one of our identified phosphorylation sites falls outside of these regions (S623 is located in the coiled coil part of the protein), the second one, S1134, falls within the N-WASP interacting SH3 domain.

In conclusion, we were able to construct a comprehensive map of signaling and translational events upon group I mGluR activation by integrating significant changes in regulation of protein phosphorylation and translation. Over time, we could monitor activation of several signaling pathways, as well as upregulation of protein signaling complexes involved in clathrin-mediated endocytosis. This multipronged analysis revealed several novel players in mGluR-stimulated AMPAR internalization, of which we could validate the involvement of Itsn1. We anticipate that our quantitative dataset on protein phosphorylation and translation in response to group I mGluR activation can be used as a rich resource for further analyses.

Acknowledgements

A.F.M.A. is supported by the Netherlands Organization for Scientific Research (NWO) through a VIDI grant (723.012.102). This research was part of the Netherlands X-omics Initiative and partially funded by NWO, project 184.034.019. H.D.M. is supported by the NWO through a ALW-Open grant (ALWOP.191), by the European Research Council (ERC starting grant 71601) and received support from a FEBS Return-to-Europe fellowship and a NARSAD Young Investigator Award. C.C.H. is supported by the NWO (NWO-ALW-VICI 865.10.010), the Netherlands Organization for Health Research and Development (ZonMW-TOP 91213017 and 91215084) and the European Research Council (ERC) (ERC Consolidator grant 617050).

Data availability

The mass spectrometry proteomics data have been deposited to the ProteomeXchange Consortium via the PRIDE partner repository with the dataset identifier PXD014043. The mass spectrometry SRM data have been deposited to the ProteomeXchange Consortium via Panorama Public (https://panoramaweb.org/23Gtf2.url) the with the dataset identifier PXD020777.

Author contributions

C.A.G.H.G. and R.P. designed and conducted proteomics sample preparation, and performed the quantitative proteomics experiments and analyzed the data; H.M.G. and L.C. designed and performed functional kinase blocker and knockdown experiments and analyzed the data. A.F.M.A. supervised the quantitative proteomics experimental setup and the mass spectrometry data. T.S.V. designed and performed the SRM experiments. The figures were designed and assembled by R.P., C.A.G.H.G., H.M.G., A.F.M.A., and C.C.H. The manuscript was written by R.P., C.A.G.H.G., H.M.G., and A.F.M.A. with input from C.C.H. A.F.M.A. and H.M.G. supervised the project and coordinated the study. Authors declare no competing financial interests.

References

1. Bhakar, A. L., Dolen, G. & Bear, M. F. The pathophysiology of fragile X (and what it teaches us about synapses). Annu. Rev. Neurosci. 35, 417–443 (2012).

2. Nicoletti, F. et al. Metabotropic glutamate receptors: from the workbench to the bedside. Neuropharmacology 60, 1017–1041 (2011).

3. Niswender, C. M. & Conn, P. J. Metabotropic glutamate receptors: physiology, pharmacology, and disease. Annu. Rev. Pharmacol. Toxicol. 50, 295–322 (2010).

4. Bashir, Z. I. et al. Induction of LTP in the hippocampus needs synaptic activation of glutamate metabotropic receptors. Nature 363, 347–350 (1993).

5. Bellone, C., Luscher, C. & Mameli, M. Mechanisms of synaptic depression triggered by metabotropic glutamate receptors. Cell. Mol. Life Sci. 65, 2913–2923 (2008).

6. Bortolotto, Z. A., Bashir, Z. I., Davies, C. H. & Collingridge, G. L. A molecular switch activated by metabotropic glutamate receptors regulates induction of long-term potentiation. Nature 368, 740–743 (1994).

7. Hu, J. H. et al. Homeostatic scaling requires group I mGluR activation mediated by Homer1a. Neuron 68, 1128–1142 (2010).

8. Popkirov, S. G. & Manahan-Vaughan, D. Involvement of the metabotropic glutamate receptor mGluR5 in NMDA receptor-dependent, learning-facilitated long-term depression in CA1 synapses. Cereb. cortex (New York, N.Y. 1991) 21, 501–509 (2011).

9. Luscher, C. & Huber, K. M. Group 1 mGluR-dependent synaptic long-term depression: mechanisms and implications for circuitry and disease. Neuron 65, 445–459 (2010).

10. Huber, K. M., Kayser, M. S. & Bear, M. F. Role for rapid dendritic protein synthesis in hippocampal mGluR-dependent long-term depression. Science 288, 1254–1257 (2000).

11. Moult, P. R., Correa, S. A., Collingridge, G. L., Fitzjohn, S. M. & Bashir, Z. I. Co-activation of p38 mitogen-activated protein kinase and protein tyrosine phosphatase underlies metabotropic glutamate receptor-dependent long-term depression. J. Physiol. 586, 2499–2510 (2008).

12. Nosyreva, E. D. & Huber, K. M. Developmental switch in synaptic mechanisms of hippocampal metabotropic glutamate receptor-dependent long-term depression. J. Neurosci. 25, 2992–3001 (2005).

13. Li, X. M. et al. JNK1 contributes to metabotropic glutamate receptor-dependent long-term depression and short-term synaptic plasticity in the mice area hippocampal CA1. Eur. J. Neurosci. 25, 391–396 (2007).

14. Liu, F. et al. Regulation of cyclin-dependent kinase 5 and casein kinase 1 by metabotropic glutamate receptors. Proc. Natl. Acad. Sci. U. S. A. 98, 11062–11068 (2001).

15. Bolshakov, V. Y., Carboni, L., Cobb, M. H., Siegelbaum, S. A. & Belardetti, F. Dual MAP kinase pathways mediate opposing forms of long-term plasticity at CA3-CA1 synapses. Nat. Neurosci. 3, 1107–1112 (2000).

16. Gallagher, S. M., Daly, C. A., Bear, M. F. & Huber, K. M. Extracellular signal-regulated protein kinase activation is required for metabotropic glutamate receptor-dependent long-term depression in hippocampal area CA1. J. Neurosci. 24, 4859–4864 (2004).

17. Rush, A. M., Wu, J., Rowan, M. J. & Anwyl, R. Group I metabotropic glutamate receptor (mGluR)-dependent long-term depression mediated via p38 mitogen-activated protein kinase is inhibited by previous high-frequency stimulation and activation of mGluRs and protein kinase C in the rat dentate gyrus in . J. Neurosci. 22, 6121–6128 (2002).

18. Hou, L. & Klann, E. Activation of the phosphoinositide 3-kinase-Akt-mammalian target of rapamycin signaling pathway is required for metabotropic glutamate receptor-dependent long-term depression. J. Neurosci. 24, 6352–6361 (2004).

19. Ronesi, J. A. & Huber, K. M. Homer interactions are necessary for metabotropic glutamate receptor-induced long-term depression and translational activation. J. Neurosci. 28, 543–547 (2008).

20. Rong, R. et al. PI3 kinase enhancer-Homer complex couples mGluRI to PI3 kinase, preventing neuronal apoptosis. Nat. Neurosci. 6, 1153–1161 (2003).
21. Banko, J. L., Hou, L., Poulin, F., Sonenberg, N. & Klann, E. Regulation of eukaryotic initiation factor 4E by converging signaling pathways during metabotropic glutamate receptor-dependent long-term depression. J. Neurosci. 26, 2167–2173 (2006).
22. Waung, M. W. & Huber, K. M. Protein translation in synaptic plasticity: mGluR-LTD, Fragile X. Curr. Opin. Neurobiol. 19, 319–326 (2009).
23. Purgert, C. A. et al. Intracellular mGluR5 Can Mediate Synaptic Plasticity in the Hippocampus. J. Neurosci. 34, 4589–4598 (2014).
24. Nakase, I., Kobayashi, N. B., Takatani-Nakase, T. & Yoshida, T. Active macropinocytosis induction by stimulation of epidermal growth factor receptor and oncogenic Ras expression potentiates cellular uptake efficacy of exosomes. Sci. Rep. 5, 10300 (2015).
25. MacGillavry, H. D., Song, Y., Raghavachari, S. & Blanpied, T. A. Nanoscale Scaffolding Domains within the Postsynaptic Density Concentrate Synaptic AMPA Receptors. Neuron 78, 615–622 (2013).
26. Shepherd, J. D. & Huganir, R. L. The Cell Biology of Synaptic Plasticity: AMPA Receptor Trafficking. Annu. Rev. Cell Dev. Biol. 23, 613–643 (2007).
27. Davidkova, G. & Carroll, R. C. Characterization of the role of microtubule-associated protein 1B in metabotropic glutamate receptor-mediated endocytosis of AMPA receptors in hippocampus. J. Neurosci. 27, 13273–13278 (2007).
28. Nadif Kasri, N., Nakano-Kobayashi, A. & Van Aelst, L. Rapid synthesis of the X-linked mental retardation protein OPHN1 mediates mGluR-dependent LTD through interaction with the endocytic machinery. Neuron 72, 300–315 (2011).
29. Waung, M. W., Pfeiffer, B. E., Nosyreva, E. D., Ronesi, J. A. & Huber, K. M. Rapid translation of Arc/Arg3.1 selectively mediates mGluR-dependent LTD through persistent increases in AMPAR endocytosis rate. Neuron 59, 84–97 (2008).
30. Zhang, Y. et al. The tyrosine phosphatase STEP mediates AMPA receptor endocytosis after metabotropic glutamate receptor stimulation. J. Neurosci. 28, 10561–10566 (2008).
31. Eichelbaum, K., Winter, M., Berriel Diaz, M., Herzig, S. & Krijgsveld, J. Selective enrichment of newly synthesized proteins for quantitative secretome analysis. Nat. Biotechnol. 30, 984–990 (2012).
32. Anggono, V. & Huganir, R. L. Regulation of AMPA receptor trafficking and synaptic plasticity. Curr. Opin. Neurobiol. 22, 461–469 (2012).
33. Dieterich, D. C., Link, A. J., Graumann, J., Tirrell, D. A. & Schuman, E. M. Selective identification of newly synthesized proteins in mammalian cells using bioorthogonal noncanonical amino acid tagging (BONCAT). Proc. Natl. Acad. Sci. U. S. A. 103, 9482–9487 (2006).
34. Koopmans, F., van Nierop, P., Andres-Alonso, M., Byrnes, A. & Cijsouw, T. SynGO: An Evidence-Based, Expert-Curated Knowledge Base for the Synapse. Neuron 103, 1–18 (2019).
35. Friocourt, G. et al. Doublecortin interacts with μ subunits of clathrin adaptor complexes in the developing nervous system. Mol. Cell. Neurosci. 18, 307–319 (2001).
36. Sanderson, T. M., Hogg, E. L., Collingridge, G. L. & Corrêa, S. A. L. Hippocampal metabotropic glutamate receptor long-term depression in health and disease: focus on mitogen-activated protein kinase pathways. J. Neurochem. 139, 200–214 (2016).
37. Zhou, Z., Hu, J., Passafaro, M., Xie, W. & Jia, Z. GluA2 (GluR2) regulates metabotropic glutamate receptor-dependent long-term depression through N-cadherin-dependent and cofilin-mediated actin reorganization. J. Neurosci. 31, 819–833 (2011).
38. Bayés, À. et al. Comparative study of human and mouse postsynaptic proteomes finds high compositional conservation and abundance differences for key synaptic proteins. PLoS One 7, e46683 (2012).
39. Heo, S. et al. Identification of long-lived synaptic proteins by proteomic analysis of synaptosome protein turnover. Proc. Natl. Acad. Sci. U. S. A. 115, E3827–E3836 (2018).
40. Szklarczyk, D. et al. STRING v10: protein–protein interaction networks,

integrated over the tree of life. Nucleic Acids Res. 43, D447–D452 (2014).
41. Montojo, J. et al. GeneMANIA Cytoscape plugin: fast gene function predictions on the desktop. Bioinformatics 26, 2927–2928 (2010).
42. Frydman, J. Folding of newly translated proteins in vivo: the role of molecular chaperones. Annu. Rev. Biochem. 70, 603–647 (2001).
43. Klein, M. E., Castillo, P. E. & Jordan, B. A. Coordination between Translation and Degradation Regulates Inducibility of mGluR-LTD. Cell Rep. 10, 1459–1466 (2015).
44. Ramachandran, K. V & Margolis, S. S. A mammalian nervous-system-specific plasma membrane proteasome complex that modulates neuronal function. Nat. Struct. Mol. Biol. (2017). doi:10.1038/nsmb.3389 [doi]
45. Sluchanko, N. N. & Gusev, N. B. 14-3-3 proteins and regulation of cytoskeleton. Biochem. 75, 1528–1546 (2010).
46. Humphrey, S. J., Azimifar, S. B. & Mann, M. High-throughput phosphoproteomics reveals in vivo insulin signaling dynamics. Nat. Biotechnol. 33, 990–995 (2015).
47. Villén, J. & Gygi, S. P. The SCX/IMAC enrichment approach for global phosphorylation analysis by mass spectrometry. Nat. Protoc. 3, 1630–1638 (2008).
48. Zarei, M., Sprenger, A., Metzger, F., Gretzmeier, C. & Dengjel, J. Comparison of ERLIC-TiO2, HILIC-TiO2, and SCX-TiO2 for global phosphoproteomics approaches. J. Proteome Res. 10, 3474–3483 (2011).
49. Post, H. et al. Robust, Sensitive, and Automated Phosphopeptide Enrichment Optimized for Low Sample Amounts Applied to Primary Hippocampal Neurons. J. Proteome Res. 16, 728–737 (2017).
50. Ye, J. et al. Optimized IMAC-IMAC protocol for phosphopeptide recovery from complex biological samples. J. Proteome Res. 9, 3561–3573 (2010).
51. Rigbolt, K. T., Vanselow, J. T. & Blagoev, B. GProX, a user-friendly platform for bioinformatics analysis and visualization of quantitative proteomics data. Mol. Cell. Proteomics 10, O110.007450 (2011).
52. Collingridge, G. L., Peineau, S., Howland, J. G. & Wang, Y. T. Long-term depression in the CNS. Nat. Rev. Neurosci. 11, 459 (2010).
53. Gladding, C. M., Fitzjohn, S. M. & Molnár, E. Metabotropic Glutamate Receptor-Mediated Long-Term Depression: Molecular Mechanisms. Pharmacol. Rev. 61, 395–412 (2009).
54. Moult, P. R. et al. Tyrosine phosphatases regulate AMPA receptor trafficking during metabotropic glutamate receptor-mediated long-term depression. J. Neurosci. 26, 2544–2554 (2006).
55. Sugawara, T., Hisatsune, C., Miyamoto, H., Ogawa, N. & Mikoshiba, K. Regulation of spinogenesis in mature Purkinje cells via mGluR/PKC-mediated phosphorylation of CaMKIIβ. Proc. Natl. Acad. Sci. 201617270 (2017). doi:10.1073/pnas.1617270114
56. Hizli, A. A. et al. Phosphorylation of Eukaryotic Elongation Factor 2 (eEF2) by Cyclin A–Cyclin-Dependent Kinase 2 Regulates Its Inhibition by eEF2 Kinase. Mol. Cell. Biol. 33, 596–604 (2013).
57. Park, S. et al. Elongation factor 2 and fragile X mental retardation protein control the dynamic translation of Arc/Arg3.1 essential for mGluR-LTD. Neuron 59, 70–83 (2008).
58. Rumbaugh, G., Adams, J. P., Kim, J. H. & Huganir, R. L. SynGAP regulates synaptic strength and mitogen-activated protein kinases in cultured neurons. Proc. Natl. Acad. Sci. U. S. A. 103, 4344–4351 (2006).
59. Walkup 4th, W. G. et al. Phosphorylation of synaptic GTPase-activating protein (synGAP) by Ca2+/calmodulin-dependent protein kinase II (CaMKII) and cyclin-dependent kinase 5 (CDK5) alters the ratio of its GAP activity toward Ras and Rap GTPases. J. Biol. Chem. 290, 4908–4927 (2015).
60. Li, J. et al. Long-term potentiation modulates synaptic phosphorylation networks and reshapes the structure of the postsynaptic interactome. Sci. Signal. 9, rs8 (2016).
61. Derkach, V. A., Oh, M. C., Guire, E. S. & Soderling, T. R. Regulatory mechanisms of AMPA receptors in synaptic plasticity. Nat. Rev. Neurosci. 8, 101 (2007).
62. Henley, J. M. & Wilkinson, K. A. Synaptic AMPA receptor composition in development, plasticity and disease. Nat. Rev. Neurosci. 17, 337 (2016).
63. Quan, A. et al. Phosphorylation of syndapin I F-BAR domain at two helix-

capping motifs regulates membrane tubulation. Proc. Natl. Acad. Sci. U. S. A. 109, 3760–3765 (2012).
64. Anggono, V. et al. PICK1 interacts with PACSIN to regulate AMPA receptor internalization and cerebellar long-term depression. Proc. Natl. Acad. Sci. U. S. A. 110, 13976–13981 (2013).
65. Mayhew, M. W. et al. Identification of phosphorylation sites in betaPIX and PAK1. J. Cell Sci. 120, 3911–3918 (2007).
66. Pechstein, A. et al. Regulation of synaptic vesicle recycling by complex formation between intersectin 1 and the clathrin adaptor complex AP2. Proc. Natl. Acad. Sci. U. S. A. 107, 4206–4211 (2010).
67. Yu, Y. et al. Mice deficient for the chromosome 21 ortholog Itsn1 exhibit vesicle-trafficking abnormalities. Hum. Mol. Genet. 17, 3281–3290 (2008).
68. Glodowski, D. R., Chen, C. C., Schaefer, H., Grant, B. D. & Rongo, C. RAB-10 regulates glutamate receptor recycling in a cholesterol-dependent endocytosis pathway. Mol. Biol. Cell 18, 4387–4396 (2007).
69. Errico, A., Deshmukh, K., Tanaka, Y., Pozniakovsky, A. & Hunt, T. Identification of substrates for cyclin dependent kinases. Adv. Enzyme Regul. 50, 375–399 (2010).
70. Gaestel, M. MAPKAP kinases - MKs - two's company, three's a crowd. Nat. Rev. cell Biol. 7, 120–130 (2006).
71. Stokoe, D., Caudwell, B., Cohen, P. T. & Cohen, P. The substrate specificity and structure of mitogen-activated protein (MAP) kinase-activated protein kinase-2. Biochem. J. 296 (Pt 3, 843–849 (1993).
72. Schmidlin, T. et al. High-Throughput Assessment of Kinome-wide Activation States. Cell Syst. 9, 366-374.e5 (2019).
73. Plattner, F., Giese, K. P. & Angelo, M. Involvement of Cdk5 in Synaptic Plasticity, and Learning and Memory. in Cyclin Dependent Kinase 5 (Cdk5) 227–260 (Springer US, 2008). doi:10.1007/978-0-387-78887-6_16
74. Contreras-Vallejos, E. et al. Searching for Novel Cdk5 Substrates in Brain by Comparative Phosphoproteomics of Wild Type and Cdk5−/− Mice. PLoS One 9, e90363 (2014).
75. Ramakers, G. M., Heinen, K., Gispen, W. H. & de Graan, P. N. Long term depression in the CA1 field is associated with a transient decrease in pre- and postsynaptic PKC substrate phosphorylation. J. Biol. Chem. 275, 28682–28687 (2000).
76. Han, M.-H. et al. The Novel Caspase-3 Substrate Gap43 is Involved in AMPA Receptor Endocytosis and Long-Term Depression. Mol. Cell. Proteomics 12, 3719–3731 (2013).
77. Hussain, N. K. et al. Endocytic protein intersectin-l regulates actin assembly via Cdc42 and N-WASP. Nat. Cell Biol. 3, 927–932 (2001).
78. Thomas, S. et al. Intersectin regulates dendritic spine development and somatodendritic endocytosis but not synaptic vesicle recycling in hippocampal neurons. J. Biol. Chem. 284, 12410–12419 (2009).
79. Kenney, J. W. et al. Eukaryotic elongation factor 2 kinase regulates the synthesis of microtubule-related proteins in neurons. J. Neurochem. 136, 276–284 (2016).
80. Schanzenbächer, C. T., Sambandan, S., Langer, J. D. & Schuman, E. M. Nascent Proteome Remodeling following Homeostatic Scaling at Hippocampal Synapses. Neuron 92, 358–371 (2016).
81. Thomas, G. M. & Huganir, R. L. MAPK cascade signalling and synaptic plasticity. Nat. Rev. Neurosci. 5, 173 (2004).
82. Ramakers, G. J. et al. Dysregulation of Rho GTPases in the alphaPix/Arhgef6 mouse model of X-linked intellectual disability is paralleled by impaired structural and synaptic plasticity and cognitive deficits. Hum. Mol. Genet. 21, 268–286 (2012).
83. Bidinosti, M. et al. CLK2 inhibition ameliorates autistic features associated with SHANK3 deficiency. Science 351, 1199–1203 (2016).
84. O'Connor, E. C., Bariselli, S. & Bellone, C. Synaptic basis of social dysfunction: a focus on postsynaptic proteins linking group-I mGluRs with AMPARs and NMDARs. Eur. J. Neurosci. 39, 1114–1129 (2014).
85. Fitzjohn, S. M. et al. A characterisation of long-term depression induced by metabotropic glutamate receptor activation in the rat hippocampus in vitro. J. Physiol. 537, 421–430 (2001).
86. Schnabel, R., Kilpatrick, I. C. & Collingridge, G. L. An investigation into

signal transduction mechanisms involved in DHPG-induced LTD in the CA1 region of the hippocampus. Neuropharmacology 38, 1585–1596 (1999).
87. Hu, J. H. et al. Preso1 dynamically regulates group I metabotropic glutamate receptors. Nat. Neurosci. 15, 836–844 (2012).
88. Li, C. et al. The different roles of cyclinD1-CDK4 in STP and mGluR-LTD during the postnatal development in mice hippocampus area CA1. BMC Dev. Biol. 7, 57 (2007).
89. Nakamura, Y. et al. PICK1 inhibition of the Arp2/3 complex controls dendritic spine size and synaptic plasticity. EMBO J. 30, 719–730 (2011).
90. Barnes, S. A. et al. Convergence of Hippocampal Pathophysiology in Syngap+/- and Fmr1-/y Mice. J. Neurosci. 35, 15073–15081 (2015).
91. Zheng, N., Jeyifous, O., Munro, C., Montgomery, J. M. & Green, W. N. Synaptic activity regulates AMPA receptor trafficking through different recycling pathways. Elife 4, 10.7554/ eLife.06878 (2015).
92. Cox, J. & Mann, M. MaxQuant enables high peptide identification rates, individualized p.p.b.-range mass accuracies and proteome-wide protein quantification. Nat. Biotechnol. 26, 1367–1372 (2008).
93. Tyanova, S. et al. The Perseus computational platform for comprehensive analysis of (prote)omics data. Nat. Methods 13, 731–740 (2016).
94. Crooks, G. E., Hon, G., Chandonia, J. M. & Brenner, S. E. WebLogo: a sequence logo generator. Genome Res. 14, 1188–1190 (2004).
95. Schneider, T. D. & Stephens, R. M. Sequence logos: a new way to display consensus sequences. Nucleic Acids Res. 18, 6097–6100 (1990).
96. Chou, M. F. & Schwartz, D. Biological sequence motif discovery using motif-x. Curr. Protoc. Bioinforma. Chapter 13, Unit 13.15-24 (2011).
97. Schwartz, D. & Gygi, S. P. An iterative statistical approach to the identification of protein phosphorylation motifs from large-scale data sets. Nat. Biotechnol. 23, 1391–1398 (2005).
98. de Graaf, E. L. et al. Signal Transduction Reaction Monitoring Deciphers Site-Specific PI3K-mTOR/ MAPK Pathway Dynamics in Oncogene-Induced Senescence. J. Proteome Res. 14, 2906–2914 (2015).

Supplemental figures

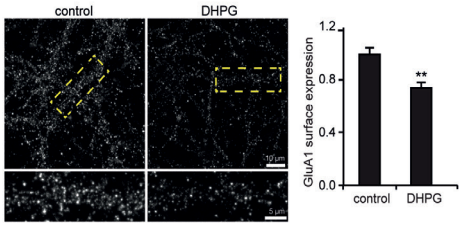

Figure S1. DHPG induces mGluR-LTD. DHPG stimulation induces significant GluA1 internalization. Data are represented as mean±SEM. ** p<0.01.

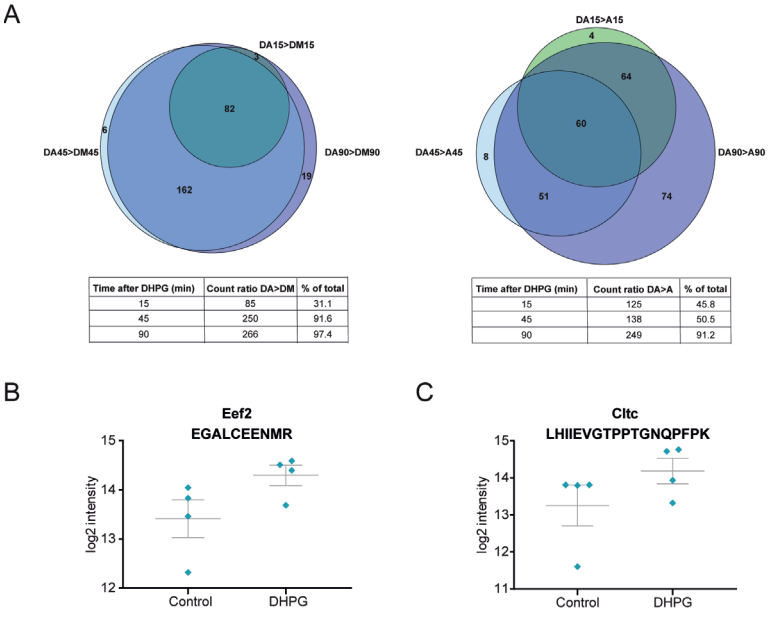

Time after DHPG (min)	Count ratio DA>DM	% of total
15	85	31.1
45	250	91.6
90	266	97.4

Time after DHPG (min)	Count ratio DA>A	% of total
15	125	45.8
45	138	50.5
90	249	91.2

Figure S2. Evaluation of the AHA & TMT dataset. **(A)** Venn diagrams showing the overlap of proteins identified in the different experimental conditions. As expected, the number of translated proteins increases over time, and the vast majority of proteins identified are stably identified among all studied time points. **(B,C)** Intensity of Eef2 and Cltc in control samples, and 5 minutes after DHPG stimulation, as measured by SRM. DA – DHPG and AHA, DM – DHPG and methionine, A – AHA only.

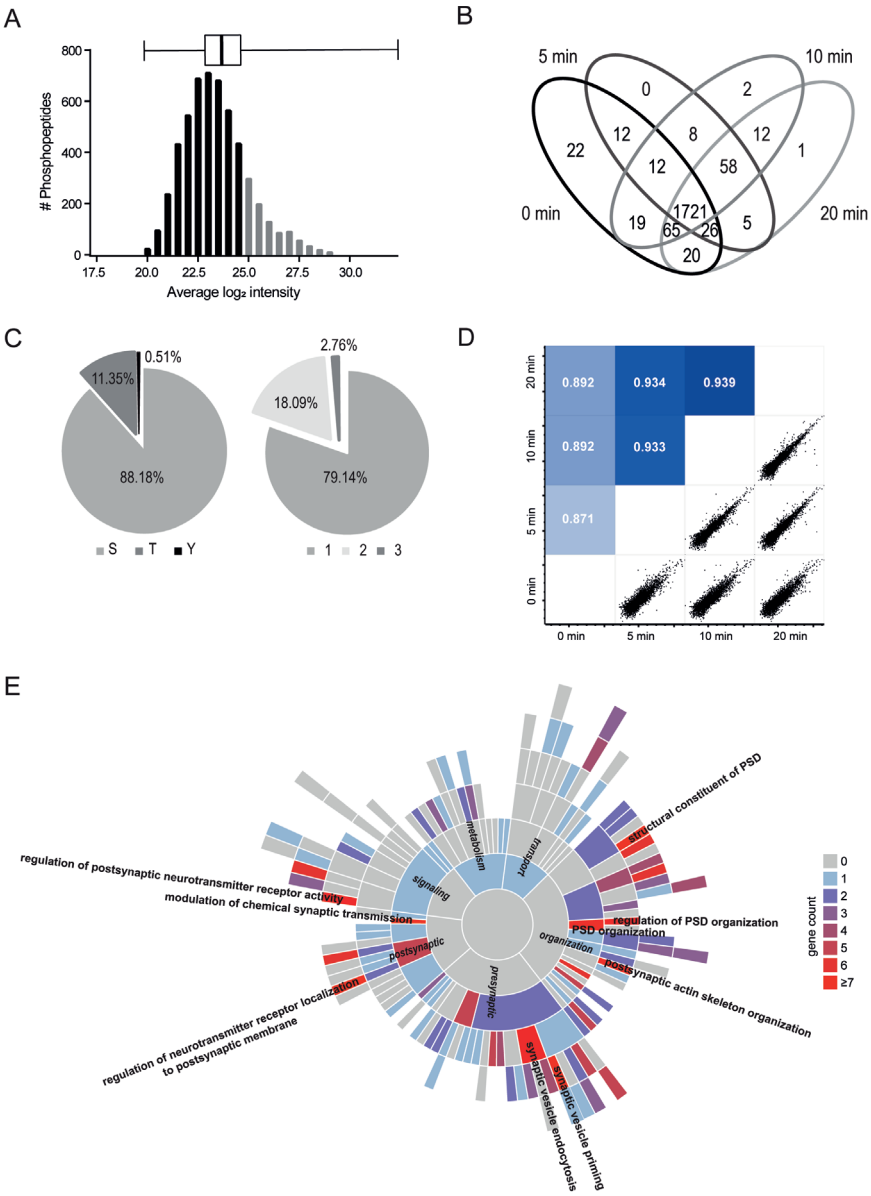

Figure S3. Evaluation of the phosphoproteomics dataset. **(A)** Distribution of phosphopeptide abundance, displaying normal distribution. Light grey bars indicate the top 25% most abundant phosphopeptides. **(B)** Venn diagram of the overlap between proteins identified in the 5, 10, and 20 minutes LTD experiment, as well as the control condition. Biological replicates were combined. **(C)** Percentages of enriched serine, threonine, and tyrosine phosphosites, and the distribution of singly, doubly and triply phosphorylated peptides. **(D)** Heatmap of Pearson correlations and correlation plots for the different biological replicates in the DHPG stimulated and control samples, showing high quantitative reproducibility between all measurements. **(E)** SynGO enrichment analysis of biological process. Processes with highest gene counts are labeled.

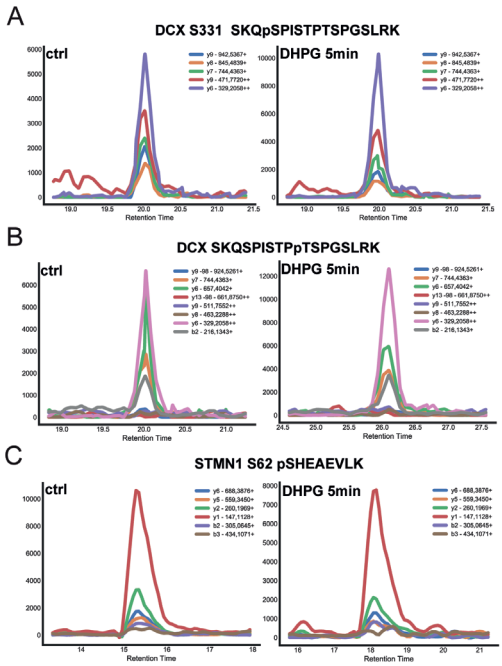

Figure S4. SRM validation of kinase phosphorylation. SRM traces of phosphorylated peptides indicating kinase activation in control samples, and 5 minutes after DHPG stimulation.

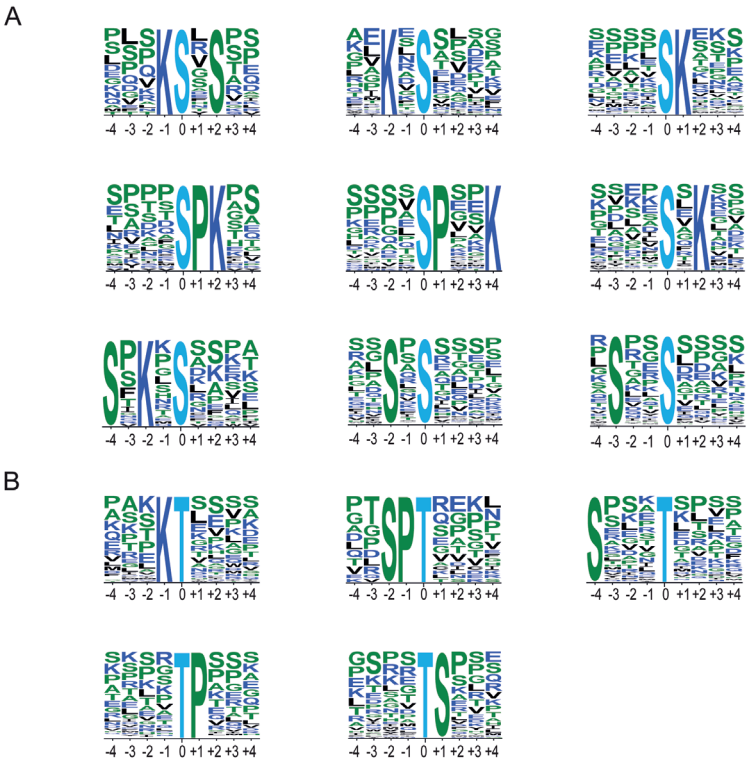

Figure S5. Phosphorylation sequence motifs. **(A)** Significantly enriched serine-directed phosphorylation motifs as generated with MotifX. **(B)** Significantly enriched threonine-directed phosphorylation motifs.

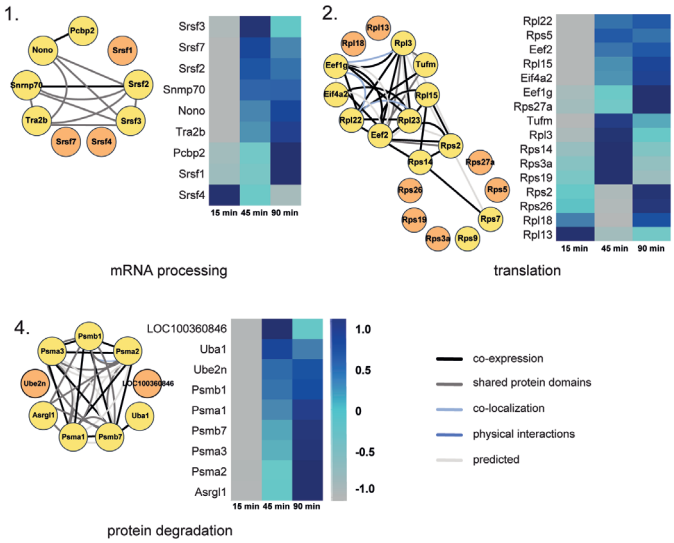

Figure S6. Supplemented interaction-based protein clusters of newly translated proteins. Protein clusters of enriched GO terms are displayed with their known interaction profiles (yellow), supplemented with less studied proteins from the translation dataset with similar function (orange). Heatmaps represent the z-score normalized ratio DHPG AHA / pool over the three measured time points.

Table S1. Overview of de novo synthesized proteins upon DHPG stimulation.

Table S2. Significantly regulated phosphorylation sites upon DHPG stimulation.

Supplemental tables can be downloaded from the online article.

Complementing the EGFR dynamic interactome using live cell proximity labeling

Charlotte AGH van Gelder[1,2], Wouter van Bergen[1,2], Pieter C van Breugel[1,2], and Maarten Altelaar[1,2]

[1]Biomolecular Mass Spectrometry and Proteomics, Bijvoet Center for Biomolecular Research and Utrecht Institute for Pharmaceutical Sciences, Utrecht University, The Netherlands, [2]Netherlands Proteomics Center, The Netherlands

Manuscript under revision

Abstract

The epidermal growth factor receptor (EGFR) is a member of the receptor tyrosine kinase family (RTK) of transmembrane receptors, known to regulate many key cellular processes, including growth, proliferation, and differentiation. Its expression, activation, trafficking, and degradation have been extensively studied, as dysregulation of EGFR activation has been linked to a vast number of cancers. Activation of EGFR by different ligands results in distinct cellular responses, and the relative distribution of EGFR in different endosome pools in a process called endosomal sorting, leading to lysosomal degradation, or cell surface recycling, respectively, is considered a fundamental process in EGFR stimulation outcome. The EGFR interactome is therefore an essential element in the study of RTK functional selectivity. Here, we aimed to complement the existing EGFR interactome with spatio-temporal information on EGFR, its interactors, and phosphorylation state. We identified and quantified EGFR stable and transient interactions at different time points after stimulation using an EGFR-APEX2 fusion construct expressed in HEK293T cells and were able to use bystander proteins to map EGFR subcellular location at each time point. Utilizing the fast and concise biotinylation of proximity proteins by APEX2, we were able to detect slight differences in early signaling kinetics between TGF-a and EGF, thereby increasing our knowledge on RTK signaling and differential trafficking.

Introduction

The epidermal growth factor receptor (EGFR) is a member of the receptor tyrosine kinase (RTK) family of transmembrane receptors, known to regulate many key cellular processes, including growth, proliferation, and differentiation 1. Its expression, activation, trafficking, and degradation have been extensively studied, as dysregulation of EGFR activation has been linked to a vast number of cancers[1,2]. Because of this, EGFR has become the model receptor, also representing lesser-studied growth factor RTKs[1].

On the extracellular domain, seven ligands are known to activate EGFR, resulting in receptor dimerization, autophosphorylation of the intracellular kinase domains, and subsequent internalization[1,3]. Interestingly, activation of EGFR by different ligands results in distinct cellular responses, which are not only regulated via differences in signal duration[4,5], but also modulation of protein-protein interactions (PPIs)[6], and the subcellular localization of the activated receptor[7–9]. More specifically, the relative distribution of EGFR in different endosome pools in a process called endosomal sorting, leading to lysosomal degradation, or cell surface recycling, respectively, is considered a fundamental process in EGFR stimulation outcome[3].

The EGFR interactome is therefore an essential element in the study of RTK functional selectivity. Classical affinity purification mass spectrometry (AP-MS) approaches, mainly antibody-based, are limited in detecting transient interactions, and do not convey any information on spatial and temporal behavior of the protein of interest, as they are often performed under non-physiological conditions[10,11]. Biotin-based proximity-labeling approaches, where the protein of interest is fused to either a promiscuous biotin ligase, or an engineered ascorbate peroxidase, can overcome these challenges[10,11]. In APEX2, an engineered ascorbate peroxidase is fused to the protein of interest, and introduced into the model system. Activation of APEX2 results in the rapid formation of biotin-phenoxy radicals within a selective 20 nm labeling radius. This fast and precise labeling in living cells allows for the generation of time-resolved 'snapshots' of the protein-of-interest's transient protein interactions, as well as subcellular location via the use of cellular compartment-specific proteins, so called 'bystander proteins'[12–14].

Recently, Francavilla *et al* published a time-resolved analysis of EGFR signaling using a multilayered proteomics approach to study interactome, phosphoproteome, ubiquitinome, and late proteome in response to differential activation with tumor growth factor alpha (TGF-a), and epidermal growth factor (EGF), respectively[3]. Here, we aimed to complement this existing EGFR interactome with spatio-temporal information on EGFR, its interactors, and phosphorylation state. We identified and quantified EGFR stable and transient interactions at different time points after stimulation using an EGFR-APEX2 fusion construct expressed in HEK293T cells and were able to use bystander proteins to map EGFR subcellular location at each time point. Utilizing the fast and concise biotinylation of proximity proteins by APEX2, we were able to detect slight differences in early signaling kinetics between TGF-a and EGF, thereby increasing our knowledge on RTK signaling and differential trafficking.

Materials and Methods

Cell culture

Human embryonic kidney 293 T-antigen (HEK293T) cells (ATCC) were cultured in Dulbecco's modified Eagle's medium (DMEM, Lonza) and supplemented with 10% fetal bovine serum (Thermo Fischer Scientific), 1% penicillin/streptomycin and L-glutamine in a humidified atmosphere with 5% CO_2 at 37 °C.

cDNA constructs and transient transfections

EGFR-GFP was a gift from Alexander Sorkin[15] (Addgene plasmid #32751). To generate the EGFR-APEX2 plasmid, the GFP moiety of pEGFR-eGFP was digested out with AgeI and NotI. APEX2, flanked with MreI and NotI restriction sites, was amplified using pcDNA3 Connexin43-GFP-APEX2 (Addgene #49385) as template. The resulting PCR product was digested with MreI and NotI and ligated into AgeI and NotI digested EGFR-eGFP, generating EGFR-APEX2. cDNA was introduced in HEK293T cells using jetPRIME transfection reagent (Polyplus) following manufacturer's protocol. In short, cells were plated at a confluency of 50-60%. For a 6-well plate format, 1 µg of DNA was introduced in 200 µl of jetPRIME buffer and 2 µl of jetPRIME reagent. Experiments were performed 24 to 48 hours after transfection.

APEX reaction and cell lysis

Cells were incubated with biotin phenol (BP, Iris Biotech) supplemented DMEM at a final concentration of 500 µM for 30 minutes at 37°C/5%CO_2. The APEX reaction was performed by introduction of 100 mM H_2O_2 (Merck) diluted in Dulbecco's phosphate buffered saline (DPBS, Lonza) to a final concentration of 1 mM for 60 seconds at room temperature. The reaction was quenched by addition of ice-cold quencher solution, consisting of 10 mM sodium ascorbate (Sigma Aldrich), 5 mM Trolox (Sigma Aldrich), and 10 mM sodium azide (Sigma) in DPBS for 20 minutes on ice. Cell pellets were collected and lysed in RIPA lysis buffer (50 mM TRIS-HCl pH 7.4, 150 mM NaCl, 0.1% sodium dodecyl sulfate, 0.1% sodium deoxycholate, and 1% Triton X-100) supplemented with 10 mM sodium ascorbate, 5 mM Trolox, 10 mM sodium azide, 1 mM PMSF (Sigma), and complete mini EDTA-free protease inhibitor cocktail (Roche). Cell lysates were sonicated for 12 rounds of 5s (Bioruptor, Diagenode) and spun down at 14,000 rpm for 10 minutes, after which supernatant was loaded onto streptavidin agarose resin (Thermo Scientific) overnight at 4 °C. Resin-bound proteins were washed twice with RIPA lysis buffer, one with 1M KCl, once with 0.1 Na_2CO_3, once with 2M urea in 10 mM Tris-HCl, and three times with 50 mM ammonium bicarbonate, respectively. Proteins were reduced with 4 mM DTT for 25 minutes at 56 °C and alkylated with 8 mM iodoacetamide for 30 minutes at room temperature in the dark. Samples were digested with LysC (1:200 enzyme substrate ratio) and trypsin (1:100) overnight at 37 °C, after which the reaction was quenched with 2% FA. Peptides were desalted using Oasis HLB columns (Waters), dried *in vacuo* and stored at -80 °C until further analysis.

LC-MS/MS

The enriched samples were analyzed with an UHPLC 1290 system (Agilent technologies) coupled to an Orbitrap Q Exactive HF X mass spectrometer

(Thermo Scientific). Before separation peptides were first trapped (Dr Maisch Reprosil C18, 3 µm, 2 cm x 100 µm) and then separated on an analytical column (Agilent Poroshell EC-C18, 2.7 µm, 50 cm x 75 µm). Trapping was performed for 5 min in solvent A (0.1% FA) and eluted with following gradient: 0 - 13% solvent B (0.1% FA in ACN) in 10s, 13 - 44% in 95 min, 44 - 100% in 3 min, and finally 100 % for 1 min. Flow was passively split to 300 nl/min. The mass spectrometer was operated in data-dependent mode. At a resolution of 35.000 m/z at 400 m/z, MS full scan spectra were acquired from m/z 375–1600 after accumulation to a target value of 3e6 with a maximum injection time of 20 ms. Up to 15 most intense precursor ions were selected for HCD fragmentation at a normalised collision energy of 27%, after the accumulation to a target value of 1e5. MS/MS was acquired at a resolution of 30,000, with an exclusion duration 16s. Charge state screening was enabled, and precursors with an unknown charge state or a charge state of 1 were excluded.

Data analysis

The raw data were analyzed using MaxQuant (version 1.6.3.4) for the identification and quantification of peptides and proteins[16]. Data were searched against a database containing SwissProt Human proteome (downloaded 10/2018). Variable modifications were methionine oxidation, protein N-terminus acetylation and biotinylation by biotin-phenol on tyrosine ($C_{18}H_{23}N_3O_3S$). A fixed modification was cysteine carbamidomethylation. The first search was performed with a mass accuracy of ± 20 ppm and the main search was performed with a mass accuracy of ± 4.5 ppm. A maximum of 5 modifications and 2 missed cleavages were allowed per peptide. The maximum charge was set to 7+. For MS/MS matching, the mass tolerance was set to 0.5 Da and the top 8 peaks per 100 Da were analyzed. MS/MS matching was allowed for higher charge states, water and ammonia loss. The false discovery rate was set to 0.01. The minimum peptide length was 7 amino acids. Match between runs was performed with a time window of 0.7 minutes. Quantification was done label free with the MaxQuant algorithm with minimal ratio label count 2 and including unique and razor peptides. Further analysis were performed using Perseus version 1.6.2.2[17], and Cytoscape[18] utilizing the GeneMANIA plugin[19].

Immunoblotting

Cell lysates were incubated with Quickstain Cy5 protein dye (GE Healthcare Bio-Sciences) for 30 minutes at room temperature, after which they were denatured and reduced in XT Sample buffer (Bio-rad) with 25 mM DTT at 95°C for 5 minutes. Proteins were separated on a 12% SDS-PAGE gel (Bio-rad) and electroblotted onto nitrocellulose membranes. Membranes were blocked in 5% non-fat milk in TBS with 0.1% Tween20 (TBS-T) and incubated with following antibodies: a-pEGFR Y1068 (1:500, Abcam), Streptavidin conjugated Alexafluor-488 (1:10,000, Invitrogen), a-rabbit horseradish peroxidase conjugate (1:2000, Dako). When multiple antibodies of the same origin were used, membranes were stripped using Restore PLUS Western Blot stripping buffer (Pierce). Detection was performed by enhanced chemiluminescent substrate (Pierce), or via fluorescence detection with the Amersham Imager 600 (GE Healthcare Bio-Sciences).

Immunofluorescence and confocal microscopy

Cells were plated onto poly-L-lysine coated glass 18 mm coverslips and cultured as normal. They were fixed with 4% paraformaldehyde / 4% sucrose in phosphate-buffered saline (PBS) for 10 minutes at room temperature. Fixed cells were blocked with 10% normal goat serum in PBS for 30 minutes at 37 °C, and stained with following antibodies: a-EGFR (1:50, Cell Signaling), a-rabbit Alexa fluor 488 (1:1000, Invitrogen), and Streptavidin conjugate Alexafluor-594 (1:2000, Invitrogen). Confocal images were taken with a Zeiss LSM 710 with 63x 1.40 oil objective. Images consist of a z-stack of 7-9 planes at 0.39 µm interval, and maximum intensity projections were generated for analysis and display.

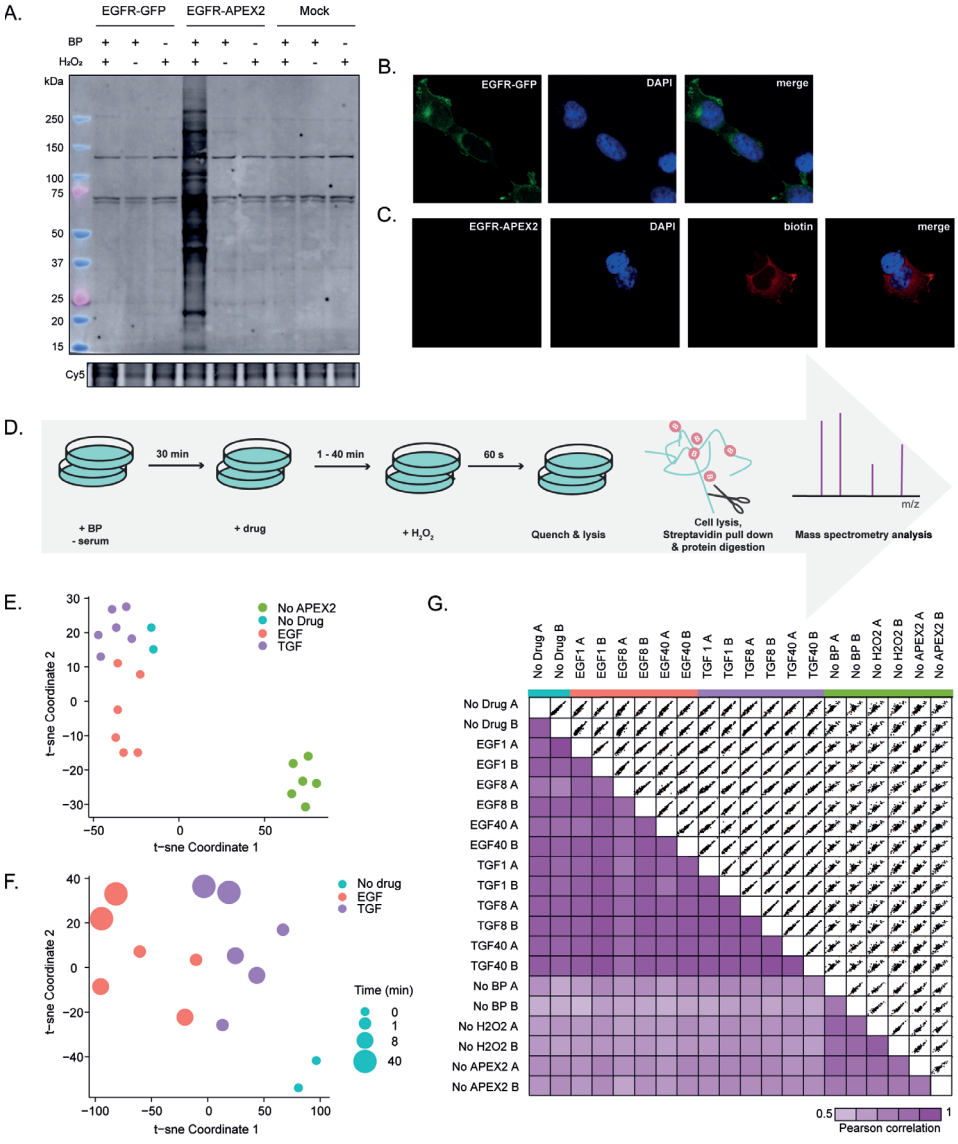

Figure 1. EGFR-APEX2 activation, localization, and data quality. **(A)** Western blot of biotinylated proteins in different 'APEX2' and 'No APEX2' conditions. Biotinylation only occurred with the APEX2 fusion construct present, after incubation with BP and subsequent stimulation with H2O2. Cy5 dye indicates protein loading. **(B)** Localization of the EGFR-GFP control construct. Expression is predominantly localized to the plasma membrane and ER. Cy5 dye indicates protein loading. **(C)** EGFR-APEX2 is localized similarly to the EGFR-GFP control construct, as the biotinylation pattern matches EGFR localization. **(D)** Experimental workflow and data quality. HEK293T cells were transfected with EGFR-APEX2 construct and incubated for 48 hours before the start of the experiment. At the start of the experiment, cell culture media was depleted from serum and supplemented with biotin phenol (BP). After 30 minutes, EGF or TGF-a was added. The APEX2 reaction was initiated by addition of H2O2, and quenched after 60 seconds, after which the cells were lysed. Biotinylated proteins were extracted from the cell lysate using streptavidin-coated beads, digested, and measured by mass spectrometry. **(E,F)** T-sne plot of all experimental conditions reveals a clear separation between 'APEX2' and 'No APEX2' conditions, as well as a defined separation of EGF and TGF-a treated samples over time, respectively. Pearson correlation plot displaying a high correlation between all 'APEX2' conditions, while 'no APEX2' and 'APEX2' conditions correlate significantly less.

Results & Discussion

EGFR-APEX2 is functional, specific, and localizes correctly

We first characterized the functionality of the newly fused EGFR-APEX2 fusion protein, where APEX2 was incorporated at the C-terminus of the EGFR. As a control, the well-characterized EGFR-eGFP control was used. First, we sought to assess the functionality of the APEX2 enzyme in the newly formed fusion protein. To address this, EGFR-APEX2 or EGFR-eGFP was introduced into HEK293T cells, and the activity of the enzyme was tested in presence of biotin phenol and H_2O_2. Western blot analysis of biotinylated proteins shows that EGFR-APEX2, and not the negative control constructs, causes biotinylation on proteins in a wide range of molecular weights. Moreover, biotinylation was exclusively observed in conditions where cells were pre-incubated with substrate (biotin-phenol) and activated with H_2O_2 (Figure 1A). Second, we assessed whether replacement of eGFP to APEX2 did not alter the functionality of the EGFR receptor. To this end, we placed the cells in starvation media without fetal bovine serum for 30 to 90 minutes and stimulated EGFR with EGF for 30 minutes. We then analyzed autophosphorylation of the receptor on tyrosine 1068 using western blot analysis and saw a clear increase in autophosphorylation after stimulation (Figure S1B), indicating that EGFR can still be activated in the presence of APEX2 at its cytoplasmic tail. Finally, we performed immunofluorescent staining experiments to visualize the localization of our fusion protein in HEK293T cells. We found that EGFR-eGFP localizes predominantly to the plasma membrane and that a smaller pool of receptors can be distinguished in the endoplasmic reticulum (Figure 1B). We observed very similar localization patterns for our EGFR-APEX2 fusion protein via visualization of biotinylated proteins, selectively in conditions where we performed the APEX2-driven biotinylation reaction (Figure 1C). Taken together, we concluded that EGFR-APEX2 was functional and suitable for further biological experiments.

Enrichment of biotinylated proteins leads to enrichment of proteins related to EGFR signaling

We sought to follow EGFR interactome dynamics upon stimulation with EGF and TGF-a. We therefore incubated HEK293T cells expressing EGFR-APEX2 with biotin-phenol (BP) in the absence of serum for 30 minutes, after which we stimulated with either EGF or TGF-a (100 ng/ml) for 1, 8, or 40 minutes. Then, we made snapshots of the EGFR interactome by addition of H_2O_2 for 60 seconds, after which the reaction was quenched and cell pellets were collected. An equal amount of cell lysate was loaded onto streptavidin-coated beads and incubated overnight to capture biotinylated proteins. After stringent washing steps, biotinylated proteins were digested off-bead and analyzed using LC-MS/MS (Figure 1D). Next to the two drug treatments, we included several 'no APEX2' negative control conditions, where we systematically excluded BP incubation, H_2O_2 stimulation, or both (Figure S1A). Visualization of all identified and quantified proteins (2,517) in a tSNE plot showed a clear separation between 'APEX2' and 'no APEX2' experimental conditions, as well as a separation between EGF, TGF-a, and unstimulated samples (Figure 2E,F). Additionally, we observed a high Pearson correlation between all 'APEX2' conditions, while 'no APEX2' and 'APEX2' conditions correlated significantly less (Figure 1G), confirming the selectivity and reproducibility of the biotin-based enrichment process.

Next, we filtered based on proteins that were identified in less than three conditions in either 'APEX2' or 'no APEX2' groups, resulting in more than 300 proteins uniquely identified in the 'APEX2' conditions (Figure 2A). Then, we tested which proteins had a significantly higher intensity profile in 'APEX2' versus the 'no APEX2' conditions (Figure 2B) and selected these proteins (fold change >2 and q-value <0.05) for further analysis, together with the 'APEX2' unique proteins, resulting in a total of 442 proteins. Among these proteins were many known EGFR interactors with significantly higher intensity in the 'APEX2' conditions, including EGFR itself, and the well-known EGFR signaling cascade proteins Grb2, and Plcg1, that are adaptor and second messenger proteins in the activation of the ras, and PKC signaling pathways, respectively. Moreover, three endogenously biotinylated proteins (Pcca, Acaca, and Pc) were much more intense in the 'no APEX2' conditions and therefore filtered out. Statistical overrepresentation analysis of Reactome pathways of the total pool of identified EGFR interactors confirmed a clear enrichment of EGF receptor and related signaling cascades (Figure 2C).

Phosphorylation of EGFR interactors

Since it is well known that EGFR signaling is highly dependent on tyrosine kinase activity, we examined to which extent we could see this reflected in our EGFR interactome datasets. To understand the extent of phosphorylation dynamics, we searched the RAW files for STY phosphorylated peptides and normalized the intensities of identified phosphosites to the relative protein ratio at each time point. Strikingly, we found that in our entire proteome dataset we identified 243 class I phosphosites (e.g. with a localization probability score higher than 0.75 and identified in at least two APEX2 replicates), corresponding to 132 unique proteins. If we consider the whole quantified proteome dataset (1,879 proteins), this results in 12.9% of our proteins being phosphorylated, all without specific phosphopeptide enrichment.

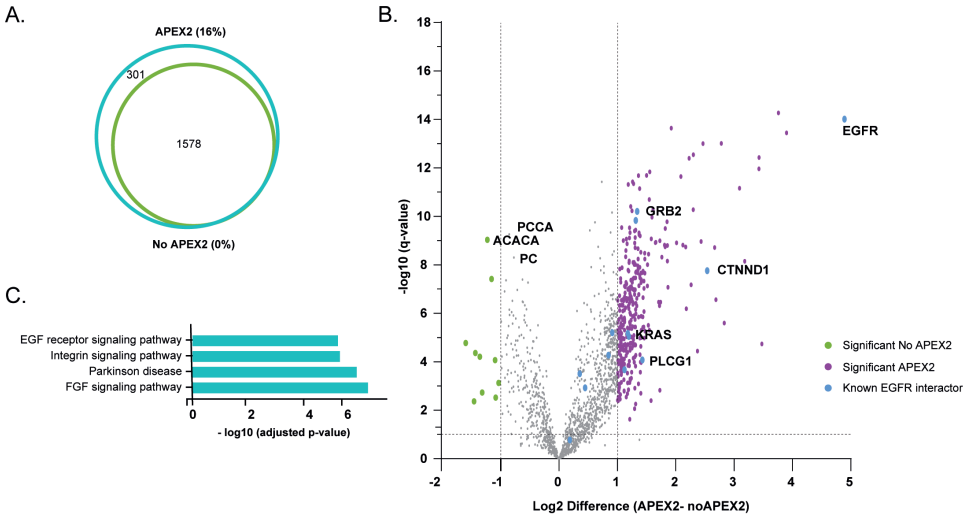

Figure 2. (A) Venn diagram illustrating the overlap in identified proteins in the 'APEX2' versus 'No APEX2' conditions. **(B)** Volcano plot of all 'APEX2' proteins versus 'No APEX2' proteins, where a clear skewed distribution of protein intensities and significance towards the 'APEX2' side can be observed, indicating the success of the enrichment strategy. **(C)** GO overrepresentation analysis showed a clear enrichment of EGFR-related biological processes amongst 'APEX2' proteins.

EGFR phosphorylation sites

Of our identified phosphosites, 41 were found to be significantly more abundant in the 'APEX2' conditions vs 'no APEX2' conditions, among which we identify three EGFR phosphorylation sites; S1166, Y1197, and T693. T693 (also often referred to as T669) is the major EGFR activation site after EGF stimulation, although it has also been shown to be constitutively active[19]. Phosphorylation is performed by p38 MAP kinase[20]. Y1197 is also known to be phosphorylated by MAP kinases upon EGF stimulation. S1166, as well as other serine and threonine phosphorylation sites located in the cytoplasmic tail of EGFR between amino acids 1047-1072, was shown to be phosphorylated by PKA, thereby positively regulation tyrosine kinase activity[21]. Altogether these results show that our EGFR-APEX2 approach is very efficient in monitoring EGFR activation, as all of these indicative phosphorylation sites have an over five times higher intensity in the 'APEX2' versus 'non-APEX2' conditions. The lack of identification of another major EGFR activation site, Y1068, which is routinely used to monitor EGFR activation in low throughput studies such as western blot analysis, can be explained by the utilized proteomics workflow. During sample preparation proteins were digested with Trypsin, with a high cleavage specificity for Lysine (K) and Arginine (R) on the N-terminal side, as indicated with the purple horizontal lines in Figure S2A. Since, in the following database search, typically only peptides with a length of maximum 25 amino acids are allowed, the peptide which contains Y1068 (indicated in the orange square) was not identified as it consists of 31 amino acids. However, searching with an extended amino acid range did indeed result in the confident identification and localization of the Y1068 activation site (Figure S2B).

Table 1. Significantly regulated phosphorylation sites in 'APEX2' upon EGFR stimulation. Phosphorylation sites with a log2 fold change >1 between EGF and TGF-a in at least one time point, or between EGF and/or TGF-a compared to control are included. Values represent log2 intensity differences between conditions.

Phosphosite	EGF 1min/ND	TGF-α 1min/ND	EGF/TGF-α 1 min	EGF/TGF-α 8 min	EGF/TGF-α 40 min
EIF5B_S66	1.97	0.99	0.98	0.07	0.36
BCLAF1_S512	-1.62	-0.73	-0.89	0.77	0.85
CHMP7_T391	0.74	0.49	0.24	-0.68	-1.69
CCDC38_S127	1.05	0.76	0.29	-0.56	0.06
NOP2_S732	1.12	0.12	1.00	0.52	1.10
TCOF1_S1228	0.38	-0.16	0.54	0.12	0.48
DDX21_S121	0.45	0.02	0.43	3.03	1.15
RRP1B_S245	1.19	0.96	0.23	0.47	0.72
NAV2_S503	2.16	-0.55	2.71	-1.58	1.78
TCOF1_S171	-0.34	0.35	-0.69	1.05	3.08
PER1_T164	-0.71	-1.70	0.99	-0.52	0.48
TOP2A_S1393	2.09	0.70	1.39	-0.69	0.23
SMARCA5_S66	1.59	1.17	0.42	0.94	-0.42
CHD4_S515	0.69	0.55	0.14	-0.54	1.41
PER1_Y167	-0.71	-1.73	1.02	-0.52	0.14
RRP1B_S732	-0.46	-1.01	0.55	-2.42	1.42
NOP56_S520	0.05	-0.16	0.21	1.78	1.53
ZMYM4_S1284	1.83	0.41	1.41	1.71	0.41
ZBTB40_S223	1.47	0.51	0.97	0.31	1.34
ECT2_T359	1.83	1.38	0.44	0.23	1.84
EIF4B_S459	-1.18	-1.34	0.16	-2.61	-1.63
MLLT4_S1275	0.31	-0.39	0.69	1.62	2.13
ABI1_S225	0.89	-0.99	1.89	1.54	2.49
EGFR_T693	1.82	1.71	0.11	0.30	0.55
DNAH7_S1252	2.49	0.22	2.27	1.73	1.91
EGFR_Y1197	0.67	0.19	0.48	-0.15	1.54

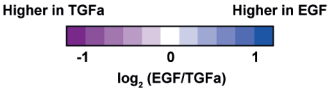

Phosphorylation dynamics upon EGFR stimulation

To identify which of these APEX2-enriched phosphorylation sites are biologically relevant in EGFR signaling dynamics, we further selected only those phosphorylation sites that showed a clear difference (at least two-fold) between EGF and TGF-a in at least one time point, or that showed a clear increase or decrease (at least two-fold) between either EGF and/ or TGF-a compared to the 'No Drug' control situation. The resulting 26 phosphorylation sites are displayed in Table 1.

We found two translation initiation factors with phosphorylation sites showing striking dynamical behavior over the time course and between the two treatment conditions. The S66 phosphorylation site of Eif5b is a known indicator of translation initiation, which, in our data, displayed very high initial activation in both EGF and TGF-a conditions, although with a much higher response in EGF-stimulated cells. This initial activation was followed by rapid de-phosphorylation at 8 minutes, which in turn was followed by re-phosphorylation at the latest time point, in both EGF and TGF-a treated cells. Eif4b displayed de-phosphorylation of S459, suggesting that de-phosphorylation of this site plays a role in the initiation of translation.

Interestingly, Eif4b remained dephosphorylated in EGF stimulated conditions over time, but conversely became phosphorylated in TGF-a conditions at later time points. Bclaf1 is a transcriptional repressor of survival genes. We observe rapid dephosphorylation in both EGF and TGF-a conditions, which hints towards activation of survival genes. Interestingly, re-phosphorylation at later time points is more pronounced in TGF-a than EGF conditions.

Temporal behavior of hallmark proteins

We next sought to identify differences in EGFR interactome dynamics between the two different stimulus conditions. We therefore investigated the behavior of three hallmark vesicle proteins over time. Rab5 is a marker of early endosomes. As internalization and early endosome encapsulation of EGFR is a common trafficking route after both EGF and TGF-a-induced EGFR activation, no bias in interaction levels is expected between the two different treatments. Indeed, the relative amount of Rab5 in close proximity to EGFR increases after both stimuli, and stabilizes after 8 minutes (Figure 3A, upper panel). As a marker of late endosomes, Rab7a is a validated indicator of protein degradation. Characteristically, the switch from Rab5 to Rab7a defines the evolution of early to late endosomes. Interestingly, we observe an initial decrease in Rab7a in the EGF treated samples compared to the TGF-a samples after 8 minutes of stimulation, which normalizes at the 40-minute time point (Figure 3A, middle panel). This unexpected difference in Rab7a localization pattern could not be explained by potential modification of the Rab7a peptides used for quantification; previous literature has shown that Rab7a undergoes multiple modifications (ubiquitination and phosphorylation) specifically in the early time points[3]. However, quantification of Rab7a in the current dataset was found not to be based on the peptides carrying earlier reported modifications. Finally, Rab11 is a marker of recycling endosomes, and can therefore be used as an example for TGF-a -mediated EGFR recycling, as the majority of EGFR recycles back to the plasma membrane upon stimulation (91% for TGF-a versus 22% in EGF-stimulated samples, respectively 3). In our data, we can indeed see a clear increase in proximity upon stimulation of the EGFR in the initial phase, which continues to increase over time for the TGF-a treated samples. In the EGF conditions however, we lose detection of Rab11 after 8 minutes, indicating that the amount of EGFR that is enclosed in Rab11 coated vesicles is below detection level (Figure 3A, lower panel). Taken together, these data clearly highlight the efficacy of the APEX2 proximity labeling protocol in deducing protein cellular location with the help of so called 'bystander' proteins.

Temporal behavior of other Rab and rap family proteins

Next to these well-established and characteristic Rab proteins, we identify several other Rab proteins. The Rab family of small GTPases are key players of intracellular membrane trafficking, regulating the formation of transport vesicles to their fusion with membranes[22]. Comparing the relative intensity of several, lesser studied members of the Rab family of proteins, as well as Ras-related GTP-binding proteins (Rap), between differential EGFR trafficking conditions, could yield relevant information on the function of these proteins. We therefore plotted the temporal behavior of all Rab and Rap proteins following TGF-a, and EGF stimulation, respectively (Figure 3B).

Rab1b and Rap1b intensities increase over time for TGF-a samples, while they are not detected, or very low abundant in the later time points for EGF-stimulated samples. As Rab1b recruitment to the Golgi is known to enhance vesicle secretion[23], it seems plausible that it facilitates receptor recycling towards the plasma membrane. Rap1b receptor binding promotes GABA receptor surface expression by facilitating receptor recycling[24], a pattern that fits TGF-a-induced EGFR trafficking. Other interesting observations include Rab3gap1 and Raph1, which are detected only after EGFR ligand activation. More specifically, both are absent in the control condition and readily detected after TGF-a addition followed by a steady increase over time. Conversely, both Rab3gap1 and Raph1 are detected after EGF stimulation only at the 8-minute time point, displaying a large difference in intensity. Rab3gap1 is the catalytic subunit of a GTPase activating protein with a high specificity for the Rab3 subfamily and converts active Rab3-GTP into its inactive form, Rab3-GDP. In synaptic vesicles, this inactivation of Rab3 results in clathrin-mediated endocytosis and recycling of these vesicles[25]. Raph1 is a known mediator of localized membrane signals, and a known interactor of Src and Abl1, and might therefore be implicated in early receptor endocytosis and cytoskeleton reorganization. Hence, both of these proteins have a likely role in the early stages of receptor endocytosis, a process that is more dominant and stable after TGF-a stimulation.

On the contrary, Rab13 seems to be more EGF-specific, as it is not detected upon TGF-a stimulation, while it increases steadily over time in the EGF conditions. Furthermore, Rap2b and Rabggta are highly abundant quickly after EGF receptor activation, and slowly decrease in intensity over time. After TGF-a stimulation, however, Rap2b is not detected in the earliest two time points. This is unexpected, as several reports describe Rap2b to be recruited by activated EGFR, thereby activating PLC-ε signaling and further downstream processes, although these data seem to be based on EGF-stimulated EGFR only[26,27]. Rabggta is a geranylgeranyl transferase and catalyzes the transfer of a geranylgeranyl lipid moiety to the c-terminus of certain Rab proteins, thereby anchoring them to their target membrane 28,29. Which membrane, however, remains unknown, and our data indicates that it might be preferentially involved in degradation-related vesicle-membranes. Overall, these data provide a good indication of the role of several lesser-studied vesicle-related proteins and give a first glance at their specificity towards different vesicle-types. Further validation studies are required for detailed characterization.

EGFR interactome significantly changes upon stimulation

We calculated the differences in protein intensity between EGF and TGF-a stimulated samples for each time point and performed Euclidean distance hierarchical clustering of all 'APEX2' proteins. In the resulting heatmap (Figure 3C) we can distinguish the relative abundance of EGFR interacting proteins in both the EGF and TGF-a conditions at the different time points, as the color scheme indicates the difference in intensity between both treatments. We can distinguish four main protein clusters, each with a distinct bias towards one of the ligands at one or more of the investigated time points. To get an indication of which proteins were noticeably biased towards one of the two signaling routes (i.e. EGF and TGF-a), we performed GO overrepresentation

analyses on cellular component (CC), biological function (BF), molecular function (MF), and Reactome Pathways (RP).

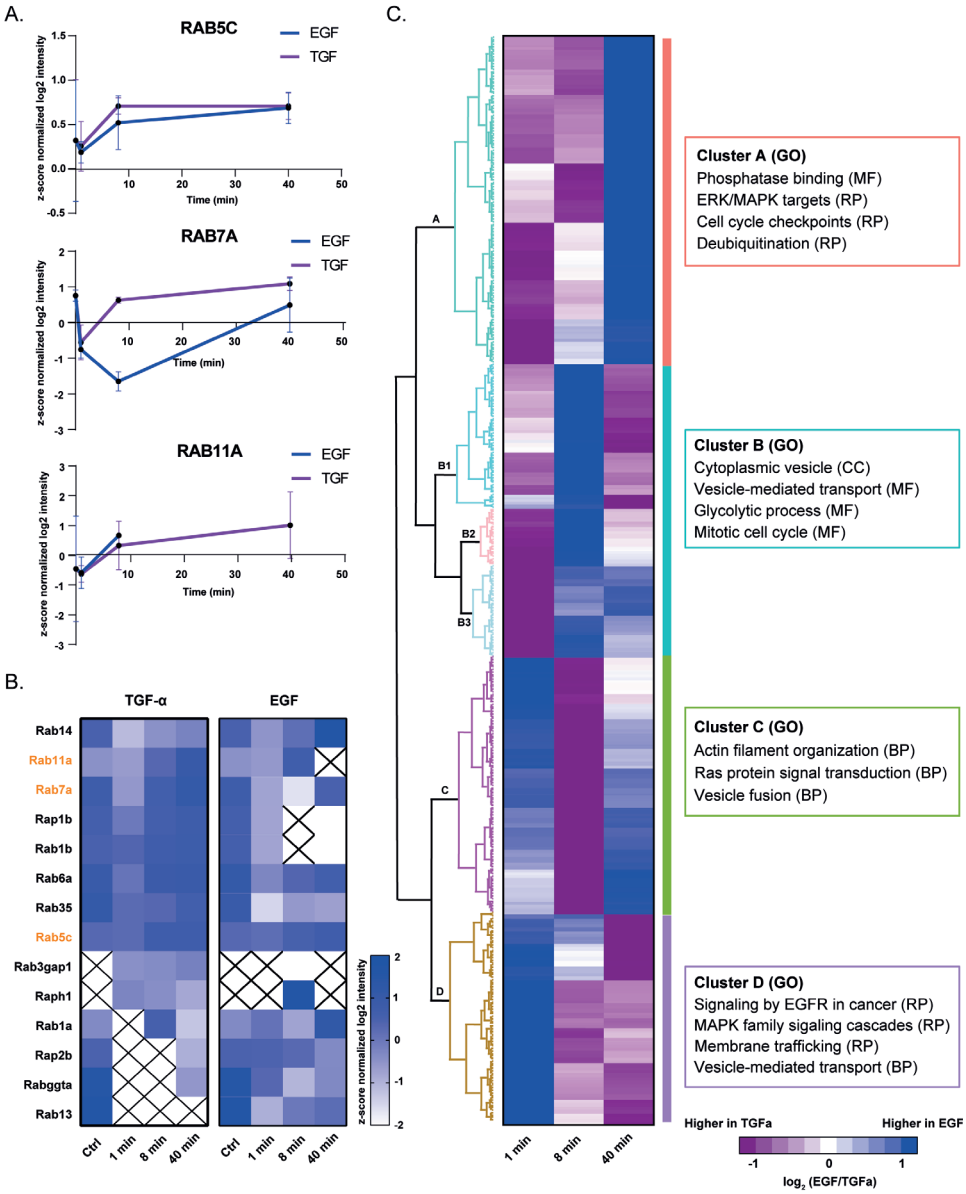

Figure 3. Stimulus-induced EGFR interactome perturbation. **(A)** Z-score normalized intensity plots of hallmark endosomal proteins following EGF and TGF-a stimulation, respectively, indicating the relative subcellular location of EGFR over different time points. **(B)** Temporal behavior of Rab family proteins yield information on vesicle-specificity and function. X – protein not identified at the specified time point. **(C)** Heatmap illustrating the differences in z-score normalized protein intensity between EGF and TGF-a stimulated samples for each time point. Hierarchical clustering based on Euclidean distance of all 'APEX2' proteins revealed four main clusters of proteins.

Cluster A contains proteins that are predominantly proximal to EGFR upon TGF-a stimulation at the early time points but shift towards EGF at the later time point. This was confirmed by GO enrichment analyses, where clear EGF-related terms are enriched, such as the dominant presence of ERK/MAPK targets. Moreover, EGF-related EGFR signaling termination was observed, as indicated by an enrichment in protein phosphatase 2 (PP2A) subunits. Activation of PP2A results in downregulation of both PI3K and MAPK pathways[30], both of which are classical EGF-related signaling pathways. Conversely, cluster D switches from EGF to TGF-a from 1 minute to 40 minutes and is therefore enriched in proteins from EGF-directed signaling pathways, including MAPK family signaling cascades. Also, proteins involved in vesicle-mediated transport and membrane trafficking are enriched, indicating TGF-a-characteristic receptor recycling and prolonged activation. Clusters B and C show a more dynamic behavior, where cluster B shifts from a bias in TGF-a at 1 minute to EGF after 8 minutes followed by an almost equal representation after 40 minutes, indicating that these proteins are active after EGFR stimulation with both TGF-a and EGF. Not surprisingly, overrepresented GO terms include general cellular processes such as cell cycle and glycolytic processes, and general vesicle-mediated transport. Cluster C displays the opposite behavior at 1 and 8 minutes, and contains proteins involved in RAS protein signal transduction, as well as the more general terms actin assembly and reorganization, and vesicle fusion.

Deducing cellular localization and biological processes from bystander proteins

Based on previous research, we expect the biggest alterations in EGFR interactome at the 40-minute time point, where we can start observing differences in receptor trafficking (e.g. degradation versus recycling)[3]. These differences in receptor distribution are expected to result in vastly different proteins in the proximity of EGFR, while more subtle differences in receptor stimulation and activation are expected to be less obvious in the study of the interactome. Hence, we further examined the proteins of clusters A and D and performed a functional network analysis on both clusters, as visualized in Figures 4A and 4B, using the STRING database in combination with GO enrichment analyses. GO terms with FDR-corrected p-values lower than 0.01 were considered for network mapping.

Figure 4A displays the interaction network of cluster D, biased towards TGF-a at the 40 min time point. We included 85 nodes, with a total of 68 edges, using a confidence cut off score of 0.6. Of these, 43 nodes were excluded for further network analysis because they were not connected to the major network. GO enrichment analyses revealed two main functional sub clusters, highlighting the presence of EGFR near recycling endosomes (green) and membrane interactors (blue), respectively. This indicates that the receptor is recycled and active, as we here identify a number of tyrosine kinases and phosphatases that are known to signal downstream of EGFR, such as tyrosine-protein kinase Lyn (Lyn) tyrosine-protein phosphatase non-receptor type 11 (Ptpn11). Membrane interaction is further supported by the presence of the well-known EGFR membrane interactor Grb2, and Moesin (Msn), where the latter functions as an anchor between microtubules and the plasma membrane[31]. Moreover, the presence of cyclin-dependent kinase

Cdk9, and the Hsp90 co-chaperone Cdc37, a protein that can stabilize protein kinases via Hsp90 interactions, further strengthen the enrichment of membrane interacting proteins.

Next, we investigated some smaller protein networks that were not directly connected to the major EGFR network, however, we believe are associated to EGFR function. First, a small complex of Rap2b and Serpinb6. Rap2b, as mentioned before, is recruited by activated EGFR and was marked as a membrane interactor. According to Reactome data, Serpbinb6 is also a membrane interacting protein, and was shown to be downregulated in EGFR tyrosine kinase domain mutants[32], indicating that it is involved in early EGFR activation and endocytosis. A second network consists of Nme1, Pola2, Txnrd1, and Glrx3. Nme1, also known as Nm23, facilitates clathrin-dependent internalization of EGFR, since knockdown of NM23 reduced EGFR endocytosis[33,34]. Txnrd1 is a key antioxidant enzyme, and inhibition of Txnrd1 has been shown to sensitize EGFR-related carcinomas to treatment 35,36. Stabilization of Glrx3, another antioxidant enzyme, increases EGFR expression in nasopharyngeal carcinoma cell lines[37]. Taken together, our results show that several other TGF-a-directed EGFR proximity proteins can in fact be added to the functional EGFR repertoire.

To plot the EGF-biased interaction network derived from the proteins in cluster A, we supplemented the group of proteins with EGFR (as it is located in cluster D), resulting in the network depicted in Figure 4B. The computed protein network consisted of a total of 134 nodes, with 155 confident edges. Again, only nodes with confident edges between major nodes of the main interaction network were kept for further analysis, so that 64 nodes were discarded. Here, GO analyses indicated clear enrichment of vesicle transport (red), protein degradation (orange) and phosphatases and other proteins that deactivate receptor signaling (purple). While vesicle transport is a quite general GO term, closer inspection of the proteins that were included in the enrichment of this term hint towards a more specified type of vesicle transport. Both V-type proton ATPase subunit C 1 (Atp6v1c1) and its catalytic subunit A (Atp6v1a) indicate EGFRs proximity to low pH vesicles, such as lysosomes.

Other proteins from cluster A that are not connected to the major network but are likely still relevant for EGF-related EGFR interactions, are, among others, Otud7b and Usp24, both of which are deubiquitinating enzymes. EGFR is ubiquitinated when activated, which eventually leads to degradation of the receptor. Deubiquitinating enzymes however, can prolong receptor activation by removing ubiquitin chains[38]. Otud7b, also known as Cezanne-1, has been shown to enhance receptor signaling by stabilizing EGF-activated EGFR[39]. Usp24 is downregulated in EGFR adenocarcinomas, as well as in EGF-treated primary lung cells. In the same cells, knockdown of Usp24 increases cell numbers and cell viability[40]. Taken together, these proteins are interesting EGFR interactors that can play a role in downstream EGFR processes that involve cell proliferation and viability.

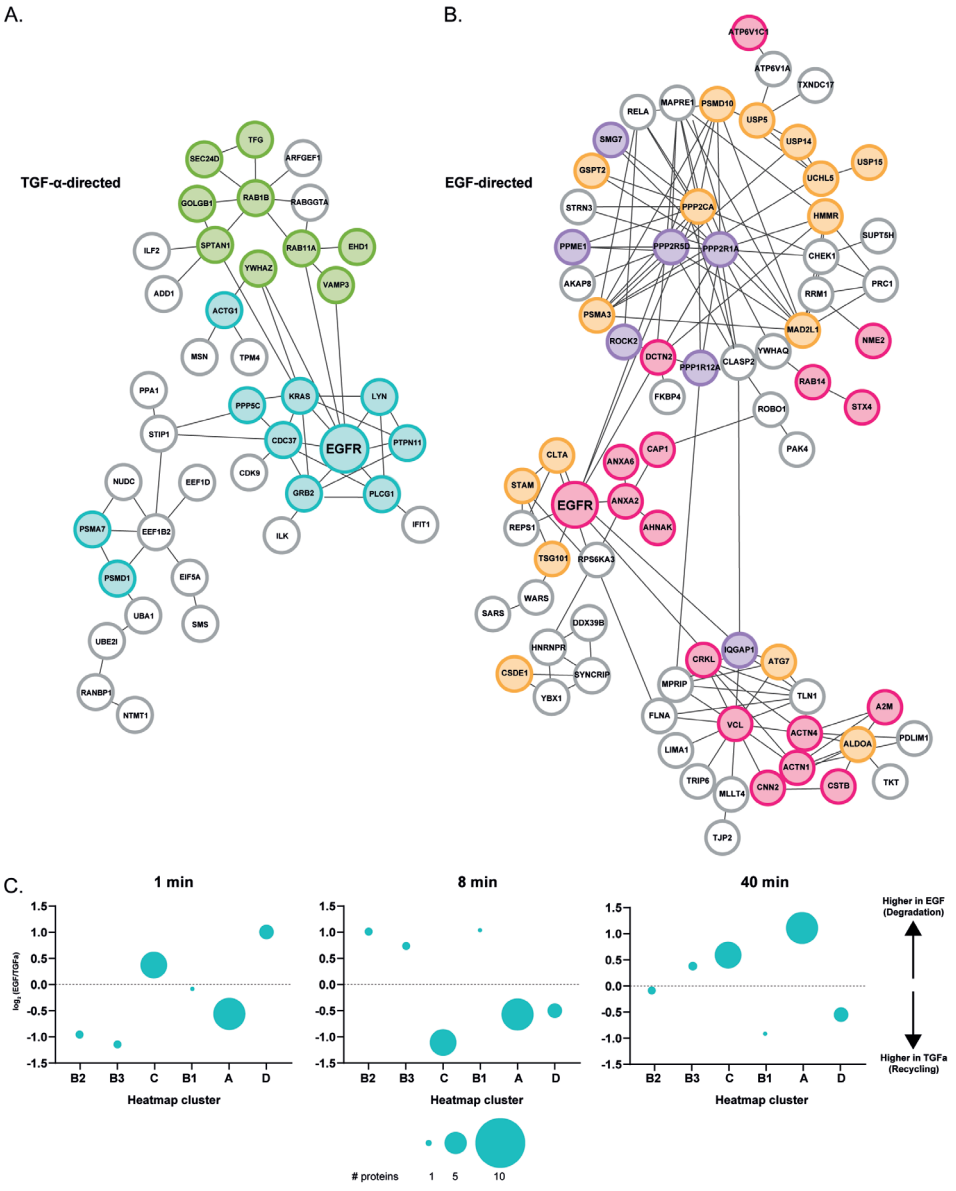

Figure 4. Protein interaction networks from heatmap clusters that are **(A)** TGF-a-directed, and **(B)** EGF-directed at the 40-minute time point. Colors indicate membership to sub clusters, as defined by enrichment in GO terms. Green – recycling endosomes, blue – membrane interactors, red – vesicle transport, orange – protein degradation, purple – phosphatases and other receptor-deactivating proteins. **(C)** Differential clustering of vesicle proteins reveals differences in timing between EGF and TGF-a signaling duration. While early signaling (1 minute, left panel) shows an equal distribution of vesicle proteins between EGF and TGF-a, differences are observed in the later time points. At the 8-minute time point, vesicle proteins are more dominantly present in the TGF-a stimulated samples, indicating that at that time point, EGFR is present in recycling vesicles (middle panel). At the late time point (40 minutes) however, we observe a shift towards EGF, and therefore towards degradation-related vesicles (right panel).

Differential clustering of vesicle proteins reveals information on timing and signaling duration

As multiple of our employed enrichment analyses clearly revealed vesicle-related proteins, we hypothesized that the localization of the different vesicle proteins at the different time points could contain information on the timing and duration of EGFR signaling. We therefore investigated the overlap of the proteins from the heatmap with the Exocarta Exosome database and found that 30 out of 441 proteins (6.8%) in the heatmap are in the Exocarta top 100 extracellular vesicle proteins. It should be noted, however, that these proteins are not exclusively found in extracellular vesicles but are considered to be identified more often in exosomes than in the general proteome. Of these, 22 are clearly EGF biased at the 40-minute time point as they can be found in cluster A.

We know that EGFR proximity proteins can reveal details on the location of the receptor via the so-called 'bystander' proteins. As activated EGFR spends the majority of its lifetime in intracellular vesicles, we hypothesized that we could use the data from all vesicle related Exocarta top 100 proteins to yield information on the timing and localization of the receptor between the different ligands. To this end, we plotted the average EGF/ TGF-a intensity ratio from all vesicle proteins in each heatmap cluster (Figure 3C) at each time point after stimulation, depicted in Figure 4C. The data in the plots clearly illustrates differential timing between the two ligands. At the earliest time point, there is no difference in the average intensity between the vesicle proteins, illustrated by the equal spread of vesicle proteins across the intensity axis. A clear shift can be observed in subsequent time points, where the majority of vesicle proteins are TGF-a focused at 8 minutes, while at the 'late', 40-minute, time point there is a clear shift for these vesicle-related proteins towards EGF, corresponding to the degradation-related proteins in heatmap cluster A. In summary, these data indicate that upon stimulation of EGFR by EGF and TGF-a, receptor recycling is initiated early in the signaling process, whereas degradation is a slower process. This evidence is strengthened further by the behavior of Rab and Rap proteins from Figure 3B, where receptor endocytosis and recycling proteins were earlier and more dominantly expressed near EGFR after TGF-a stimulation, compared to EGF stimulation.

Conclusion

In conclusion, we showed that with a label free APEX2 live cell proximity method we were able to map EGFR subcellular location at different time points after stimulation. Utilizing the fast and concise biotinylation of proximity proteins by APEX2, we were able to detect slight differences in early signaling kinetics between TGF-a and EGF, and identified ligand-specific vesicle-related proteins, thereby increasing our knowledge on RTK signaling and differential trafficking.

Data availability

The mass spectrometry proteomics data have been deposited to the ProteomeXchange Consortium via the PRIDE partner repository (http://www.ebi.ac.uk/pride/archive/) with the data set identifier PXD024136.

Acknowledgements

This research was part of the Netherlands X-omics Initiative and partially funded by NWO, project 184.034.019 and the Horizon 2020 program INFRAIA project Epic-XS (Project 823839). We would like to thank Bohui Li for help with the generation of the t-sne plots.

References

1. Bakker, J., Spits, M., Neefjes, J. & Berlin, I. The EGFR odyssey – from activation to destruction in space and time. J. Cell Sci. 130, 4087–4096 (2017).
2. Ayati, A. et al. A review on progression of epidermal growth factor receptor (EGFR) inhibitors as an efficient approach in cancer targeted therapy. Bioorg. Chem. 99, 103811 (2020).
3. Francavilla, C. et al. Multilayered proteomics reveals molecular switches dictating ligand-dependent EGFR trafficking. Nat. Struct. Mol. Biol. 23, 608–618 (2016).
4. Kiyatkin, A., van Alderwerelt van Rosenburgh, I. K., Klein, D. E. & Lemmon, M. A. Kinetics of receptor tyrosine kinase activation define ERK signaling dynamics. Sci. Signal. 13, eaaz5267 (2020).
5. Purvis, J. E. & Lahav, G. Encoding and Decoding Cellular Information through Signaling Dynamics. Cell 152, 945–956 (2013).
6. Zheng, Y. et al. Temporal regulation of EGF signalling networks by the scaffold protein Shc1. Nature 499, 166–171 (2013).
7. Sousa, L. P. et al. Suppression of EGFR endocytosis by dynamin depletion reveals that EGFR signaling occurs primarily at the plasma membrane. Proc. Natl. Acad. Sci. 109, 4419–4424 (2012).
8. Vieira, A. V., Lamaze, C. & Schmid, S. L. Control of EGF Receptor Signaling by Clathrin-Mediated Endocytosis. Science. 274, 2086–2089 (1996).
9. Villaseñor, R., Nonaka, H., Del Conte-Zerial, P., Kalaidzidis, Y. & Zerial, M. Regulation of EGFR signal transduction by analogue-to-digital conversion in endosomes. Elife 4, (2015).
10. Trinkle-Mulcahy, L. Recent advances in proximity-based labeling methods for interactome mapping. F1000Research 8, 135 (2019).
11. Kim, D. I. & Roux, K. J. Filling the Void: Proximity-Based Labeling of Proteins in Living Cells. Trends Cell Biol. 26, 804–817 (2016).
12. Hung, V. et al. Spatially resolved proteomic mapping in living cells with the engineered peroxidase APEX2. Nat. Protoc. 11, 456–475 (2016).
13. Lobingier, B. T. et al. An Approach to Spatiotemporally Resolve Protein Interaction Networks in Living Cells. Cell 169, 350-360.e12 (2017).
14. Paek, J. et al. Multidimensional Tracking of GPCR Signaling via Peroxidase-Catalyzed Proximity Labeling. Cell 169, 338-349.e11 (2017).
15. Tyanova, S., Temu, T. & Cox, J. The MaxQuant computational platform for mass spectrometry-based shotgun proteomics. Nat. Protoc. 11, 2301–2319 (2016).
16. Tyanova, S. et al. The Perseus computational platform for comprehensive analysis of (prote)omics data. Nat. Methods 13, 731–740 (2016).
17. Shannon, P. Cytoscape: A Software Environment for Integrated Models of Biomolecular Interaction Networks. Genome Res. 13, 2498–2504 (2003).
18. Montojo, J. et al. GeneMANIA Cytoscape plugin: fast gene function predictions on the desktop. Bioinformatics 26, 2927–2928 (2010).
19. Assiddiq, B. F. et al. EGFR S1166 Phosphorylation Induced by a Combination of EGF and Gefitinib Has a Potentially Negative Impact on Lung Cancer Cell Growth. J. Proteome Res. 11, 4110–4119 (2012).
20. Winograd-Katz, S. E. & Levitzki, A. Cisplatin induces PKB/Akt activation and p38MAPK phosphorylation of the EGF receptor. Oncogene 25, 7381–7390 (2006).
21. Imami, K. et al. Temporal Profiling of Lapatinib-suppressed Phosphorylation Signals in EGFR/HER2 Pathways. Mol. Cell. Proteomics 11, 1741–1757 (2012).
22. Homma, Y., Hiragi, S. & Fukuda, M. Rab family of small GTPases: an updated view on their regulation and functions. FEBS J. febs.15453 (2020).
23. Halberg, N. et al. PITPNC1 Recruits RAB1B to the Golgi Network to Drive Malignant Secretion. Cancer Cell 29, 339–353 (2016).
24. Zhang, Z. et al. GABAB receptor promotes its own surface expression by recruiting a Rap1-dependent signaling cascade. J. Cell Sci. 128, 2302–2313 (2015).
25. Südhof, T. C. Function of Rab3 GDP–GTP Exchange. Neuron 18, 519–522 (1997).
26. Zhu, Z., Di, J., Lu, Z., Gao, K. & Zheng, J. Rap2B GTPase: structure, functions, and regulation. Tumor Biol. 37, 7085–7093 (2016).
27. Stope, M. B. et al. Rap2B-Dependent Stimulation of Phospholipase C-ε by Epidermal Growth Factor Receptor Mediated by c-Src Phosphorylation of RasGRP3. Mol. Cell. Biol. 24, 4664–4676 (2004).
28. Leung, K. F., Baron, R. & Seabra, M. C. Thematic review series: Lipid Post translational Modifications. Geranylgeranylation of Rab GTPases. J. Lipid Res. 47, 467–475 (2006).
29. Shinde, S. R. & Maddika, S. Post translational modifications of Rab GTPases. Small GTPases 9, 49–56 (2018).
30. Tohmé, R. et al. Direct activation of

PP2A for the treatment of tyrosine kinase inhibitor–resistant lung adenocarcinoma. JCI Insight 4, (2019).
31. Solinet, S. et al. The actin-binding ERM protein Moesin binds to and stabilizes microtubules at the cell cortex. J. Cell Biol. 202, 251–260 (2013).
32. Peraldo-Neia, C. et al. Epidermal Growth Factor Receptor (EGFR) mutation analysis, gene expression profiling and EGFR protein expression in primary prostate cancer. BMC Cancer 11, 31 (2011).
33. Boissan, M. et al. Nucleoside diphosphate kinases fuel dynamin superfamily proteins with GTP for membrane remodeling. Science. 344, 1510–1515 (2014).
34. Boissan, M., Schlattner, U. & Lacombe, M.-L. The NDPK/NME superfamily: state of the art. Lab. Investig. 98, 164–174 (2018).
35. Xiaobo, C. et al. TUSC2(FUS1)-erlotinib Induced Vulnerabilities in Epidermal Growth Factor Receptor(EGFR) Wildtype Non-small Cell Lung Cancer(NSCLC) Targeted by the Repurposed Drug Auranofin. Sci. Rep. 6, 35741 (2016).
36. Dai, B. et al. KEAP1-Dependent Synthetic Lethality Induced by AKT and TXNRD1 Inhibitors in Lung Cancer. Cancer Res. 73, 5532–5543 (2013).
37. He, F. et al. Glutaredoxin 3 promotes nasopharyngeal carcinoma growth and metastasis via EGFR/Akt pathway and independent of ROS. Oncotarget 7, 37000–37012 (2016).
38. Fang, Y., Fu, D. & Shen, X.-Z. The potential role of ubiquitin c-terminal hydrolases in oncogenesis. Biochim. Biophys. Acta - Rev. Cancer 1806, 1–6 (2010).
39. Pareja, F. et al. Deubiquitination of EGFR by Cezanne-1 contributes to cancer progression. Oncogene 31, 4599–4608 (2012).
40. Wang, S.-A. et al. EGF-mediated inhibition of ubiquitin-specific peptidase 24 expression has a crucial role in tumorigenesis. Oncogene 36, 2930–2945 (2017).

Supplemental figures

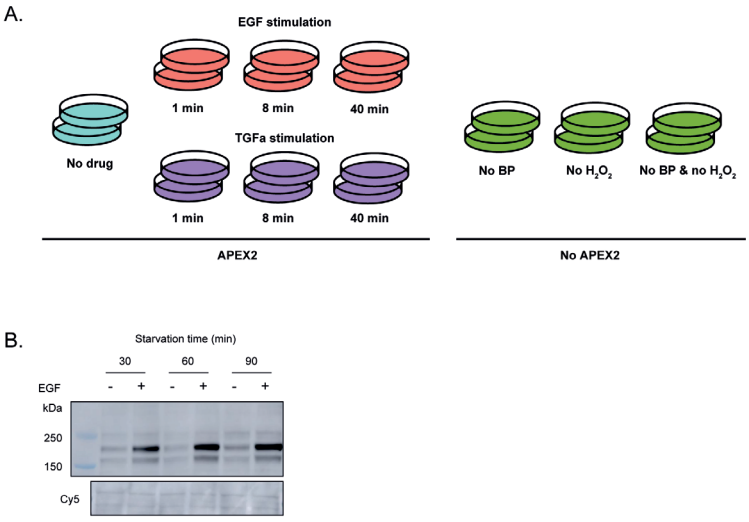

Figure S1. (A) Experimental conditions utilized in this study. Duplicate biological replicates were prepared for each experimental condition. Samples belonging to the 'APEX2' conditions were both incubated with BP and stimulated using H_2O_2, as described in the experimental workflow, and stimulated with either EGF or TGF-a for 1-40 minutes, respectively. The 'No APEX2' condition comprised of samples that were deprived from one or more of the APEX2 reagents, being BP, H_2O_2, or both, respectively. **(B)** Western blot of EGFR Y1068 phosphorylation after different periods of serum starvation.

A.

```
       960         970         980         990        1000
WMIDADSRPK FRELIIEFSK MARDPQRYLV IQGDERMHLP SPTDSNFYRA
      1010        1020        1030        1040        1050
LMDEEDMDDV VDADEYLIPQ QGFFSSPSTS RTPLLSSLSA TSNNSTVACI
      1060        1070        1080        1090        1100
DRNGLQSCPI KEDSFLQRYS SDPTGALTED SIDDTFLPVP EYINQSVPKR
```

B.

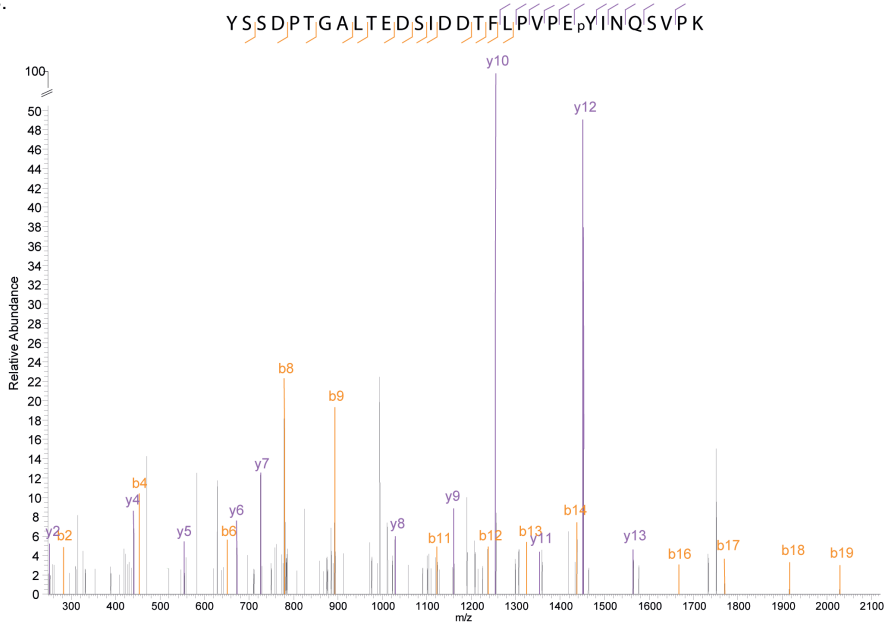

Figure S2. Mass spectrum of the Y1068 EGFR phosphorylated activation site. **(A)** Partial amino acid sequence of the human EGFR receptor. Purple vertical lines indicate tryptic cleavage sites. The orange square indicates the tryptic peptide containing the Y1068 activation site. **(B)** Mass spectrum of the phosphorylated Y1068 EGFR activation site.


4

Live cell proximity labeling of mGluR5: Mechanisms of intracellular receptor trafficking and nuclear localization

Charlotte AGH van Gelder[1,2], Pieter C. van Breugel[1,2], and Maarten Altelaar[1,2]

[1]Biomolecular Mass Spectrometry and Proteomics, Bijvoet Center for Biomolecular Research and Utrecht Institute for Pharmaceutical Sciences, Utrecht University, The Netherlands, [2]Netherlands Proteomics Center, The Netherlands.

Manuscript in preparation

Abstract

The g-protein coupled receptor (GPCR) superfamily of proteins can induce a wide array of intracellular signaling cascades, depending, among others, on their g protein subunit compositions. Classically, focus has been on GPCR signaling on the plasma membrane. However, activated receptors have been found abundantly on several intracellular locations, including endosomes, the endoplasmic reticulum (ER), and the nucleus. The metabotropic glutamate 5 receptor (mGluR5) has been studied extensively for its role in synaptic plasticity, where stimulation of postsynaptic mGluR5 decreases synaptic strength through internalization of AMPA receptors in a process most often referred to as mGluR5 long term depression (LTD). As intracellular mGluR5 were shown to be able to induce LTD independently of plasma membrane (PM) mGluR5, in depth study of localization and activation mechanisms of inner nuclear membrane (INM)-mGluR5 is essential for understanding their role in synaptic plasticity and other biological processes. Recent studies have shown that INM-mGluR5 and PM-mGluR5 originate from different receptor pools. INM-mGluR5 displays mature glycosylation patterns, indicating that these proteins are processed as far as the cis/medial-Golgi, before trafficking to the nucleus, however, how INM-mGluR5 traffics from here back to the INM is unknown. In this study, we investigate the trafficking mechanism of INM-mGluR5 using an engineered ascorbate peroxidase (APEX2) tag fused to mGluR5 and ΔINM-mGluR5. Proximity labeling of mGluR5 interactors and bystander proteins revealed location specific mGluR5 proteins, among which several subsets of proteins that are likely involved in the different localization routes of various subcellular mGluR5 receptor pools. Moreover, we identify Casein Kinase 2 as a selective nuclear mGluR5 interactor. Through deglycosylation experiments, we validate the trafficking of nuclear mGluR5 to the cis and medial Golgi. Using knockdown approaches, we validate the role of the coatomer (COPI) complex in subsequent retrograde transport to the ER, and hypothesize on the role of Endoplasmic Reticulum Associated protein Degradation (ERAD)-related proteins in release and stabilization of nuclear-bound mGluR5 in the cytoplasm before transport into the inner nuclear membrane.

Introduction

G protein-coupled receptors (GPCRs) are large seven transmembrane domain receptors that transduce extracellular signals into cells. This superfamily, consisting of more than 800 predicted members, can induce a wide array of intracellular signaling cascades, depending, among others, on their g protein subunit compositions. Moreover, GPCR activation can induce g protein independent signaling, mostly via β-arrestin scaffold proteins[1]. Classically focus has been on GPCR signaling on the plasma membrane. However, activated receptors have been found abundantly on several intracellular locations, including endosomes, the endoplasmic reticulum (ER), and the nucleus. Some of these receptor pools originate from the plasma membrane, where they are activated and subsequently internalized. However, a growing body of evidence shows that for some GPCRs, separate pools are located on intracellular membranes, which can be activated independent of their plasma membrane located versions[2,3]. Activation of intracellular receptors can be induced by both intracellular and plasma membrane permeable ligands, and can couple to entire different signaling cascades[4,5].

The metabotropic glutamate 5 receptor (mGluR5) has been studied extensively for its role in synaptic plasticity, where stimulation of postsynaptic mGluR5 decreases synaptic strength through internalization of AMPA receptors in a process most often referred to as mGluR5-LTD[6]. Moreover, mGluR5 functioning is essential in neurodevelopment, and aberrations have been implicated in many neurological disorders, including autism spectrum disorders, chronic pain, and addiction[7]. Studies have shown that more than half of mGluR5 in hippocampal neurons can be found associated with intracellular membranes, most predominantly on the ER and the inner nuclear membrane (INM), where it couples to $g_{q/11}$ and subsequently causes calcium release of internal storages[6,8,9]. Moreover, intracellular mGluR5 have been shown to be capable of LTD induction independently of plasma membrane (PM) mGluR5, highlighting the potential importance of INM-mGluR5 in other biological processes, and the localization and activation of INM-mGluR5 in general[10–12].

Recent work of Sergin *et al* has given some insight in the localization strategy of INM-mGluR5[13]. Deletion of sequential amino acid stretches in the c-terminal tail of mGluR5 in HEK293 cells revealed a 25 amino acid domain necessary for nuclear localization. They also show that indeed, INM-mGluR5 and PM-mGluR5 originate from different pools, using a labeled ligand receptor binding site pair to follow PM-mGluR5 trafficking upon glutamate stimulation. Moreover, it was shown that INM-mGluR5 displays mature glycosylation patterns, indicating that these proteins are processed as far as the *cis/medial*-Golgi, before trafficking to the nucleus. It is still unknown however, how INM-mGluR5 traffics from here back to the INM.

In this study, we aimed to investigate the trafficking mechanism of INM-mGluR5 using an engineered ascorbate peroxidase (APEX2) tag fused to mGluR5 and ΔINM-mGluR5, where we deleted 25 amino acids needed for INM localization. Proximity labeling of mGluR5 interactors and bystander

proteins revealed location specific mGluR5 proteins, among which several subsets of proteins that are likely involved in the different localization routes of different mGluR5 receptor pools.

Materials and Methods

Cell culture

Human embryonic kidney 293 T-antigen (HEK293T) cells (ATCC) were cultured in Dulbecco's modified Eagle's medium (DMEM, Lonza) and supplemented with 10% fetal bovine serum (Thermo Fischer Scientific), 1% penicillin/streptomycin and L-glutamine in a humidified atmosphere with 5% CO2 at 37 °C.

cDNA constructs and transient transfections

pRK5-CMV-Myc-SNAP-mGluR5a-HA-FRB was a kind gift of H.D. MacGillavry. To generate plasmid pRK5-CMV-Myc-SNAP-mGluR5a-APEX2, the HA-FRB region of plasmid pRK5-CMV-Myc-SNAP-mGluR5a-HA-FRB was replaced by the APEX2 region. In brief, pRK5-CMV-Myc-SNAP-mGluR5a-HA-FRB was digested with XbaI (Thermo Fisher Scientific; ER0681) and SalI (Thermo Fisher Scientific; ER0641) to remove the HA-FRB region. The APEX2 region flanked with XbaI and SalI restriction sites was generated by PCR using Phusion High-Fidelity DNA Polymerase (Thermo Fisher Scientific; F530), primers 2103 and 2104 and pcDNA3 Connexin43-GFP-APEX2(Addgene plasmid number 49385) as template DNA. The resulting PCR product was digested with XbaI and SalI and ligated using Rapid DNA Ligation Kit (Thermo Fisher Scientific; K1422) into XbaI and SalI digested pRK5-CMV-Myc-SNAP-mGluR5a-HA-FRB to generate pRK5-CMV-Myc-SNAP-mGluR5a-APEX2.

To generate plasmid pRK5-CMV-Myc-SNAP-mGluR5a(delIMN)-APEX2 a part of pRK5-CMV-Myc-SNAP-mGluR5a-APEX2 was amplified out by PCR using primers 2170 and 2208. The resulting PCR product was cloned into pJET1.2-Blunt vector (Thermo Fisher Scientific CloneJET PCR Cloning Kit; K1231) generating pJet_PCR_2170-2208_mGluR5a-APEX2(partial). This plasmid was used as template to generate pJet_mGluR5a(delIMN)-APEX2(partial). In brief, mutagenic primers 2278 and 2279 were used for a mutagenic PCR reaction. The generated PCR product was then phosphorylated by T4 Polynucelotide Kinase (T4 PNK,NEB; M0201S) and plasmid template was removed by DpnI (Thermo Fisher Scientific; ER1705) digestion before ligation with T4 DNA ligase (Thermo Fisher Scientific; EL0011)) and transformation to Alpha-Select Silver Efficiency competent cells (Bioline; BIO-85026). From the subsequent obtained pJet_mGluR5a(delIMN)-APEX2(partial) plasmid, the region containing the IMN deletion was digested out by NheI (Thermo Fisher Scientific; ER0972) and SalI digestion and ligated into pRK5-CMV-Myc-SNAP-mGluR5a-APEX2 digested with NheI and SalI to generate pRK5-CMV-Myc-SNAP-mGluR5a(delIMN)-APEX2.

cDNA was introduced in HEK293T cells using jetPRIME transfection reagent (Polyplus transfection) following manufacturer's protocol. In short, cells were plated at a confluency of 50-60%. For a 6-well plate format, 1 µg of DNA was introduced in 200 µl of jetPRIME buffer and 2 µl of jetPRIME reagent. Experiments were performed 24 to 48 hours after transfection.

Table 1. Primers

#	Primer	Sequence
2103	Fw_XbaI-APEX2 (#2)	acagcgTCTAGAGGGCGCGCCAAGGG
2104	Rv_APEX2-XhoI-SalI (#2)	acagcgGTCGACCTCGAGTTAGGCATCAGCAAACC
2170	Seq_Fw3_mGluR5a	CTGCCTCGGTCTGCTAG
2208	Seq_Rv_SV40 PolyA	GTAACCATTATAAGCTGCAATAAACAAG
2278	Fw_mGluR5a_del_INM_localization	TCCAACGGAAAATCTGTGACTTGGG
2279	Rv_mGluR5a_del_INM_localization	TGATTTGCCGTCTCCTACATGCATG
2121	Fw_MreI-APEX2 (#1)	acagcgCGCCGGCGGGGCGCGCCAAGGG
2122	RV_APEX2-NotI (#1)	acagcgGCGGCCGCTCGAGTTAGGCATCAGCAAACC

siRNA and transient transfections
Transfections were performed using Lipofectamine 2000 reagent (Invitrogen) following manufacturer's instructions. In short, receptor cDNA and siRNA were diluted in Opti-MEM without serum. Lipofectamine 2000 was diluted in Opti-MEM, and was incubated for 5 minutes at room temperature. Then diluted cDNA and siRNA were added to the diluted Lipofectamine 2000 and incubated for 20 minutes at room temperature to allow complex formation. The mix was introduced into the host cells and incubated for 48 hours in a humidified atmosphere with 5% CO2 at 37 °C.

APEX2 reaction and cell lysis
Cells were incubated with biotin phenol (BP, Iris Biotech) supplemented DMEM at a final concentration of 500 µM for 30 minutes at 37°C/5%CO2. The APEX2 reaction was performed by introduction of 100 mM H2O2 (Merck) diluted in Dulbecco's phosphate buffered saline (DPBS, Lonza) to a final concentration of 1 mM for 60 seconds at room temperature. The reaction was quenched by addition of ice-cold quencher solution, consisting of 10 mM sodium ascorbate (Sigma Aldrich), 5 mM Trolox (Sigma Aldrich), and 10 mM sodium azide (Sigma) in DPBS for 20 minutes on ice. Cell pellets were collected and lysed in RIPA lysis buffer (50 mM TRIS-HCl pH 7.4, 150 mM NaCl, 0.1% sodium dodecyl sulfate, 0.1% sodium deoxycholate, and 1% Triton X-100) supplemented with 10 mM sodium ascorbate, 5 mM Trolox, 10 mM sodium azide, 1 mM PMSF (Sigma), and complete mini EDTA-free protease inhibitor cocktail (Roche).

Subcellular fractionation
Cell pellets were resuspended in resuspension buffer (25 mM HEPES pH 7.5, 50 mM NaCl, 5 mM KCl, complete mini EDTA-free protease inhibitor cocktail (Roche), and phosSTOP phosphatase inhibitor cocktail (Roche)) for 20 minutes on ice. The cell suspension was passed 100 times through a dounce tissue grinder with pestle B, after which the nuclei and mitochondria were pelleted via centrifugation at 1,200 rpm for 10 minutes at 4 °C. The nuclear fraction was washed two times in resuspension buffer and subsequently lysed in tris buffered saline (TBS) with 1% triton X-100, complete mini EDTA-free protease inhibitor cocktail (Roche), and phosSTOP phosphatase inhibitor

cocktail (Roche) for 15 minutes on ice. Protein content was determined per fraction using the Pierce BCA protein assay kit (Thermo Scientific). Proteins were reduced with 4 mM DTT for 25 minutes at 56 °C and alkylated with 8 mM iodoacetamide for 30 minutes at room temperature in the dark. Samples were digested with LysC (1:200 enzyme substrate ratio) and trypsin (1:100) overnight at 37 °C, after which the reaction was quenched with 2% FA. Peptides were desalted using Oasis HLB columns (Waters), dried in vacuo en stored at -80 °C until further analysis.

Deglycosylation experiments
Deglycosylation of subcellular fractions was performed following the protocols of New England Biolabs, (Ipswich, MA). In short, samples were denatured in denaturing buffer (0.5% SDS and 1% β-mercaptoethanol) at 55 °C for 10 min. The denatured samples (10 µg each) were then subjected to digestion with 0.01 µg of EndoH (kindly provided by Prof. Dr. G.J. Boons, Utrecht University) in a 20-µl reaction mixture containing 50 mM sodium citrate, pH 5.5, 0.5% SDS, and 1% β-mercaptoethanol or with 1.6 units of PNGase F (Roche) in a 20-µl reaction mixture containing 50 mM sodium phosphate, pH 7.5, 0.5% SDS, 1% Nonidet P-40, and 1% β-mercaptoethanol for 4 hours at 37 °C. The reactions were quenched by the addition of Sample Buffer.

Immunoblotting
Cell lysates were incubated with Quickstain Cy5 protein dye (GE Healthcare Bio-Sciences) for 30 minutes at room temperature, after which they were denatured and reduced in XT Sample buffer (Bio-rad) with 25 mM DTT at 95°C for 5 minutes. Proteins were separated on a 12% SDS-PAGE gel (Bio-rad) and electroblotted onto nitrocellulose membranes. Membranes were blocked in 5% non-fat milk in TBS with 0.1% Tween20 (TBS-T) and incubated with following antibodies: a-mGluR5 (Sigma-Aldrich) 1:1000, a-COPB1 (Thermo) 2 ug/mL, a-GAPDH (Genetex) 1:5000, a-lamin A/C (BD Biosciences) 1:1000, streptavidin conjugate Alexafluor-488 (Invitrogen) 1:10 000, a-rabbit horseradish peroxidase conjugate (Dako) 1:2000, and a-mouse horseradish peroxidase conjugate (Dako) 1:2000. When multiple antibodies of the same origin were used, membranes were stripped using Restore PLUS Western Blot stripping buffer (Pierce) to avoid cross-contamination of the secondary antibody. Detection was performed by enhanced chemiluminescent substrate (Pierce), or via fluorescence detection with the Amersham Imager 600 (GE Healthcare Bio-Sciences).

Co-immunoprecipitation (co-IP) and in-gel digestion
Brains were obtained from female adult rats and homogenized in 10x volume/weight in tissue lysis buffer (50mM TrisHCl, 150mM NaCl, 0.1% SDS, 0.2% NP-40, and protease inhibitors (Roche)). Brain lysates were centrifuged at 16,000 g for 15 min at 4°C and protein content of the supernatant was determined using the Pierce BCA protein assay kit (Thermo Scientific). 2 mg of brain lysate was incubated with 50 µl magnetic protein G beads (Dynabeads Protein G, Life Technologies AS., Oslo, Norway) per IP, were washed three times with 1 ml PBS and subsequently 10 µg of antibodies were added to the beads in 1ml PBS for antibody-beads coupling overnight at 4°C. After removing the unbound antibody, the beads were mixed with the whole cell lysate extract (6mg) and incubated overnight at 4°C while rotating. Subsequently,

the beads were washed three times with 1ml lysis buffer and proteins were eluted off the beads by incubating with 50 µl 2X Laemmli buffer and boiling for 10 min at 95°C. The eluted proteins were reduced (25mM DTT) at 56°C for 1 hour, and alkylated (90mM chloroacetamide) for 30 min in the dark. For in-gel digestion, eluted proteins were resolved by SDS-PAGE using 4–12% or 12% Criterion XT Bis-Tris precast gels (Bio-Rad Laboratories). After fixing for 20 min in 40% (v/v) EtOH/10% (v/v) acetic acid (Merck) and staining with Coomassie Brilliant Blue (Thermo Scientific) each sample line was excised, and in-gel digested according to the standard protocol described by Schevhenko *et al*[14] with minor modifications. Briefly, gel pieces were washed with 50 mM ammonium bicarbonate (Fluka) pH 8.5 and dehydrat¬ed using 100% acetonitrile (Biosolve). After repeating several hydration/dehy¬dration cycles, 150 ng of trypsin (Promega) was added for overnight incubation at 37 °C.

Immunofluorescence and confocal microscopy

Cells were plated onto poly-L-lysine coated glass 18 mm coverslips and cultured as normal. They were fixed with 4% paraformaldehyde / 4% sucrose in phosphate-buffered saline (PBS) for 10 minutes at room temperature. Fixed cells were blocked with 10% normal goat serum in PBS for 30 minutes at 37 °C, and stained with DAPI and a-mGluR5 (Sigma-Aldrich). Confocal images were taken with a Zeiss LSM 710 with 63x 1.40 oil objective. Images consist of a z-stack of 7-9 planes at 0.39 µm interval, and maximum intensity projections were generated for analysis and display.

Analysis of biotinylated proteins

Enrichment of biotinylated proteins

Cell lysates were sonicated for 12 rounds of 5s (Bioruptor, Diagenode) and spun down at 14,000 rpm for 10 minutes, after which supernatant was loaded onto streptavidin agarose resin (Thermo Scientific) overnight at 4 °C. Resin-bound proteins were washed twice with RIPA lysis buffer, one with 1M KCl, once with 0.1 Na2CO3, once with 2M urea in 10 mM Tris-HCl, and three times with 50 mM ammonium bicarbonate, respectively. Proteins were reduced with 4 mM DTT for 25 minutes at 56 °C and alkylated with 8 mM iodoacetamide for 30 minutes at room temperature in the dark. Samples were digested with LysC (1:200 enzyme substrate ratio) and trypsin (1:100) overnight at 37 °C, after which the reaction was quenched with 2% FA. Peptides were desalted using Oasis HLB columns (Waters), dried in vacuo and stored at -80 °C until further analysis.

LC-MS/MS

The enriched samples were analyzed with an UHPLC 1290 system (Agilent technologies) coupled to an Orbitrap Q Exactive HF X mass spectrometer (Thermo Scientific). Before separation peptides were first trapped (Dr Maisch Reprosil C18, 3 µm, 2 cm x 100 µm) and then separated on an analytical column (Agilent Poroshell EC-C18, 2.7 µm, 50 cm x 75 µm). Trapping was performed for 5 min in solvent A (0.1% FA) and eluted with following gradient: 0 - 13% solvent B (0.1% FA in ACN) in 10s, 13 - 44% in 95 min, 44 - 100% in 3 min, and finally 100 % for 1 min. Flow was passively split to 300 nl/min. The mass spectrometer was operated in data-dependent mode. At a

resolution of 35.000 m/z at 400 m/z, MS full scan spectra were acquired from m/z 375–1600 after accumulation to a target value of 3e6 with a maximum injection time of 20 ms. Up to 15 most intense precursor ions were selected for HCD fragmentation at a normalised collision energy of 27%, after the accumulation to a target value of 1e5. MS/MS was acquired at a resolution of 30,000, with an exclusion duration 16s. Charge state screening was enabled, and precursors with an unknown charge state or a charge state of 1 were excluded.

Data analysis
The raw data were analyzed using MaxQuant (version 1.6.3.4) for the identification and quantification of peptides and proteins[15]. Data were searched against a database containing SwissProt Human proteome (downloaded 10/2018). Variable modifications were methionine oxidation, protein N-terminus acetylation and biotinylation by biotin-phenol on tyrosine (C18H23N3O3S). A fixed modification was cysteine carbamidomethylation. The first search was performed with a mass accuracy of ± 20 ppm and the main search was performed with a mass accuracy of ± 4.5 ppm. A maximum of 5 modifications and 2 missed cleavages were allowed per peptide. The maximum charge was set to 7+. For MS/MS matching, the mass tolerance was set to 0.5 Da and the top 8 peaks per 100 Da were analyzed. MS/MS matching was allowed for higher charge states, water and ammonia loss. The false discovery rate was set to 0.01. The minimum peptide length was 7 amino acids. Match between runs was performed with a time window of 0.7 minutes. Quantification was done label free with the MaxQuant algorithm with minimal ratio label count 2 and including unique and razor peptides. Further analysis were performed using Perseus version 1.6.2.2[16].

Results

ΔINM-mGluR5-APEX2 does not localize on the nucleus
To study the interactome of mGluR5 in living cells, we made use of a fully functional construct with an frb tag in the c-terminal tail and replaced this with an APEX2 tag. Upon incubation with its substrate, biotin phenol (BP), and activation with H_2O_2, APEX2 catalyzes the addition of a biotin moiety to tyrosine residues. After cell lysis, these biotinylated proteins can then be enriched using streptavidin-coated beads, and analyzed via western blot and mass spectrometric analysis (Figure 1A).

To compare the interactome of differentially localized mGluR5, we deleted a stretch of 25 C-terminal amino acids (852-876) that was previously identified to be crucial for localization to the inner nuclear membrane (Figure 1B)[13]. Deletion of this INM localization signal was confirmed with Sanger sequencing. We assessed ΔINM-mGluR5-APEX2 localization via confocal microscopy, and saw a clear decrease in co-localization with the nuclear stain DAPI compared to mGluR5-APEX2 (Figure 1C,D). We then tested activation specificity of the APEX2 fusion proteins via western blot and observed biotinylated proteins solely in the conditions where we incubated with substrate, BP and H_2O_2, whereas endogenously biotinylated proteins could be observed in all conditions (Figure S1).

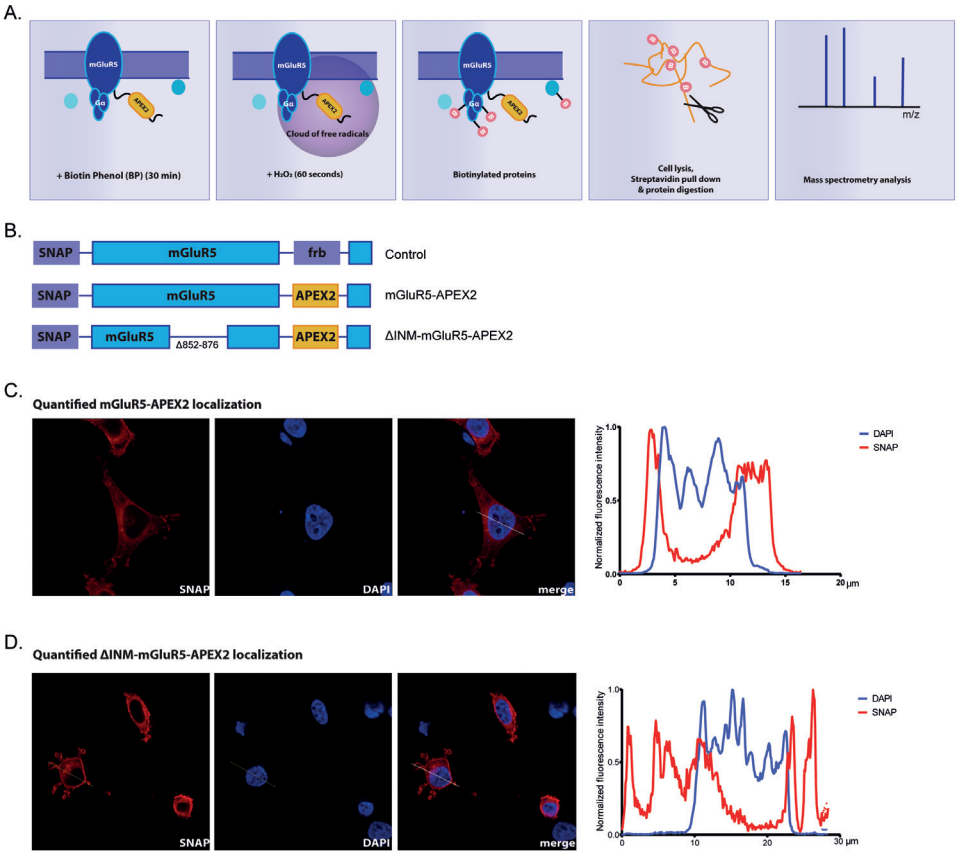

Figure 1. Creation of the mGluR5-ΔINM-mGluR5-APEX2 construct and experimental procedures. **(A)** Workflow of the APEX2 experiment. mGluR5-APEX2, or ΔINM-mGluR5-APEX2 are introduced into the host cell and incubated with biotin phenol. Biotinylation by APEX2 is activated by the addition of H_2O_2 for 60 seconds. This creates a cloud of free radicals, so that proteins in close proximity (~20 nm) of the APEX2 tag can be biotinylated on tyrosine residues. After cell lysis, biotinylated proteins are enriched using streptavidin, and enriched proteins are digested, and subsequently analyzed by mass spectrometry. **(B)** Schematic representation of the constructs used in this study. **(C,D)** Quantification of fluorescence intensity across mGluR5 and nucleus shows that upon deletion of the nuclear localization signal, no overlap between nuclear and mGluR5 localization signal is detected.

Deletion of nuclear localized mGluR5 reveals a subset of proteins specific for the INM-mGluR5 local environment

We next sought to compare the mGluR5 direct environment and interactome by transfecting transiently HEK293T cells with either mGluR5-APEX2 or ΔINM-mGluR5-APEX2. The APEX2 reaction was performed one day after transfection, and cell pellets were collected and lysed. Biotinylated proteins were enriched using streptavidin-coated beads and digested overnight. Mass spectrometric analysis of the samples resulted in the confident identification of 527 proteins (quantified in at least two out of three biological replicates). Initial analyses showed a clear enrichment of

our target and interacting proteins in all APEX2 conditions versus negative controls, illustrated by significant increase in protein abundance of, among others, mGluR5 (Figure 2A). Similar analyses on all confidently assigned proteins identified 64 proteins with a significantly higher abundance in the full mGluR5 condition compared to ΔINM-mGluR5 (Figure 2B), which were enriched for the GO Cellular Component (CC) categories nucleus, ribonucleoprotein complex, and nucleolus (Figure 2C).

Next to differences in protein abundances, we also identified proteins that were solely present in either the full mGluR5-APEX2 (42 proteins), and ΔINM-mGluR5-APEX2 (8 proteins), respectively (Figure 2D). Although derived indirectly, we suggest that the proteins that were only detected in the full mGluR5-APEX2, and not in ΔINM-mGluR5-APEX2, are specific for the nuclear mGluR5 pool. We hypothesized that these proteins could provide useful insights in the mechanism by which nuclear mGluR5 is processed and transported to be localized on the inner nuclear membrane. Based on this hypothesis, closer inspection of nuclear mGluR5-specific proteins (Supplemental Table 1) led us to shortlist three subsets of proteins for further investigation, which will be discussed in more detail.

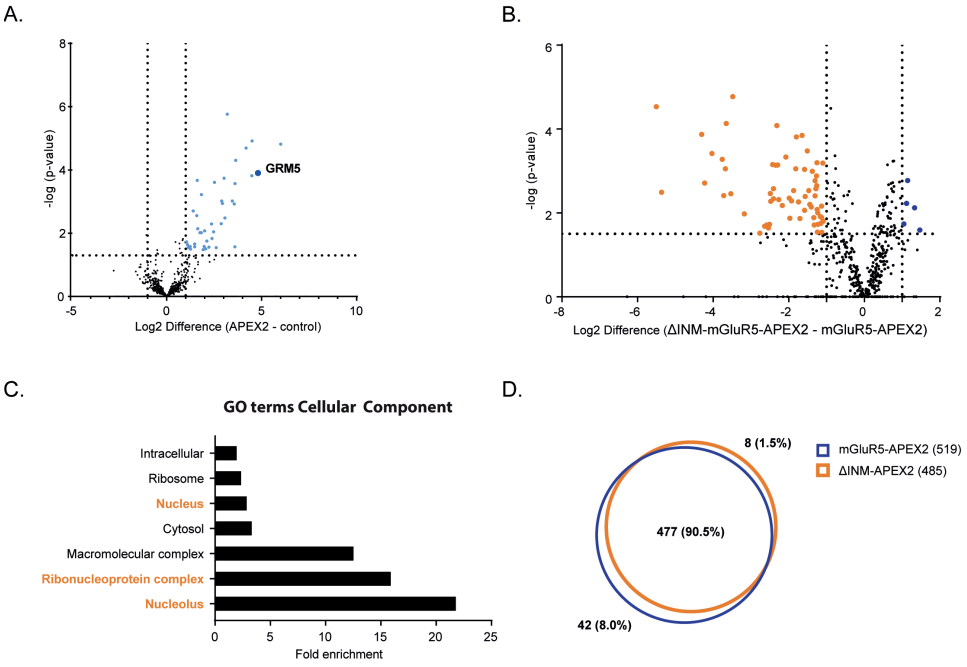

Figure 2. Mass spectrometry-based comparisons of mGluR5-APEX2 and ΔINM-mGluR5-APEX2 cellular environment using proximity-proteins. **(A)** Vulcano plot of all 'APEX2' proteins versus control proteins, where a skewed distribution of protein intensities and significance towards the 'APEX2' side can be observed, indicating the success of the enrichment strategy. **(B)** Vulcano plot illustrating differentially expressed proteins in the full mGluR5-APEX2 versus ΔINM-mGluR5-APEX2. **(C)** GO overrepresentation analysis on Cellular Component showed a clear enrichment in nucleus-related proteins. **(D)** Venn diagram illustrating the overlap in identified proteins from mGluR5-APEX2 and ΔINM-mGluR5-APEX2 experiments, with 42 proteins being uniquely identified in the mGluR5-APEX2 experiments, indicating that these are unique for nuclear mGluR5.

Nuclear casein kinase II is specific for INM-mGluR5

Casein kinase 2 (Csnk2) is an abundantly expressed and studied serine-threonine-selective protein kinase. The tetrameter comprises of two catalytic alpha, and two regulatory beta subunits[17]. Both subunits were identified to be in close proximity of nuclear, but not of plasma membrane mGluR5. To assess whether casein kinase is a stable interactor or rather a dynamic, transient, or bystander protein of INM mGluR5, we performed pull-down experiments of endogenous mGluR5 from rat whole brain lysate. Here, we established that both the catalytic subunit a, as well as the regulatory β subunit are indeed mGluR5 interactors. Also, casein kinase 1 was found as a direct interactor of mGluR5 in whole brain lysates, indicating that both kinases from this family are directly involved with mGluR5 in whole brain lysates (Figure 3A). Interestingly, both Csnk2 and Csnk1 subunits were found to be much more abundantly present in the IP samples than some of the known mGluR5 interactors. As the whole brain lysate that was used for this experiment is extremely complex and contains a wide variety of cell types, these results indicate that the interaction of Csnk1 and Csnk2 with mGluR5 is conserved in many different cell types, as compared to cell-type specific interactions such as with the post synaptic density Homer and Shank proteins (Figure 3B).

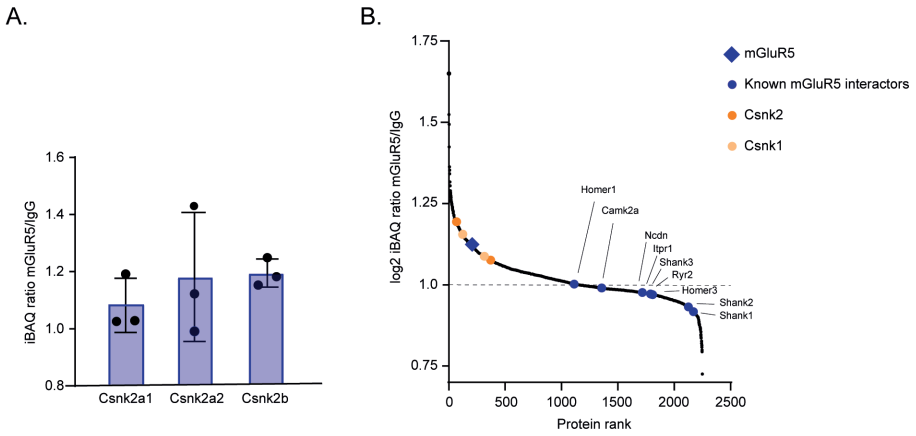

Figure 3. Pull down of mGluR5 in a rat whole brain lysate identify Csnk2 as mGluR5 interactors. **(A)** Both the alpha and beta subunits of casein kinase II are clear interactors of mGluR5, as well as Csnk1. **(B)** Both Csnk1 and Csnk2 subunits have a much higher ratio than known mGluR5 interactors, indicating that they are conserved in a variety of cell types. N=3, data are represented as mean ± SD.

A recent phosphoproteomics study investigated potential candidates of Csnk2 using the specific and selective Csnk2 ATP competitive inhibitor CX-4945, also known as Silmitaseratib[18]. The potential phosphorylation sites, determined by downregulation of phosphorylation upon Csnk2 inhibition, were subjected to linear motif analysis, resulting in enrichment for an acidophilic motif with a glutamic or aspartic acid residue in the +1 and/or +3 positions of the phosphorylated serine residue. Interestingly, the deleted amino acid sequence of ΔINM-mGluR5 contains the SxxE motif, which could very well be a target of Csnk2, explaining the bias of Csnk2 for nuclear mGluR5.

A.

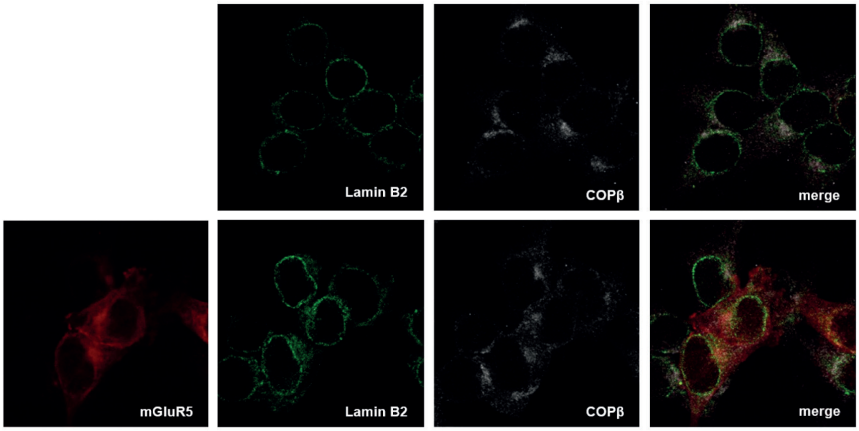
Lamin B2
COPβ
merge
mGluR5
Lamin B2
COPβ
merge

B.

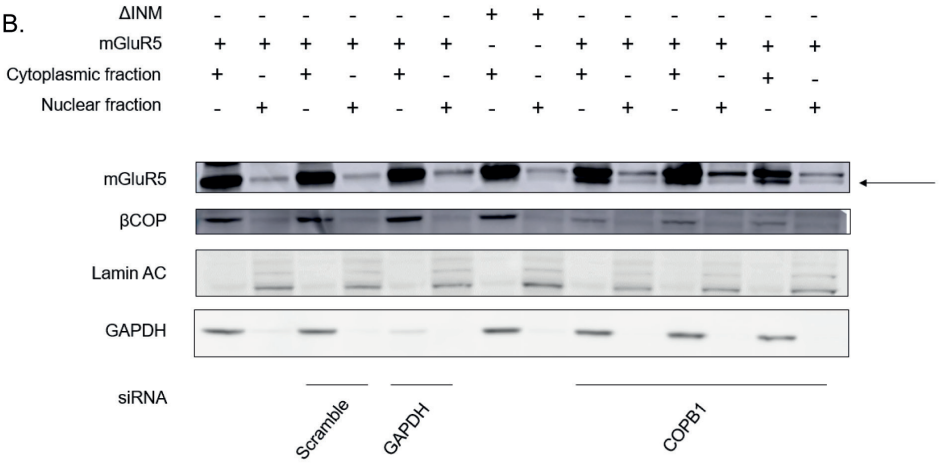
ΔINM - - - - - - + + - - - - - -
mGluR5 + + + + + + - - + + + + + +
Cytoplasmic fraction + - + - + - + - + - + - + -
Nuclear fraction - + - + - + - + - + - + - +
mGluR5
βCOP
Lamin AC
GAPDH
siRNA
Scramble
GAPDH
COPB1

C.

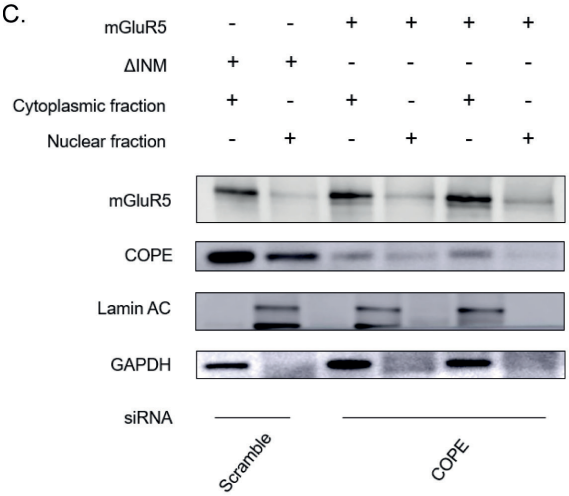
mGluR5 - - + + + +
ΔINM + + - - - -
Cytoplasmic fraction + - + - + -
Nuclear fraction - + - + - +
mGluR5
COPE
Lamin AC
GAPDH
siRNA
Scramble
COPE

Figure 4. Knock down of the βCOP and εCOP subunits of the COPI complex, responsible for retrograde Golgi to ER transport, result in a decrease of nuclear mGluR5. **(A)** Localization of the βCOP subunit of the COPI complex. **(B)** Western Blot analysis of mGluR5 expression in different cellular fractions following knock down of a Coatomer I complex subunit, βCOP. Knock down of βCOP did not only result in a decrease of mGluR5 in the nuclear fraction, it also resulted in the formation of a second molecular weight band of mGluR5 (indicated with the black arrow). **(C)** Similar results are obtained with the knock down of an alternative COPI subunit, εCOP.

Nuclear mGluR5 uses the COPI complex for retrograde Golgi to ER transport

Transport of newly synthesized proteins from the Endoplasmic Reticulum (ER) to the Golgi network is closely regulated and executed by the coatomer complex (COPII). Retrograde transport from the trans-Golgi to the cis-Golgi, and back to the ER is carried out by the COPI complex, existing of α, β, β', γ, δ, ε and ζ subunits. In our APEX2 experiments, the β and ε subunits were found to be uniquely present near nuclear mGluR5, which raised the question whether INM mGluR5 utilizes the COPI transport system to travel from the Golgi back to the ER, on its way to the inner nuclear membrane.

First, we investigated the intracellular localization of COPβ using confocal microscopy, where we observed a dense staining of COPβ on the ER, and further spreading out towards the Golgi (Figure 4A). We hypothesized that, if the COPI complex indeed is responsible for correct nuclear localization of mGluR5, knock down of COPβ would result in a decrease of mGluR5 on the inner nuclear membrane. Therefore, we co-transfected our mGluR5-APEX2 or ΔINM-mGluR5-APEX2 constructs in HEK293T cells with siRNA for COPβ, and analyzed relative mGluR5 content. Western blot analysis of subcellular cytoplasmic and nuclear fractions, characterized by marker proteins GAPDH and Lamin A/C, respectively, showed a decrease in mGluR5 in the nuclear fraction in the ΔINM-mGluR5-APEX2 samples, as expected (Figure 4B). Co-transfection of mGluR5-APEX2 cDNA and siRNA for GAPDH resulted in knockdown of GAPDH in the cytoplasmic fraction, while co-transfection with scramble siRNA did not have any effect on mGluR5 localization and intensity. Knock down of βCOP using three different siRNAs however, seemed to result in the formation of two separate molecular weight bands of mGluR5, as indicated with an arrow. Similar results are obtained with the knock down of the other COPI subunit, COPε (Figure 4C). These doublet bands presumably reflect the glycosylation state of the mGluR5 at the moment of sample processing. This implicates that COPI might not be solely responsible for mGluR5 localization to the nucleus per se, but also for correct glycosylation of mGluR5. We therefore sought to investigate the extent of glycosylation of both mGluR5 receptor pools.

mGluR5 destined for the inner nuclear membrane travels to the *cis/medial* Golgi

To determine whether the doublet band observed in the western blots is in fact caused by altered glycosylation of nuclear versus plasma membrane mGluR5, we performed deglycosylation experiments. Here, we treat subcellular fractions with different deglycosylation enzymes. Proteins are glycosylated in the ER, where oligosaccharides high in mannose are typically attached to the protein. Endo-β-N-acetylglucosaminidase H (EndoH) cleaves high mannose and most hybrid glycans, but not complex

glycans. This means that proteins originating from the ER are sensitive to EndoH, but not proteins that have travelled through different compartments of the Golgi apparatus, as here glycans are adjusted to be more complex. Peptide-N-glycosidase (PNGaseF) on the other hand, hydrolyzes all types of N-glycan chains, removing them from the protein completely. Hence, mGluR5 that is sensitive to EndoH treatment can be assumed to be residing in the ER, while resistant protein has traveled at least to the cis/medial Golgi. Indeed, we see that both plasma membrane mGluR5, as well as nuclear mGluR5 are mostly resistant to EndoH (Figure 5). This confirms that nuclear mGluR5 travels to and partially through the Golgi, strengthening the role of COPI in INM-mGluR5 trafficking.

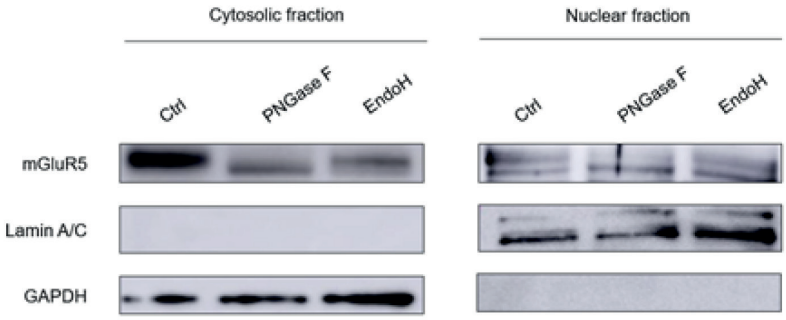

Figure 5. Deglycosylation of cytoplasmic and nuclear mGluR5 pools to investigate global glycosylation patterns. Both plasma membrane and nuclear mGluR5 are largely unaffected by EndoH treatment, indicating that they have traveled through the *cis/medial* Golgi.

Other interesting proteins to be investigated

Our results indicate that at least a part of the nuclear mGluR5 pool is transported from the Golgi back to the ER via the COPI complex. What is still unclear however, is how mGluR5 is dissociated from the ER so that it can be released into the cytoplasm. In our list of unique nuclear mGluR5 interactors, we find two members of the endoplasmic reticulum associated protein degradation (ERAD) protein complex; Derlin-1 and Erlin-2. The ERAD targets misfolded proteins of the ER for ubiquitination and subsequent degradation by the proteasome or other protein degradation mechanisms. Many uncertainties still exist on the mechanisms of the ERAD system, from target recognition, ER membrane passage, and release into the cytosol[19]. Dislocation, the process of retrograde transport from the ER into the cytosol, is thought to occur via proteinacious pores[20]. One protein that has been implicated in this retro-translocation from the ER lumen into the cytosol is Derlin-1, a multi-spanning membrane protein that is required for turnover of a subset of ERAD substrates[20,21]. As it is a transmembrane protein, it functions as a transporter for its substrates. Upon release into the cytoplasm, ERAD substrates can be directed into one of two possible pathways: the proteasome-mediated degradation, or endosomal-lysosomal pathway, which is regulated by ubiquitination. Erlin-2, another ERAD protein that was found to be uniquely expressed near nuclear mGluR5, was shown to be positively involved in K63-linked ubiquitination. Interestingly, K63-

linked cellular proteins are largely protected from proteasome-mediated degradation, and are directed towards the endosomal pathway[22]. Current efforts involving siRNA investigate the involvement of these ERAD components into the cellular localization of mGluR5 onto the inner nuclear membrane.

Rab-14 is known to be involved in membrane trafficking between the Golgi complex and endosomes[23]. Interestingly, the same study noted a high level of staining on the rough endoplasmic reticulum and the nuclear envelope as well. Hence, further investigation into the localization of Rab-14, and its co-localization with mGluR5 is encouraged.

Finally, nuclear mGluR5 needs to be directed from the cytosol onto the inner nuclear membrane. Passage through the nuclear membrane is likely accomplished via nuclear pore complexes. Several nuclear pore complex proteins were found to be uniquely expressed in proximity of mGluR5 (supplemental table 1). Stable integration into the inner nuclear membrane, was suggested to be regulated via chromatin interactions[13].

An overview of proposed trafficking of mGluR5 into the INM is depicted in Figure 6. In short, both nuclear and plasma membrane mGluR5 receptor pools are translated and N-glycosylated in the ER, and transported to the Golgi apparatus using the COPII complex. There, plasma membrane mGluR5 travels through the Golgi and is released at the *trans* Golgi, after which it is directed towards the plasma membrane. Nuclear mGluR5 travels at least to the *cis* and *medial* Golgi, after which retrograde transport to the ER is ensured by the COPI complex. From there, INM-mGluR5 is believed to be released from the ER but protected from degradation through involvement of the ERAD complex. Next, free cytosolic mGluR5 is hypothesized to be transported into the nucleus via the nuclear pore complex, where INM mGluR5 is inserted and retained via chromatin interactions.

Discussion

In this study, we used APEX2 for proximity labeling in living cells to study the differential interactome of plasma membrane versus nuclear localized mGluR5. We identified several proximity proteins that were specific for the nuclear mGluR5 pool, including two subunits of Csnk2, which we validated to be a true interaction using immunopurification of mGluR5 in a rat whole brain lysate. Although the sequence containing the putative mGluR5 localization signal contains a known Csnk2 recognition motif, future studies need to be carried out to understand the effect of the mGluR5-Csnk2 interaction on localization bias or subcellular fraction-specific signaling, for instance with the help of Csnk2 inhibition.

Next to unique protein interactions, the list of specific INM-mGluR5 proximity proteins yielded information of intracellular mGluR5 trafficking of the nuclear mGluR5 receptor pool. First, we identified several subunits of the COPI complex responsible for retrograde transport from the Golgi apparatus to the ER, COPβ and COPε, knock down of which resulted in a decrease of mGluR5 in nuclear subcellular fractions. Moreover, knockdown of these proteins resulted in alternative glycosylation patterns of both mGluR5

receptor pools. Mass spectrometry-based glycoproteomics experiments and deglycosylation experiments are being performed to further characterize this shift in N-glycosylation and its functionality. Moreover, fractionation of additional subcellular mGluR5 receptor pools, including newly translated mGluR5 still residing in the ER and Golgi apparatus, as well as fully functional ER residing receptors, would give further insight into the exact differences between plasma membrane and nuclear mGluR5, more specifically.

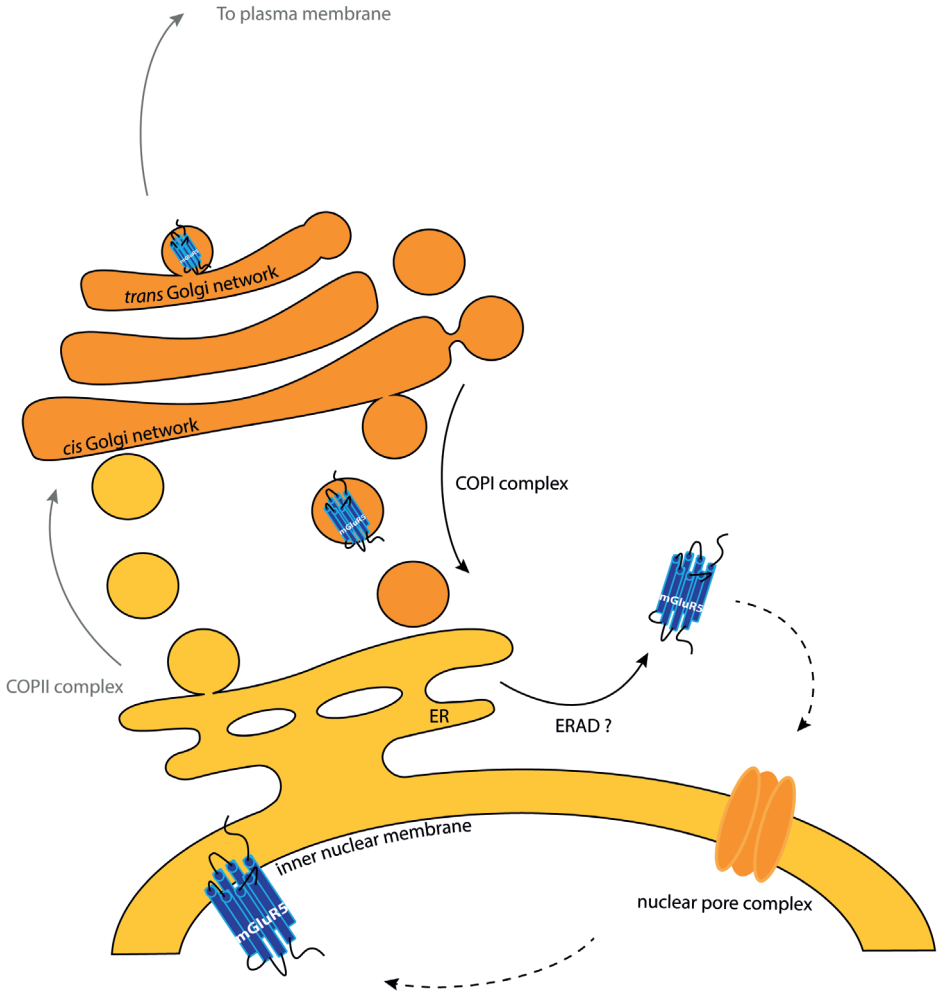

Figure 6. Proposed mechanism of nuclear mGluR5 localization. After translation in the Endoplasmic Reticulum (ER), both nuclear and plasma membrane mGluR5 pools are transported to the Golgi network using the coatomer II complex (COPII). There, the receptor pools travel from the cis to trans Golgi network, and depending on their glycosylation pattern are plasma membrane, or nucleus bound. The nuclear mGluR5 pool is transported back to the ER using the Coatomer I complex (COPI). Next, the receptor dissociates from the ER and is released into the cytosol via Endoplasmic Reticulum Associated Degradation (ERAD) complex members. From there, the nuclear mGluR5 pool transports towards the nucleus via the nuclear pore complex using affinity for chromatin, and finally is attached to the inner nuclear membrane.

Finally, we identified subunits of the ERAD system, responsible for retro-translocation from the ER lumen into the cytosol of, among others, faulty proteins. Knock down experiments will have to prove whether Derlin-1 in the case of mGluR5 indeed acts as part of a translocation pore, in which case silencing of Derlin-1 would lead to accumulation of mGluR5 in the ER. In the case of Erlin-2, knock down would result in an increase of K63-ubiquitinated mGluR5 in the cytoplasm. Analysis of mGluR5 sequence shows that it has three di-gly (KK) sequences that could serve as K63 ubiquitin anchors, of which two are located on the N-terminal tail, and one on the C-terminus. Moreover, both Erlin-1 and Erlin-2 were found to be stable mGluR5 interactors in rat whole brain lysate.

Next, we aim to use phosphoproteomics and N-linked glycoproteomics to study mGluR5 post translational modifications. Creating a map of known phosphorylation and glycosylation sites and occupancy will serve as a database for future studies, such as cell type-specific, as well as location- and stimulus-specific, analysis of mGluR5. This is especially interesting for the study of mGluR5-mediated long term depression (LTD) in cortical, striatal, and hippocampal neurons, where nuclear, but not plasma membrane mGluR5 was shown to be essential for LTD induction. Moreover, mGluR5 protein-protein interactions, as well as receptor dimerization and subcellular trafficking, has been shown to be essential in diseases as schizophrenia[24].

In conclusion, we show that INM-mGluR5 can be distinguished from plasma membrane mGluR5 via location-specific mGluR5 proximity proteins, revealing detailed information on receptor trafficking and localization mechanisms.

Acknowledgements

We thank Dr. Harold D. MacGillavry for kindly providing us the mGluR5-frb plasmid and help with the confocal microscopy experiments. We thank Dr. Riccardo Stucchi for help with isolation and lysis of rat brains, and Dr. Stamatia Rontogianni for help with the IP protocol. We thank Rosanne van Beek and Prof. Dr. G.J. Boons for kindly providing us with EndoH, and Dr. Karli Reiding and Dr. Albert Bondt for help with glycosylation experiments. This research was part of the Netherlands X-omics Initiative and partially funded by NWO, project 184.034.019 and the Horizon 2020 program INFRAIA project Epic-XS (Project 823839).

References

1. Willard SS, Koochekpour S. Glutamate, Glutamate Receptors, and Downstream Signaling Pathways. Int J Biol Sci. 2013;9(9):948-959.

2. Mohammad Nezhady MA, Rivera JC, Chemtob S. Location Bias as Emerging Paradigm in GPCR Biology and Drug Discovery. iScience. 2020;23(10):101643.

3. Bhosle VK, Rivera JC, Chemtob S. New insights into mechanisms of nuclear translocation of G-protein coupled receptors. Small GTPases. January 2017:1-10.

4. Jong Y-JI, O'Malley KL. Mechanisms Associated with Activation of Intracellular Metabotropic Glutamate Receptor, mGluR5. Neurochem Res. 2017;42(1):166-172.

5. Jong Y-JI, Kumar V, O'Malley KL. Intracellular Metabotropic Glutamate Receptor 5 (mGluR5) Activates Signaling Cascades Distinct from Cell Surface Counterparts. J Biol Chem. 2009;284(51):35827-35838.

6. Jong Y-JI, Kumar V, Kingston AE, Romano C, O'Malley KL. Functional Metabotropic Glutamate Receptors on Nuclei from Brain and Primary Cultured Striatal Neurons. J Biol Chem. 2005;280(34):30469-30480.

7. Vincent K, Cornea VM, Jong Y-JI, et al. Intracellular mGluR5 plays a critical role in neuropathic pain. Nat Commun. 2016;7(1):10604.

8. Kumar V, Jong Y-JI, O'Malley KL. Activated Nuclear Metabotropic Glutamate Receptor mGlu5 Couples to Nuclear G q/11 Proteins to Generate Inositol 1,4,5-Trisphosphate-mediated Nuclear Ca 2+ Release. J Biol Chem. 2008;283(20):14072-14083.

9. O'Malley KL, Jong Y-JI, Gonchar Y, Burkhalter A, Romano C. Activation of Metabotropic Glutamate Receptor mGlu5 on Nuclear Membranes Mediates Intranuclear Ca 2 + Changes in Heterologous Cell Types and Neurons. J Biol Chem. 2003;278(30):28210-28219.

10. Purgert CA, Izumi Y, Jong Y-JI, Kumar V, Zorumski CF, O'Malley KL. Intracellular mGluR5 Can Mediate Synaptic Plasticity in the Hippocampus. J Neurosci. 2014;34(13):4589-4598.

11. Kumar V, Fahey PG, Jong Y-JI, Ramanan N, O'Malley KL. Activation of Intracellular Metabotropic Glutamate Receptor 5 in Striatal Neurons Leads to Up-regulation of Genes Associated with Sustained Synaptic Transmission Including Arc/Arg3.1 Protein. J Biol Chem. 2012;287(8):5412-5425.

12. Jong Y-JI, Harmon SK, O'Malley KL. Intracellular GPCRs Play Key Roles in Synaptic Plasticity. ACS Chem Neurosci. 2018;9(9):2162-2172.

13. Sergin I, Jong Y-JI, Harmon SK, Kumar V, O'Malley KL. Sequences within the C Terminus of the Metabotropic Glutamate Receptor 5 (mGluR5) Are Responsible for Inner Nuclear Membrane Localization. J Biol Chem. 2017;292(9):3637-3655.

14. Shevchenko A, Tomas H, Havli J, Olsen J V, Mann M. In-gel digestion for mass spectrometric characterization of proteins and proteomes. Nat Protoc. 2006;1(6):2856-2860.

15. Tyanova S, Temu T, Cox J. The MaxQuant computational platform for mass spectrometry-based shotgun proteomics. Nat Protoc. 2016;11(12):2301-2319.

16. Tyanova S, Temu T, Sinitcyn P, et al. The Perseus computational platform for comprehensive analysis of (prote)omics data. Nat Methods. 2016;13(9):731-740.

17. Litchfield DW. Protein kinase CK2: structure, regulation and role in cellular decisions of life and death. Biochem J. 2003;369(1):1-15.

18. Rusin SF, Adamo ME, Kettenbach AN. Identification of Candidate Casein Kinase 2 Substrates in Mitosis by Quantitative Phosphoproteomics. Front Cell Dev Biol. 2017;5.

19. McCracken AA, Brodsky JL. Evolving questions and paradigm shifts in endoplasmic-reticulum-associated degradation (ERAD). BioEssays. 2003;25(9):868-877.

20. Meusser B, Hirsch C, Jarosch E, Sommer T. ERAD: the long road to destruction. Nat Cell Biol. 2005;7(8):766-772.

21. Ye Y, Shibata Y, Yun C, Ron D, Rapoport TA. A membrane protein complex mediates retro-translocation from the ER lumen into the cytosol. Nature. 2004;429(6994):841-847.

22. Zhang X, Cai J, Zheng Z, et al. A novel ER–microtubule-binding protein, ERLIN2, stabilizes Cyclin B1 and regulates cell cycle progression. Cell Discov. 2015;1(1):15024.

23. Junutula JR, De Maziére AM, Peden AA, et al. Rab14 Is Involved in Membrane Trafficking between the Golgi Complex and Endosomes. Mol Biol Cell. 2004;15(5):2218-2229.

24. Matosin N, Fernandez-Enright F, Lum JS, Newell KA. Shifting towards a model of mGluR5 dysregulation in schizophrenia: Consequences for future schizophrenia treatment. Neuropharmacology. 2017;115:73-91.

Supplemental information

Table S1. Proteins identified in APEX2 experiments that are unique for INM-mGluR5.

Uniprot ID	Gene name	Description
Q9UBU9	NXF1	Nuclear RNA export factor 1
O14579	COPE	Coatomer subunit epsilon
P00492	HPRT1	Hypoxanthine-guanine phosphoribosyltransferase
P05089	ARG1	Arginase-1
Q9UJV9	DDX41	Probable ATP-dependent RNA helicase DDX41
A0JLT2	MED19	Mediator of RNA polymerase II transcription subunit 19
Q96GA3	LTV1	Protein LTV1 homolog
P53618	COPB1	Coatomer subunit beta
Q5SY16	NOL9	Polynucleotide 5-hydroxyl-kinase NOL9
P19784	CSNK2A2	Casein kinase II subunit alpha
P18754	RCC1	Regulator of chromosome condensation
Q9H9B4	SFXN1	Sideroflexin-1
Q86XI2	NCAPG2	Condensin-2 complex subunit G2
Q9NPI1	BRD7	Bromodomain-containing protein 7
P78362	SRPK2	SRSF protein kinase 2
Q15020	SART3	Squamous cell carcinoma antigen recognized by T-cells 3
P27708	CAD	CAD protein
Q9Y295	DRG1	Developmentally-regulated GTP-binding protein 1
Q5T9A4	ATAD3B	ATPase family AAA domain-containing protein 3B
Q8N1F7	NUP93	Nuclear pore complex protein Nup93
P67870	CSNK2B	Casein kinase II subunit beta
P08243	ASNS	Asparagine synthetase [glutamine-hydrolyzing]
Q92900	UPF1	Regulator of nonsense transcripts 1
Q99729	HNRNPAB	Heterogeneous nuclear ribonucleoprotein A/B
Q9BUN8	DERL1	Derlin-1
Q9Y450	HBS1L	HBS1-like protein
Q9Y4W2	LAS1L	Ribosomal biogenesis protein LAS1L
Q7Z7K6	CENPV	Centromere protein V
O75533	SF3B1	Splicing factor 3B subunit 1
P61106	RAB14	Ras-related protein Rab-14
O94905	ERLIN2	Erlin-2
P17980	PSMC3	26S protease regulatory subunit 6A
Q12769	NUP160	Nuclear pore complex protein Nup160
Q9Y5A9	YTHDF2	YTH domain-containing family protein 2
Q9Y277	VDAC3	Voltage-dependent anion-selective channel protein 3
P22102	GART	Trifunctional purine biosynthetic protein adenosine-3
P08621	SNRNP70	U1 small nuclear ribonucleoprotein 70 kDa
O14646	CHD1	Chromodomain-helicase-DNA-binding protein 1
P50990	CCT8	T-complex protein 1 subunit theta
P26641	EEF1G	Elongation factor 1-gamma
P11586	MTHFD1	C-1-tetrahydrofolate synthase, cytoplasmic
P17066	HSPA6	Heat shock 70 kDa protein 6

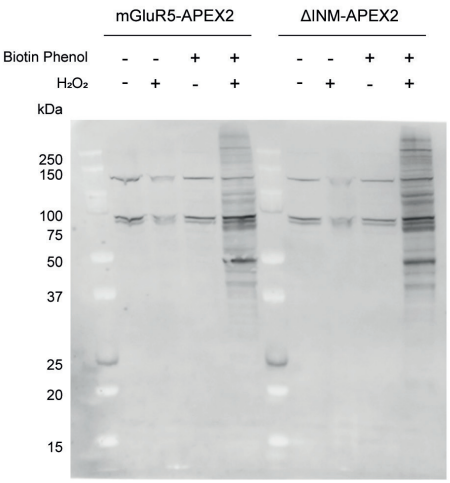

Figure S1. Proof of concept of APEX2 biotinylation experiment.

Summarizing discussion

Nederlandse samenvatting

Summarizing discussion

Introduction

One of the most fascinating features of the brain is its ability to adapt to its surroundings. Synaptic plasticity, the dynamic process of functional and structural alterations in synaptic strength, is essential for brain functioning and underlies a variety of processes such as learning and memory. The basics of synapse biology and synaptic plasticity were introduced in **chapter 1**. While the molecular mechanisms underlying such rapid plasticity processes are not fully understood, a general consensus exists on the important role of proteins. As proteins can undergo interactions (protein-protein interactions; PPIs) and can be regulated by up to 300 different post translational modifications (PTMs), it is essential to study all layers of information in the biological sample in a high-throughput and unbiased manner. The use of mass spectrometry (MS) based proteomics has increased exponentially in the last decades and is now considered the golden standard in proteomics research. The general workflow of an MS experiment was outlined in **chapter 1**.

Advancements in the modeling of brain complexity

In neuroproteomics experiments, the nature of the sample material inherently poses challenges for standard proteomics workflows. Limitations such as low sample amount caused by the use of terminally differentiated, non-dividing cells, and the heterogeneity in cell types have delayed the development of the neuroproteomics field. However, in **chapter 2** we describe a shift from the use of whole brain homogenates, towards the use of tissue from specific brain regions, and more recently towards more defined and homogeneous primary cultures.

Induced pluripotent stem cells

The shift towards the study of single neuronal subtypes was further advanced via the use of induced pluripotent stem cells (iPSCs). These are human adult somatic cells, most often fibroblasts, that are reprogrammed to that they are pluripotent; they can differentiate into the three germ layers: endoderm, mesoderm, and ectoderm, and are therefore ultimately able to generate any cell type[1]. Because the input material does not require actual brain tissue but rather non-invasively acquirable skin cells, iPSCs offer the possibility to study patient-derived material. This does not only allow for proteomic screening of specific genetic backgrounds, but also for the use of isotype controls. For instance, a mutated gene can be inserted or deleted using CRISPR/Cas9 or other gene editing techniques. Isotype controls are especially interesting for biomarker and other discovery studies, which currently have to deal with massive sample variety, caused by differences in patient gender, age, and genetic background, thereby hampering the identification of relevant, often low abundant, candidate proteins.

For neuroproteomics studies, differentiation of iPSCs into one specific subtype of neuron also increases the amount of available sample as iPSCs, in contrast to neurons, can be multiplied in culture. The use of iPSC-derived neuronal cell types have resulted, among many other studies, in

the creation of valuable resources for the neuroscience community. These include but are not limited to a proteomics resource of the developing neuronal stem cells in Rett syndrome[2], and proteomes of both motor and glutamatergic neurons during differentiation[3].

A limitation of iPSC is their maturation state, as the generated differentiated neurons often resemble an embryonic and immature phenotype. Current efforts to mature the differentiated neurons will make them more suitable for the study of many neurodegenerative diseases, such as Alzheimer's disease (AD)[4]. This does not mean that current approaches are not suitable for the study of these diseases. For example, iPSC technology has been successfully applied to generate a three-dimensional culture of iPSC-derived neurons from a patient with a specific mutation in the PSEN1 gene, which is common in early onset AD[5]. Another example generated patient-specific iPSC-derived neurons and astrocytes of four AD patients, two with sporadic and two with familial AD, of which the familial AD patients harbored different mutations. Interestingly, all neurons showed differential manifestation of cellular stress, which is typical for AD neurons, as they contain intracellular oligomers of the amyloid-β peptide[6].

Although very promising and versatile, iPSC technology is currently still limited in the amount of neuronal cell fates that can be recreated in vitro. This is caused by the lack of specific markers for many neuronal cell types, making it difficult to eliminate the potential creation of mixed population of neurons, as validating markers are often not available. Moreover, many differentiation protocols require an extensive mix of growth factors, which makes it a costly and time-consuming procedure. In the future, high-throughput and automated differentiation protocols will likely circumvent many of the current technical limitations.

Brain organoids

Another trend in neuroscience is the creation of brain organoids, and more complex assembloids. These are organoids that resemble different subsets of a distinct brain region, such as the dorsal or ventral forebrain, so that they contain either cortical glutamatergic, or GABAergic neurons, respectively[7]. The uses of brain organoids are extremely versatile, as they reflect the developing brain, including migration into different cortical layers, anatomical structures, and many different neuronal and glial cell types. They therefore also allow for the study of the formation and functioning of neurons, synapses, and even neural pathways and tracts. Recent efforts have shown beautiful examples of spontaneously developing brain organoids with a plethora of cell types and anatomical structures[8]. However, brain organoids still lack many important features of in vivo brains, such as an immune and vascular system[9]. Recent studies have even shown integration of neuronal protrusions and connections between two differentially cued brain organoids, making it possible to closely mimick interactions between brain regions.

Examples of the use of brain organoids in proteomics include choroid plexus (ChP) brain organoids; choroid plexus is present in each brain ventricle and makes the cerebrospinal fluid (CSF). Proteomics of CSF-like fluid showed that the CSF composition of the organoids matured extensively over time. Moreover, single-cell RNA sequencing and characterization of the ChP organoids showed that the epithelial cells increasingly matured and that the numbers of stromal cells increased in older organoids, resembling the molecular profiles of in vivo human ChP tissue[10].

Trends in mass spectrometry-based proteomics techniques

The study of neuronal proteins using neuroproteomics has increased rapidly in the last decades, and advancements in mass spectrometry-based proteomics has broadened our understanding of neuroplasticity exponentially. In **chapter 2**, we discussed the trends in mass spectrometry-based neuroproteomics for the study of synaptic PPIs and protein signaling dynamics. Focusing on studies from the last five years, we observed a shift towards label free quantification methods, as separation techniques have become more stable, allowing for the analysis of bigger sample sets without significant changes in retention times. At the same time, a shift towards the use of live cell labeling techniques was observed, ranging from bio-orthogonal amino acids for the study of newly translated proteins, and biotin-based proximity labeling approaches.

Combining multiple labeling and enrichment techniques to map intracellular signaling

In **chapter 3**, we aimed to map the molecular events following mGluR5 stimulation with DHPG, which is often used as a model for LTD, as it results in the internalization of AMPA receptors. mGluR-LTD has been studied extensively with classical biochemical approaches, which allows for the study of only one or two proteins simultaneously. There was a lack of proteome-wide studies on the mechanism of induction and maintenance of mGluR-LTD, which we addressed by following the synthesis of new proteins and phosphorylation dynamics of primary hippocampal neurons stimulated with DHPG over several time points.

A number of challenges were associated with these aims. First, a big dynamic range in protein expression profiles was expected, as the post synaptic density is very crowded, and only a fraction of proteins are expected to change expression upon mGluR5 stimulation. Moreover, we studied relatively short time points for protein translation, ranging from 15 to 90 minutes. Also, protein translation occurs locally in the dendrites, further increasing sample complexity. Finally, the use of primary hippocampal neurons from rat embryos resulted in limited amount of cells and material. To overcome these challenges, we integrated quantitative phosphoproteomics with the analysis of newly synthesized proteins via bio-orthogonal amino acids (azidohomoalanine) in a pulsed labeling strategy. From the phosphoproteomics dataset we identified several kinases with important roles in DHPG-induced mGluR5 activation, which we confirmed using small molecule kinase inhibitors. Furthermore, changes in the AMPA receptor endocytosis pathway in both protein synthesis and protein phosphorylation were identified. Integration of both proteomics datasets

allowed for the creation of a detailed map of molecular events following mGluR5 activation with DHPG, and provides a resource for further studies.

What can be appreciated from the results presented in this chapter, is that the application of enrichable labels in living cells, as well as the use of a sensitive and automated enrichment method allowed for the identification and quantification of hundreds of newly translated proteins and more than 10,000 phosphorylation sites, with less than 100 µg of protein input per sample.

The use of live cell proximity labeling to study receptor dynamics and location

In **chapter 4** we introduce the use of APEX2, a proximity labeling method, for the study of receptor PPIs and differential trafficking after stimulation with different ligands. To assess whether this method was sensitive and reproducible enough to detect slight differences in signal transduction pathways, we chose a well-studied receptor with implications in many cellular processes. EGFR is known to regulate many key cellular processes, including growth, proliferation, and differentiation, and its expression, activation, trafficking, and degradation have been extensively studied, as dysregulation of EGFR activation has been linked to a vast number of cancers. Using EGF and TGF-a, we identified and quantified EGFR stable and transient interactions at different time points after stimulation. We were able to use bystander proteins to map EGFR subcellular location at each time point, and detected slight differences in early signaling kinetics between the two ligands, which was made possible by the use of the fast and concise biotinylation of proximity proteins by APEX2.

Applying live cell proximity labeling to study receptor trafficking and location bias

In **chapter 5** we continued to use APEX2, and fused it to mGluR5 to study receptor localization bias. We deleted a 25 amino acid sequence in the receptor c-terminal tail, which contains the nuclear localization signal to the inner nuclear membrane (INM) of mGluR5, ΔINM-APEX2, and identified a subset of proteins that were specifically localized to the nuclear fraction of mGluR5. Using siRNA and western blot validation approaches, we confirm the role of these so called 'bystander' proteins in the differential trafficking of mGluR5 nuclear versus plasma membrane pools. We identified casein kinase 2 as an INM-mGluR5-specific kinase, and confirmed the direct interaction of mGluR5 with the catalytic subunit of the kinase in whole brain lysates. We also identified a potential Csnk2 motif in the amino acid sequence required for nuclear localization of mGluR5. Next, we validated the role of COPI for the retrograde transport of nuclear mGluR5 from the Golgi to the endoplasmic reticulum. Knock down of the βCOP, a subunit of COPI, resulted in decreased nuclear mGluR5 levels and altered mGluR5 glycosylation patterns. Finally, we im to use mass spectrometry to study localization-based differential glycosylation and phosphorylation of mGluR5.

Conclusion

In conclusion, the work described in this thesis illustrates that mass spectrometry-based proteomics has grown to be an indispensable tool in the study of synapse biology. The combination of enrichment and labeling methods has allowed us to create a multidimensional picture of protein expression levels, translation of new proteins, protein-protein interactions, protein activity, and subcellular location. This multifactorial approach has aided to the understanding of synaptic plasticity processes on the molecular level.

References

1. Takahashi K, Yamanaka S. Induction of Pluripotent Stem Cells from Mouse Embryonic and Adult Fibroblast Cultures by Defined Factors. Cell. 2006;126(4):663-676.

2. Varderidou-Minasian S, Hinz L, Hagemans D, Posthuma D, Altelaar M, Heine VM. Quantitative proteomic analysis of Rett iPSC-derived neuronal progenitors. Mol Autism. 2020;11(1):38.

3. Varderidou S, Verheijen BM, Schätzle P, Hoogenraad CC, Pasterkamp RJ, Altelaar M. Deciphering the protein dynamics of iPSC-derived neurons. J Proteome Res. May 2020:acs.jproteome.0c00070.

4. Penney J, Ralvenius WT, Tsai L-H. Modeling Alzheimer's disease with iPSC-derived brain cells. Mol Psychiatry. 2020;25(1):148-167.

5. Hernández-Sapiéns MA, Reza-Zaldívar EE, Cevallos RR, Márquez-Aguirre AL, Gazarian K, Canales-Aguirre AA. A Three-Dimensional Alzheimer's Disease Cell Culture Model Using iPSC-Derived Neurons Carrying A246E Mutation in PSEN1. Front Cell Neurosci. 2020;14.

6. Kondo T, Funayama M, Tsukita K, et al. Focal Transplantation of Human iPSC-Derived Glial-Rich Neural Progenitors Improves Lifespan of ALS Mice. Stem Cell Reports. 2014;3(2):242-249.

7. Birey F, Andersen J, Makinson CD, et al. Assembly of functionally integrated human forebrain spheroids. Nature. 2017;545(7652):54-59.

8. Velasco S, Kedaigle AJ, Simmons SK, et al. Individual brain organoids reproducibly form cell diversity of the human cerebral cortex. Nature. 2019;570(7762):523-527.

9. Marx V. Reality check for organoids in neuroscience. Nat Methods. 2020;17(10):961-964.

10. Silva-Vargas V, Doetsch F. Exploring the source of human brain fluids. Science. 2020;369(6500):143-144.

Nederlandse samenvatting

Een van de meest fascinerende eigenschappen van de hersenen is de mogelijkheid om zich aan te passen aan de omgeving. Synaptische plasticiteit is het dynamische proces waarin de structuur en functionaliteit van een synaps constant wordt aangepast aan de hand van prikkels. Dit is essentieel voor het normaal functioneren van de hersenen en vormt de basis van veel hersenprocessen zoals leren en geheugenvorming. Dit proefschift laat zien hoe met behulp van massaspectrometrie het proteoom van synapsen bestudeerd kan worden. Hierbij is vooral gekeken naar de metabotropische glutamaat 5-receptor (mGluR5) en zijn rol in synaptische plasticiteit. In de verschillende hoofdstukken worden verschillende label- en verrijkingstechnieken toegepast om met behulp van massaspectrometrie het proteoom van cellijnen en primaire neuronen te bestuderen. Er wordt gekeken naar de translatie van nieuwe eiwitten, eiwitsignalering, dynamische eiwit-eiwitinteracties en receptor-internalisatie.

In het eerste deel van **hoofdstuk 1** worden de belangrijkste principes van de anatomie en signaleringsmechanismen van neuronen geïntroduceerd. Daarnaast wordt mGluR5 en de rol hiervan in synaptische plasticiteit beschreven. In het tweede deel worden de basisprincipes en de opkomende technologieën in massaspectrometrie-gebaseerde proteomics geïntroduceerd. Ook wordt een gebruikelijk proteomics-experiment beschreven, waarbij de nadruk ligt op de technische aspecten.

De vooruitgang in massaspectrometrie-gebaseerde proteomics heeft ervoor gezorgd dat zeer dynamische neuronale processen in specifieke cellulaire onderdelen zoals synapsen kunnen worden bestudeerd, ondanks hun korte duur en lage concentraties. In **hoofdstuk 2** bediscussiëren we de trends in massaspectrometrie-gebaseerde neuroproteomics van de synaps. We beschouwen de keuzes tussen verschillende types biologisch materiaal; label- en verrijkingstechnieken die gebruikt kunnen worden voor het bestuderen van eiwit-eiwitinteracties en eiwitsignalering alsmede data analyse en interpretatie. We eindigen met een notie over recente bevindingen die de vooruitgang van neuroproteomics kunnen bespoedigen.

In **hoofdstuk 3** integreren we kwantitatieve hogeresolutie-fosfoproteomics met de analyse van nieuw-gesynthetiseerde eiwitten met behulp van bio-ortogonale aminozuren. Om mGluR5-geïnduceerde eiwitfosforylatie en –translatie te volgen over tijd combineren we een gepulseerde labelstrategie met een op tandem mass tag label-gebaseerde kwantificatie van gekweekte hippocampale neuronen die gestimuleerd worden met DHPG. We identificeren verschillende kinases met belangrijke functies in DHPG-gerelateerde mGluR-signalering, wat we bevestigen door middel van inhibitie van de kinases met behulp van kleine moleculen. Daarnaast hebben we veranderingen in translatie en fosforylatie van eiwitten die kenmerkend zijn voor de signaleringsroute voor AMPA-receptor endocytose ontdekt. Een van deze eiwitten, Intersectin-1, is vervolgens gevalideerd als een cruciale speler in die signaleringsroute. Deze studie heeft verschillende nieuwe inzichten in de moleculaire mechanismen van

mGluR-geïnduceerde plasticiteit gegenereerd en biedt een overzicht van het proces over tijd.

In **hoofdstuk 4** beschrijven we de optimalisatie en validatie van APEX2 gefuseerd met de epidermal growth factor receptor (EGFR). We laten zien dat we met behulp van dit protocol, waarmee we alleen eiwitten labelen die zich bevinden in de zeer dichte nabijheid van APEX2, subtiele veranderingen in de locatie van EGFR kunnen onderscheiden. We bestuderen op die manier de verschillen in de locatie van de receptor in de tijd na stimulatie met EGF of TGF-a, waar de eerste resulteert in degradatie van de receptor en de tweede in het recyclen van de receptor naar het plasmamembraan. We hebben stabiele en vluchtige interactoren van de EGFR geïdentificeerd en gekwantificeerd op verschillende momenten na stimulatie en we konden zogenoemde 'omstandereiwitten' gebruiken om de subcellulaire locatie van EGFR op elk tijdspunt te bepalen. Door gebruik te maken van de snelle en precieze biotinylatie van eiwitten in de nabijheid van EGFR door APEX2 konden we zeer kleine verschillen in de vroege signaleringskinetiek tussen TGF-a en EGF onderscheiden, waardoor we de kennis over signalering van EGFR hebben uitgebreid.

In **hoofdstuk 5** gebruikten we APEX2 opnieuw en fuseerden we het label aan mGluR5 om alternatieve localisatie van de receptor in de cel te bestuderen. Hiertoe werd een sequentie van 25 aminozuren in het c-terminale domein van de receptor verwijderd. Deze bevat het localisatiesignaal naar het binnenste membraan van de nucleus. Biotinylatie-experimenten met deze versie van de mGluR5 leverden een subset van eiwitten op die specifiek gelocaliseerd zijn nabij de nucleaire fractie van mGluR5 in de cel. Door gebruik te maken van siRNA en western blot validatie-experimenten kunnen we unieke eiwitten betrokken bij het transport van mGluR5 naar de nucleus bestuderen. Ook zijn de rol van het coatomer I complex voor het retrograde transport van het golgisysteem naar het endoplasmatisch reticulum en casein kinase 2 als specifieke kinase voor nucleair mGluR5 bevestigd. Tezamen vormt dit een goede basis voor de studie naar verschillende functies van mGluR5, die afhankelijk kunnen zijn van zijn locatie in de cel.

About the author

List of publications

Acknowledgements

About the author

Charlotte van Gelder was born on the 29th of May 1990 in Heerlen, the Netherlands. She obtained a bachelor's degree with honours from the bachelor College of Pharmaceutical Sciences at Utrecht University in 2014. Her research internship at the department of Psychoneuropharmacology at the Utrecht Institute for Pharmaceutical Sciences under supervision of Dr. Ronald Oosting and Dr. Erik Hendriksen was focused on the assessment of a potential antidepressant in an animal model for depression. Moreover, she participated in the Honours Programme of Pharmaceutical Sciences, during which she co-authored a book on pharmacy and pharmaceutical sciences for nonprofessionals, titled 'Farmacie, van pillen tot patiëntenzorg'. During her bachelor studies, she discovered her fascination for the brain, and she applied for the selective master's programme Neuroscience and Cognition at Utrecht University. She followed the Clinical and Experimental Neuroscience track, during which she performed two research internships. The first internship was under the supervision of Prof. dr. Maarten Altelaar at Utrecht University. Here, she studied the role of newly translated proteins in mGluR5-dependent long term depression; a project that she continued to work on during her PhD. For her second internship she moved to Uppsala, Sweden. Under supervision of Prof. dr. Klas Kullander and Dr. Fabio Caixeta, she investigated the role of the vesicular aminergic-associated transporter slc10a4 in serotonergic neurons. In May 2016, she graduated and started her PhD under supervision of Prof. dr. Maarten Altelaar and Prof. dr. Albert Heck at the Biomolecular Mass Spectrometry and Proteomics group of Utrecht University. During this time, she was part of the Future Medicine Fellows, with whom she organized a seminar series and summer school on Gene and Cellular Therapies. Her research was focused on the use of a variety of enrichment and labeling approaches in combination with mass spectrometry-based proteomics to study the role of the metabotropic glutamate 5 receptor in synapse functioning, the results of which are presented in this dissertation.

List of publications

Van Gelder C.A.G.H. and Altelaar M. Neuroproteomics of the synapse: subcellular quantification of protein networks and signaling dynamics. *Manuscript accepted for publication*.

Van Gelder C.A.G.H.*, Penning R.*, Veth T.S., Catsburg L.A.E., Hoogenraad C.C., MacGillavry H.D., and Altelaar M. Temporal quantitative proteomics of mGluR-induced protein translation and phosphorylation in neurons. Mol Cell Proteomics (2020) mcp.RA120.002199.

Laarse S.A.M.*, **van Gelder C.A.G.H.***, Bern M., Akeroyd M., Olsthoorn M.M.A., and Heck A.J.R. Targeting proline in (phospho)proteomics. FEBS J (2020) febs.15190.

van Gelder C.A.G.H. and Lau C. 'De toekomst', in Addink M. *Farmacie: van pillen tot patiëntenzorg*. (2015). ISBN: 9789491141164.

Van Gelder C.A.G.H., van Bergen W., van Breugel P.C., and Altelaar M. Complementing the EGFR dynamic interactome using live cell proximity labeling. *Manuscript under revision*.

Schmidlin T., Debets D.O., **van Gelder C.A.G.H.**, Stecker K.E., Rontogianni S., van den Eshof B.L., Kemper K., Lips E.H., van den Biggelaar M., Peeper D.S., Heck A.J.R., and Altelaar M. High-throughput assessment of kinome-wide activation states. Cell Syst (2019) 9(4):366-374.e5.

Van de Loo A.J., van Andel N., **van Gelder C.A.G.H.**, Janssen, B.S., Titulaer J., Jansen J., and Verster J.C. The effects of alcohol mixed with energ drink (AMED) on subjective intoxication and alertness: results from a double-blind placebo-controlled clinical trial. Hum Psychopharmacol Clin Exp (2016) 31(3):200-205.

Jamalpoor A., **van Gelder C.A.G.H.***, Yousef Yengej F.A.*, Zaal E.A., Berlingerio, S.P., Veys K.R., Pou Casellas C., Voskuil K., Essa K., Ammerlaan C.M.E., Rega L.R., van der Welle R., Lilien M.R., Rookmaaker M.B., Clevers H., Klumperman J., Levtchenko E.N., Berkers C.R., Verhaar M.C., Altelaar M., Masereeuw R., and Janssen M.J. Cysteamine-bicalutamide combination therapy corrects proximal tubule phenotype in cystinosis. *Manuscript under revision*.

Man J.H.K., **van Gelder C.A.G.H.**, Breur M., van der Knaap M.S., Altelaar M., and Bugiani M. Astrocyte heterogeneity proteome in the normal human brain. *Manuscript submitted*.

Jamalpoor A., van Eerde A.M., Lilien M.R., **van Gelder C.A.G.H.**, Zaal E.A., Valentijn F.A., Broekhuizen R., Zielhuis E., Egido J.E., Altelaar M., Berkers C.R., Masereeuw R., and Janssen M.J. The lysosomal V-ATPase B1 subunit in proximal tubule is linked to nephropathic cystinosis. *Manuscript submitted*.

*Authors contributed equally.

Acknowledgements

They say time flies when you are having fun. And although on an adventure like this one you never reach the top in a straight line, I really enjoyed the journey. I have had the opportunity to work with many great people during my PhD, and I have had the greatest support team by my side, cheering me up and arming me with motivational speeches.

First, I would like to thank my supervisor **Maarten**, for encouraging me to apply for a PhD position in this lab by writing my own proposal. The project I initially wrote did not end up in this thesis, but that is ok, because science never really goes as planned. Thank you so much for allowing me to pursue almost all of my ideas and suggestions, and for giving me the freedom to try a little bit of everything. Your relaxed approach of supervision allowed for a lot of independence, which I really enjoyed. Nevertheless, you were also very approachable and helpful in difficult professional and personal situations. I really appreciate your mentorship.

Albert, it was a great pleasure to work in a lab surrounded with people from many different cultural and scientific backgrounds. Our weekly group meetings taught me so much about a wide variety of subjects, and I feel very lucky having to have met and befriend so many talented people.

In a lab as big as Biomass, chaos is always lurking around the corner. Luckily, the help of some amazing people has averted many crises. **Mirjam**, thank you for always being there to answer all my questions and for making sure the wet lab was a nice place to work in. Thank you **Soenita**, for teaching me cell culture basics when I was a student, and for all the nice cakes and chats. Wellicht zien we elkaar volgend jaar weer gewoon op Pinkpop! **Pieter**, your plasmid creations have proven to be an essential part of my work, and I am happy with the results we obtained using them, some of which are in this thesis. Additional exciting results are on the way, and I am looking forward sharing them. Thank you for teaching me some basic microbiology, I learned a lot from you. **Arjan**, thanks for showing me what a mass spec looks like from the inside. **Ceri**, thank you for your help during LC issues and in the cell culture lab. **Geert**, thanks for keeping the computers running smooth and for keeping our precious data save and accessible at all times. **Corine,** your organizational skills are admirable, thank you for answering all my questions. I hope we can soon run in an event again, perhaps another Science Park marathon next year?

During the years, I have had the opportunity to supervise a number of students during their internships. Their contributions to this thesis and to my personal growth have been invaluable. **Wouter**, your work has a prominent spot in this thesis, and I am very proud of the obtained results. Thank you so much for your enthusiasm and hard work, and I am happy that you decided to come back to the lab for your PhD. I am sure that you will do great, and I am looking forward to see the results of your work in a couple of years. **Renske**, how lucky that you were just about to dive into your first neuroproteomics project when I was looking for an internship! Thank you for sharing your knowledge and project with me, I am happy our joint effort

is now finally finished and online for everyone to see. Luckily, I was not the only one working on neuroproteomics after you left, and I really appreciate the support of the other 'neuro people'. **Suzy**, thank you for teaching me how to work with iPSCs and the basics of neuronal differentiation. Our daily trips to the iPSC lab were fun and I learned a lot! **Riccardo Stucchi**, I really enjoyed our discussions on the struggles and highlights of proteomics experiments in neurons.

The image of a grey and old man in a room without windows, working day after day, crunching away at a bench, is something we typically imagine when we think of a scientist. And although we do spend a tremendous amount of time at a bench, repeating experiments over and over, our labs do have windows. More importantly, we do not have to do all the science alone. I have collaborated with some very enthusiastic and talented scientists from various disciplines. I am grateful for all the help from our collaborators from the cell biology department, **Harold**, **Lisa**, and **Nicky**. You have been invaluable in my PhD project and have helped me with countless questions, and experiments. Thank you so much for your efforts and resources. **Amer**, I enjoyed working on projects that were very different from what I typically worked on. Thank you for the good discussions and nice collaboration. **Jodie**, it was so nice to witness the progress of your project over time, and to be a part of another neuroscience project. I learned a lot from the discussions on the biological relevance of our proteomics data, and I am looking forward to see more of the results. **Tim**, I am a bit worried that your efforts to teach me targeted mass spectrometry have been futile, as I still get a tiny panic attack every time I open Skyline. Thank you so much for helping me out with the SRM rebuttal experiments and for trying to figure out mGluR5 phosphorylation (which I am sure we will figure out in the near future). Also, when are you starting CrossFit? **Albert Bondt** and **Karli**, thank you for giving me a peak into the world of glycoproteomics! It is work in progress, but I am sure it is worth the trouble.

Being part of the Future Medicine Fellows has been such an experience! Thanks so much to my fellow FMFs **Katja**, **Amer**, **Rick**, **Lourens**, **Carl**, **Gerlof**, **Saar**, **Donna**, and **Tom** for trying to bridge all different aspects of pharmaceutical sciences together. It was a lot of fun organizing the Summer School and seminar series together. Thank you **Ed** and **Paul** for your guidance, both with the FMF and PhD committee.

Office Z606 a.k.a. the girls on fire: **Marie**, **Bohui**, and **Donna**. This office has been my second home (and also an additional storage space for random stuff, when do you think we will be able to finally use that barbecue?). You girls have been great, thanks for all the good times!

In order to keep up with all the hard work, it needs to be alternated with some distractions every now and then. My lunch times have provided that, thanks to my lunch buddies. **Sander**, thanks for all the nice coffee breaks and conversations during our internships. **Alba**, our time together in the lab was short, but it was nice to be a part of such a nice group of people. **Matina**, I am forever grateful that you asked Corine to place me into the office with you and Alba when you heard I was coming back to the lab

for my PhD. You were actually the one that brought me to Unscared and introduced me to CrossFit, and I have been in love with it ever since. Thank you so much for positive vibes and encouraging words. **David**, muchas gracias for all the great brainstorms, good conversations, and adventures. **Harm**, ik kan me nog herinneren dat je een poging hebt gedaan ons SDS page te leren tijdens het eerste jaar van mijn bachelor. Je hebt me enorm veel protocollen geleerd tijdens mijn stage en PhD. Dankjewel voor alle goede gesprekken. Die vrijdaglunch houden we erin! **Saar**, ons allereerste kopje koffie als kennismaking was tijdens mijn allereerste week. Ik durf niet te zeggen hoeveel koffie ondertussen geïmporteerd is om onze (lees jouw) consumptie bij te houden, maar ik ben enorm blij dat we atijd samen koffie konden drinken, ventileren, discussiëren en werken. Bedankt voor je altijd eerlijke en waardevolle mening, nacho's van The Basket en je steun als paranimf tijdens mijn verdediging.

Kyle, as you like to tell to everyone who wants to hear, we only became friends when you were almost leaving the lab. But hey, we have been friends ever since, and that has been some years now. You are my favorite concert buddy, and I cannot wait until they bring back the metal to the concert halls! On a more serious note, you have helped me through the first lockdown with our Friday pizza and beer meetings, and I hope I can come over to visit you and **Dallas** again soon.

Although the corona crisis changed the last year of my PhD tremendously, the lab has always had a great social and sportive network. **Marie** and **Julia**, my fellow crazy plant ladies, thanks for making me feel like a normal person even though I basically live in a jungle. **Sem**, **Esther**, **Arjan**, **Kelly D**, **Esther**, **Vojta** thank you for the good times during the Pheidippides relay run and USP marathon and the fun times during the Friday borrels. **Tomislav**, you better read this on a Friday, otherwise it does not count.

Er was gelukkig ook nog tijd voor een leven buiten het lab. Special thanks to my CrossFit buddies **Franziska**, **Tijmen**, and **Jeroen**, who have really tried to keep me fit and happy during the lock downs and closing of the gyms. Thanks for all the good times and peer pressure during the workouts. **Jeroen**, jouw aanwezigheid heeft van het afgelopen jaar, in alle onwaarschijnlijkheid, een geweldig jaar gemaakt. Bedankt voor de mooie werkplek, ontbijtjes, peptalks en knuffels. De afgelopen maanden als Prinsesbaas waren geweldig, maar ik durf wel te gokken dat de tijd die nog komt nóg leuker wordt.

Jiska, we waren onafscheidelijk vanaf mijn eerste dag op het Christelijk Lyceum. En ondanks dat we twee compleet verschillende routes hebben genomen zijn we allebei terecht gekomen in de massa spectrometrie. Je bent een goede vriendin en voorbeeld en ik ben dankbaar dat ik je al mijn halve leven ken.

Nienke, het is bijna onmogelijk om jarenlang twee straten bij elkaar vandaan te hebben gewoond, dezelfde lievelingsplekken te hebben en elkaar toch niet te kennen, maar toch was het zo. Gelukkig hebben we elkaar uiteindelijk in Utrecht ontmoet en hebben we een paar jaar geleden

het goede voornemen gehad om elke week samen te eten. Thanks voor alle gezellige etentjes en mental support!

Linda, **Simon**, **Tarah** en **Alex**, wat zijn onze levens enorm veranderd sinds we elkaar leerden kennen bij de Graaf! Ik ben enorm blij dat onze vriendschappen met ons zijn meegegroeid en dat ik altijd bij jullie terecht kan voor een biertje of een kopje thee en een hoop gezelligheid. Je kan me niet veel gelukkiger maken dan mij een middagje laten spelen met **Elin**, **Ivar** en **Tijl**. Maar nu genoeg gepraat over gevoelens, wanneer gaan we bier drinken?

Lieve **Steph**, ik kan geen grote stap in m'n leven bedenken waarin jij niet aan mijn zijde was om mij te steunen. Je gelooft altijd in mij en bent m'n grootste fan en ik kan je niet genoeg bedanken voor alles wat je voor me hebt gedaan. Ik ben enorm trots op ons en alles wat we hebben bereikt! Je bent niet alleen mijn kleine zusje, maar vooral ook mijn beste vriendin. Dat we samen de omslag en layout voor deze thesis hebben gemaakt staat symbool voor wat jij voor mij betekent. Ik vind het een enorme eer dat jij en mijn lieve nichtje samen mijn paranimf willen zijn (en dat ik dus stiekem drie paranimfen heb)!